Response to nitrosative stress of *Escherichia coli*

by

Jing Wang

A thesis submitted to

The University of Birmingham

For the degree of

DOCTOR OF PHILOSOPHY

School of Biosciences

University of Birmingham

April 2015

Abstract

Escherichia coli encounters nitrosative stress from various sources. It was shown in a previous study that several genes, including the *hcp* gene, were highly expressed during anaerobic growth under conditions of nitrosative stress, thus indicating a possible role for Hcp in the nitrosative stress response. The hybrid cluster protein (Hcp) contains a regular 4Fe-4S (or 2Fe-2S) centre and an unusual hybrid 4Fe-2S-2O cluster. The focus of this study was to determine the function of Hcp.

First the phenotype of an *hcp* mutant in a genetic background lacking all known NO reductases was determined. The growth of the *hcp* mutant was inhibited by various sources of nitrosative stress, including nitrate, nitrite, and nitric oxide. Aconitase, an Fe-S protein that is especially sensitive to inactivation by NO, was inactivated in the *hcp* mutant under nitrosative stress conditions. The growth defect of the *hcp* mutant was complemented by native Hcp protein. Glutamic acid 492, which coordinates the hybrid cluster, was mutated by site-directed mutagenesis to valine, alanine, glycine and aspartic acid. Only the E492D substitution complemented the mutation. The role of Hcp was shown to protect *E. coli* from nitrosative stress, and the hybrid cluster is critical for its function.

In an attempt to extrapolate the function of Hcp through protein interaction, the bacterial two-hybrid system was used to test the interaction between Hcp and several protein candidates. No protein interaction was observed between Hcp and AcnB, YtfE, NsrR, or with itself. Direct interaction between Hcp and Hcr was demonstrated. In *E. coli*, the gene *hcp* is found in a two-gene operon *hcp-hcr*. Hcr is the NADH-dependent

oxidoreductase of Hcp. Phenotype study of the *hcp*$^{+}$*hcr* strain showed that it was still resistant to nitrosative stress. Possibly an alternative oxidoreductase of Hcp exists in *E. coli*, and Hcp accepts electrons from other sources than Hcr to fulfill its function.

To test whether Hcp is an NO reductase, the NO reduction ability of bacteria with or without the *hcp* gene was compared. Gas analysis of the headspace of anaerobic cultures showed that when treated with NO, the *hcp*$^{+}$ strain lacking all known NO reductases was still capable of reducing sub-micro molar NO into N_2O, while the further deletion of *hcp* completely abolished NO reduction. The *hcp*$^{+}$*hcr* mutant was also capable of reducing NO to N_2O, however, its tolerance to NO is lower than that of the *hcp*$^{+}$*hcr*$^{+}$ parent strain. This provides the first *in vivo* evidence that Hcp is a high affinity, low capacity NO reductase in *E. coli*, reducing NO to N_2O.

Acknowledgements

First of all, I would like to thank Prof. Jeff Cole, for revising this thesis and his supervision. A similar thank-you also goes to co-supervisor Prof. Steve Busby. I am grateful to Chinese Scholarship Council for funding my PhD study for the past three years.

I thank Prof. Lars Bakken for giving me the opportunity to complete the critical robotic experiments in Norway, and those working in his lab, Lars M, Junaid, Natalie, especially Linda for her kindness during my stay, and for completing additional experiments for our joint publication. I would like to thank everyone on the ground floor that I've worked with: Claire for her four isogenic strains, Sarah, Charlene and Ian for their help in my first year of PhD, Basema for accommodating me during the revision of this thesis, MSc students Pete, Parisa, Stan, Tania, Matthew, Ana, and especially Lisa and John for sharing proteins and unpublished data. I want to thank Prof. Ian Henderson and the whole Busby group sharing the same office: Dave, Laura, Yasir, Doug, Rita, Riddhi, Jack, Banda, Ghada, George, Bihe, Far. Also I want to thank other fellow IMIers and people from the System Biology that I have been fortunate enough to know: James, Lisa L, Shuangxi, Rohit, Feng, Isaac, Daniel. For those other people that happened in my PhD that don't belong the above mentioned classifications: Alfredo, Kay, Hongyan, Jianming, Masha, Sharna, Elisa, thank you for your help and inspiration.

Last but not the least, I want to thank my family, especially my mom and my sister for their support during my PhD. I hope I have made you proud.

Contents

List of Figures

List of Tables

List of abbreviations

Amp	Ampicillin
ATP	Adenosine triphosphate
bp	Base pairs
Carb	Carbenicillin
Chlor	Chloramphenicol
CD	Circular dichroism
CR	Cloning region
DCPIP	2,6-dichloroindophenol
DMSO	Dimethyl sulfoxide
E. coli	*Escherichia coli*
EPR	Electro paramagnetic resonance
FdhN	Formate:menaquinone oxido-reductase
Fis	Factor for inversion stimulation
Fnr	Regulator of fumarate and nitrite reduction
GC	Gas chromatograph
GSNO	S-nitrosoglutathione
Hcp	Hybrid cluster protein
Hcr	Hcp oxidoreductase
HPLC	High pressure liquid chromatography
IHF	Integration host factor
IMAC	Immobilized-metal affinity chromatography
IPTG	Isopropyl-β-D-1-thiogalactopyranoside
Km	Kanamycin

LB	Lennox broth
LB-Ca^{2+}	Lennox broth supplemented with 2 mM $CaCl_2$
MS	Minimal salts
MK	Menaquinone
MKH_2	Menaquinol
NA	Nutrient agar
NADP(H)	Nicotinamide adenine dinucleotide phosphate (reduced form)
NAD^+	Nicotinamide adenine dinucleotide
NAP	Nitrate reductase in the periplasm
NAR	Nitrate reductase
ND	Not determined
NIR	Nitrite reductase
NRF	Nitrite reduction by formate
NO	Nitric oxide
NOSW	Nitric oxide saturated water
nt	Nucleotide
N-terminal	Amino terminal
OD	Optical density
ONPG	Orthonitrophenyl-β-D-galactopyranoside
PCR	Polymerase chain reaction
ppmv	Parts per million by volume
RIC	Repair of iron centres
RNA	Ribonucleic acid
RNAP	RNA polymerase

RNS	Reactive nitrogen species
ROS	Reactive oxygen species
TCA	Tricarboxylic acid
TMA(O)	Trimethylamine (*N*-oxide)

CHAPTER 1
INTRODUCTION

Escherichia coli is a facultative anaerobe capable of growing under both aerobic and anaerobic conditions. Hence it can be found in many diverse environments. It is capable of using the same ATP synthase during aerobic and anaerobic respiratory growth (reviewed by Cole, 1996). *E. coli* is able to sense and respond to oxygen in the environment, which releases more free energy than other electron acceptors. The expression of other terminal reductases are repressed by oxygen. When oxygen is not available, in order to survive, *E. coli* can also reduce less energy-efficient, alternative terminal electron acceptors, among which nitrate is the preferred option (Unden *et al.*, 1995; Unden and Bongaerts, 1997). However, the metabolism of nitrate and nitrite can cause nitrosative stress inside the bacteria, for which *E. coli* has developed several detoxifying systems, one of which was identified and studied in this thesis.

In this introduction, first the transcription factors responsible for the control of anaerobic respiration will be introduced. Nitrate and nitrite reductases will be described, then the generation of nitric oxide and nitrosative stress, its toxicity *in vivo* and detoxification in *E. coli*. NsrR is a NO sensor and its transcriptional control is triggered by nitric oxide. Two genes *ytfE* and *hcp* from the *nsrR* regulon will be described. The gene *hcp* is the focus of this study. Detailed information on Hcp structure, *hcp* gene regulation and putative functions will be given. Finally the aim of this work will be introduced.

1.1. Anaerobic bacterial respiration and its regulation

During anaerobic respiration, proton motive force and therefore ATP, are generated *via* the transfer of electrons through the electron transfer chain. Electrons are derived from

various electron donors, such as formate, NADH, H_2, glycerol 3-phosphate, and lactate, and transferred *via* electron mediators such as ubiquinone (Q) or menaquinone (MQ), then finally to the various electron acceptors such as nitrate, nitrite, TMAO, DMSO and fumarate (Collins and Jones, 1981; Tyson *et al*., 1997). For instance, nitrate could be reduced to nitrite *via* a short electron transfer chain. In this reduction process, electrons flow from the quinone pool *via* the *b*-type cytochrome NarI and the iron-sulphur protein NarH to the active nitrate reductase NarG (Richardson and Sawers, 2002). The standard apparent reduction potential of biochemical half reactions involved in this study is summarised in Table 1.1 (Alberty, 2004). In a general respiration process, when a variety of electron acceptors, including oxygen, nitrate, dimethyl sulfoxide (DMSO) and fumarate, are present at the same time, corresponding respiratory enzymes are synthesized in a hierarchical manner. Transcription factors that are responsive to different electron acceptors regulate the hierarchical control so that the thermodynamically most favorable electron acceptor is utilized before the others.

1.2. Major transcription factors involved in anaerobiosis

1.2.1 FNR as a direct oxygen sensor

The top level of control of adaptation to anaerobic growth is mediated by a global transcription factor, FNR (the regulator of fumarate and nitrite reduction), which regulates the expression profile of more than 100 genes during the transition from aerobic to anaerobic respiration **(**Constantinidou *et al*., 2006; Grainger *et al.*, 2007). FNR is an iron-sulfur protein in which the [4Fe-4S] acts as an oxygen sensor (Jayaraman *et al.*, 1988; Spiro and Guest, 1990). In the presence of oxygen, the iron-sulfur centre is degraded, FNR is inactivated and dissociates from a functional

dimer into inactive monomers that are unable to bind to the DNA. Active FNR acts both as an activator and a repressor (Kiley and Reznikoff, 1991). During anaerobic growth conditions, genes involved in aerobic respiration are repressed by FNR (reviewed in Spiro and Guest, 1990). Transcription initiation of many operons for anaerobic respiration is activated by the Fnr protein, such as the *dmsABC* and *narGHJI* operons encoding the DMSO reductase and the respiratory enzymes cytochrome *b*-linked nitrate reductase (Guest *et al.*, 1996). At most target promoters, two FNR monomers bind to an inverted repeat consensus sequence TTGAT-N_4-ATCAA, resulting in the activation of transcription initiation by RNA polymerase (Jayaraman *et al.*, 1988).

1.2.2. The Nar two-component sensor and response regulators

The second level of control is mediated by the dual two component system NarXL-NarQP. They modulate the expression of operons involved in anaerobic respiration, according to the availability of nitrate and nitrite (Stewart, 1993). This accounts for the established priorities of operons involved in nitrate and nitrite reduction above other anaerobically expressed operons. The Nar two component system consists of two homologous sensors, NarX and NarQ, which are responsible for detecting nitrate and nitrite, and two homologous response regulators, NarL and NarP, which are responsible for regulating the expression level of various operons important for nitrate and nitrite respiration (Lin *et al.*, 2007; stewart and Bledsoe, 2005; Filenko, 2005).

In this dual interacting two-component regulatory system NarXL-NarQP, NarX and NarQ sensors are histidine kinases that span across the membrane. In the presence of

Table 1.1. **Standard reduction potential of reactions involved in this study**

Half Reaction	Number of electrons	E^o/V
$O_{2(aq)} + 4e + 4H^+ \rightarrow 2H_2O$	4	0.849
$NO_3^- + 2e + 2H^+ \rightarrow NO_2^- + H_2O$	2	0.410
$NO_2^- + 2H^+ + e \rightarrow NO_{(g)} + H_2O$	1	0.374
$NO_2^- + 8H^+ + 6e \rightarrow NH_4^+ + 2H_2O$	6	0.338
$NO_{(g)} + H^+ + e \rightarrow ½\ N_2O_{(g)} + ½\ H_2O$	1	1.164
$½\ N_2O_{(g)} + H^+ + e \rightarrow ½\ N_2 + ½\ H_2O$	1	1.347
$Ferredoxin_{ox} + e \rightarrow Ferredoxin_{red}$	1	-0.403
$Fe^{3+} + e \rightarrow Fe^{2+}$	1	+0.200~-0.236
Fe-S clusters*	1	-0.5 ~ +0.3

*reference from Meyer, 2008, all other figures from Alberty, 2004.

nitrate and nitrite, a conserved histidyl residue in the sensor regulator is autophosphorylated at the expense of ATP, producing ADP. Intra-molecular transfer of the phosphate group between sensor and response regulators enables signal transduction. A conserved aspartyl residue in the receiver domain of the response regulators is phosphorylated (Stewart, 2003, Stewart and Bledsoe, 2003). NarL and NarP have an increased DNA binding affinity when they are phosphorylated by NarX and NarQ sensors. However, the phosphorylated response domain could also be dephosphorylated by several mechanisms. For instance, a phosphor group could also be removed from the response regulators under the stimulation of an unphosphorylated sensor. The final state of phosphorylated response regulators are determined by the relative rates of transmitter autokinase and phosphatase activity (Stewart, 1998; Noriega *et al.,* 2010).

The Nar two-component system forms a cross-regulation network *in vivo*, but it is not symmetric in terms of kinetic preference between different pairs of sensor and regulator, as well as the response of sensors NarX and NarQ to nitrate or nitrite (Noriega *et al.,* 2010). *In vitro* phosphoryl transfer time-course reactions demonstrated that NarL is the preferred response regulator for receiving signals from phosphor transfer. NarX has a pronounced kinetic preference to NarL over NarP, while NarQ interacted with both of the two response regulators, but has a relatively slight preference over NarL (Noriega *et al.,* 2010). Hence the Nar two-component system is also referred to as NarXL and NarQP. The scheme of phosphorylation between sensors and regulators is depicted in Fig 1.1. NarX responds preferentially to nitrate while NarQ is capable to respond to both nitrate and nitrite (Rabin and Stewart, 1993, Wang *et al.,* 1999). Phosphorylated NarL activates 51 operons and represses 41 operons, while phosphorylated NarP

Figure 1.1.

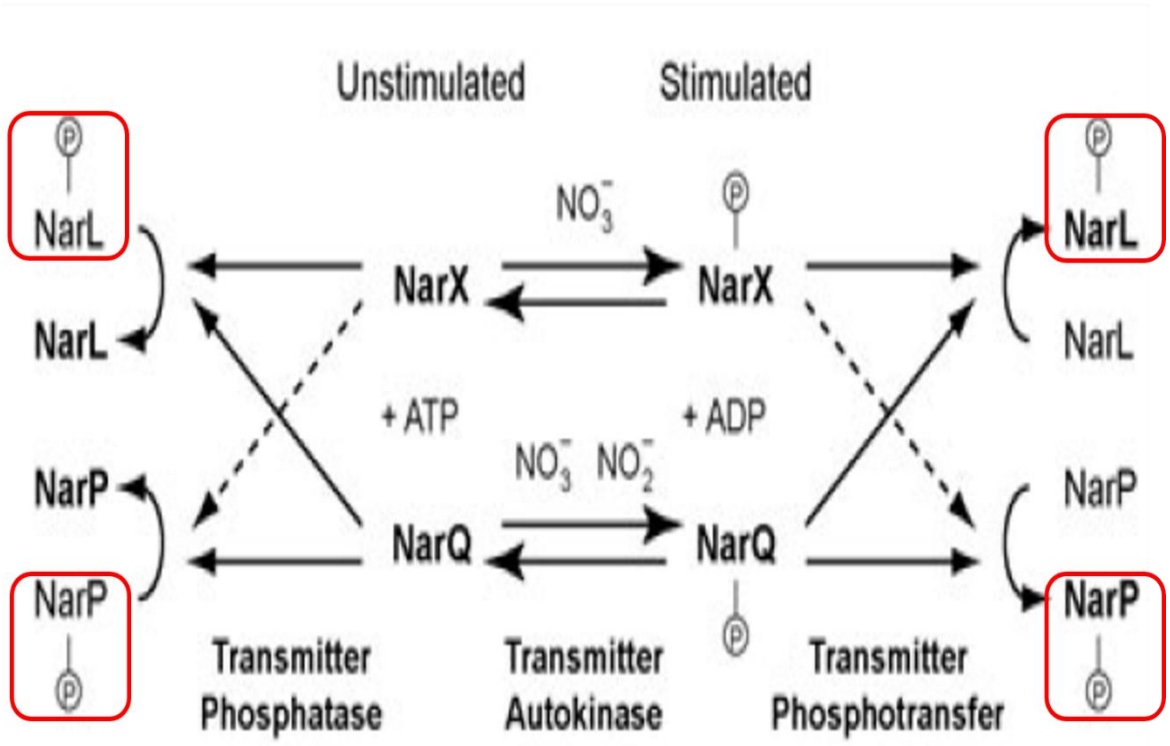

Model of asymmetry in the Nar dual component cross-regulation network

It is hypothesized that the presence of the nitrate/nitrite and ligand binding determine the two-state equilibrium achieved between the NarX and NarQ sensor populations. Phospho-sensors phosphorylate the response regulators, while in reverse, dephospho-sensors are also capable of catalyzing the dephosphorylation of phospho-response regulators. The phosphorylated response regulators (in squares) then bind to the control regions of target operons, activate or repress their transcription. Dashed arrows represent relatively slow reactions. Adapted from Noriega *et al*., 2010.

activates 14 operons and represses 37 operons (Constantinidou *et al*, 2006).

1.3 Nitrate and nitrite

Nitrate assimilation and dinitrogen fixation are performed by bacteria to incorporate inorganic nitrogen into the biological nitrogen cycle, which is essential for providing the material used in the nucleic acid and protein synthesis (Richardson, 2001). Nitrate can be reduced by nitrate reductases to yield energy in anaerobic respiration (Richardson, 2000). If the final product is nitrogen, the reduction process is termed denitrification, which is one of the foci in the environmental research. In denitrification, various intermediate nitrogen oxides are generated, causing the green-house effect and public health issues (Richardson *et al*., 1998). Nitrite can also act as a terminal electron acceptor to provide energy. However, nitrite is cytotoxic, especially at acidic conditions where NO can be generated *via* nonenzymatic acidic disproportionation. In the laboratory, one way to make nitric oxide is by adding acid into the solution of a nitrite in the presence of a reducing agent, which was later adopted in this study for generating gaseous NO.

1.3.1. The nitrate reductases Nar and Nap

More than one nitrate reductase is present in *E. coli*. The complexity is essential for the bacteria to survive in transient environmental conditions (Cole, 1996). The genes encoding two of the nitrate reductases are anaerobically expressed and are subject to transcriptional control. The *E. coli* genome encodes three distinct nitrate reductases, with two that are membrane-bound at the cytoplasmic side and one in the periplasm. The two sets of cytoplasmic nitrate reductase genes, *narGHJI* and *narZYWV*, encode

two membrane bound protein complexes (Forget, 1974, Enoch and Lester, 1975, Chaudhry and Macgregor, 1983, Blasco *et al.*, 1990, Iobbi-Nivol *et al.*, 1990). In the presence of nitrate, the *narGHJI* operon is up-regulated by NarL while the *narZYWV* operon is still poorly expressed. The periplasmic nitrate reductase and its electron transfer partners of *E. coli*, Nap proteins, are important during anaerobic growth in low-nitrate environments (Potter *et al*., 1999; Wang *et al*., 1999; Stewart *et al*., 2002). Figure 1.2 shows the cellular location of nitrate reductase subunits.

Nar and Nap function with different nitrite reductases in response to the availability of nitrate (Spector *et al.*, 1999, Iobbi-Nivol *et al.*, 1990, Iobbi *et al.*, 1987). When nitrate is abundant, the respiratory nitrate reductase NarG, which is located on the cytoplasmic side of the membrane, works with the cytoplasmic nitrite reductase NirB. When nitrate is scarce and nitrite is abundant, Nap works with periplasmic nitrite reductase Nrf (Fig 1.3).

1.3.2. The nitrite reductases Nir and Nrf

Two nitrite reductases are present in *E. coli*, one in the cytoplasm and the other one in the periplasm. The cytoplasmic NADH-dependent nitrite reductase Nir functions primarily to detoxify nitrite to ammonia. Expression of the *nir* operon is activated by Fnr and phosphorylated NarL and NarP (Browning *et al.*, 2005, Tyson *et al.*, 1993). The *nir* operon is co-regulated with the *NarGHJI* operon so that nitrite is reduced as rapidly as nitrite is formed as the product of nitrate reduction (Page *et al.*, 1990). No energy is conserved directly during this process, and therefore no proton gradient is generated (Cole and Brown, 1980, Wang and Gunsalus, 2000). The Nir system is encoded by the

Figure 1.2.

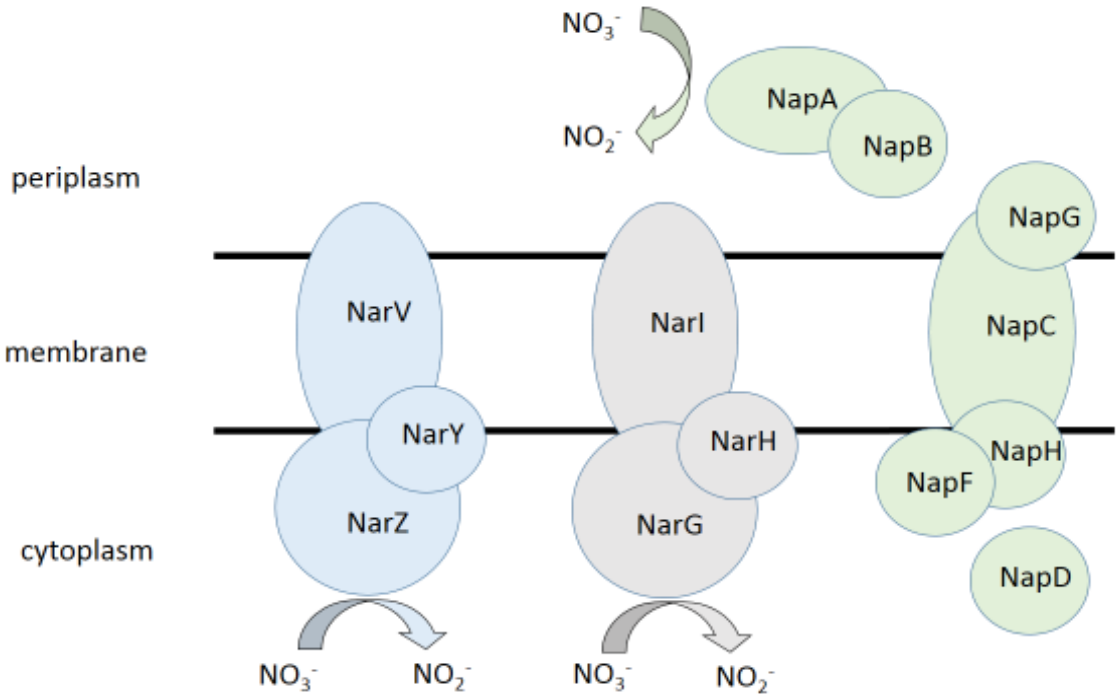

Distribution of nitrate reductase subunits in *E. coli*

The two cytoplasmic nitrate reductase complexes are NarZYV (blue) and NarGHI (grey). The periplasmic Nap complex is shaded green. The chaperone components of these complexes were not shown for simplicity of the diagram. Adapted from Vine and Cole (2011a).

nirBDEC operon and *cysG* operon: *nirBD* encode the structural enzyme subunits of the nitrite reductase; *nirC* encodes a nitrite transport protein; *cysG* is required for the synthesis of sirohaem, which is a haem group that serves the binding site for sulfite or nitrite in the sulfite or nitrite reductases (Peakman *et al.*, 1990, Jia *et al.*, 2009, Clegg *et al.*, 2002, Vega and Garrett, 1975; Murphy *et al.*, 1974).

The periplasmic cytochrome *c* nitrite reductase NrfA reduces nitrite directly to ammonia (Table 1.1). The catalytic subunit of NrfA is a homo-dimer of two penta-haem cytochromes. It is located in the periplasm and interacts with other membrane-associated subunits of the Nrf complex. As shown in Fig 1.4, the six electron reduction of nitrite to ammonia is proposed to proceed through enzyme-bound intermediates, NO and hydroxylamine (Einsle *et al.*, 2002). The mechanism was based on the crystallographic observation of reaction intermediates and density functional calculations using computer programs and a simplified active site model [Fe(P)(NH3)(X)], with X being various reaction intermediates as distal ligands.

Regulation of the *nrf* operon is very complex (Browning *et al.*, 2010). High concentrations of nitrate repress its expression and low concentrations of nitrate activate its expression. Under anaerobic conditions, it is activated by Fnr and NarL (or NarP), but repressed by two nucleoid associated proteins IHF and Fis in response to rich medium (Tyson *et al.*, 1997, Browning *et al.*, 2005). It was found that NsrR, a nitric oxide sensitive repressor, modulates expression of the *nrf* operon (Browning *et al.*, 2010). NrfA also reduces nitric oxide to ammonia, facilitating NO detoxification (van Wonderen *et al.*, 2008).

Figure 1.3.

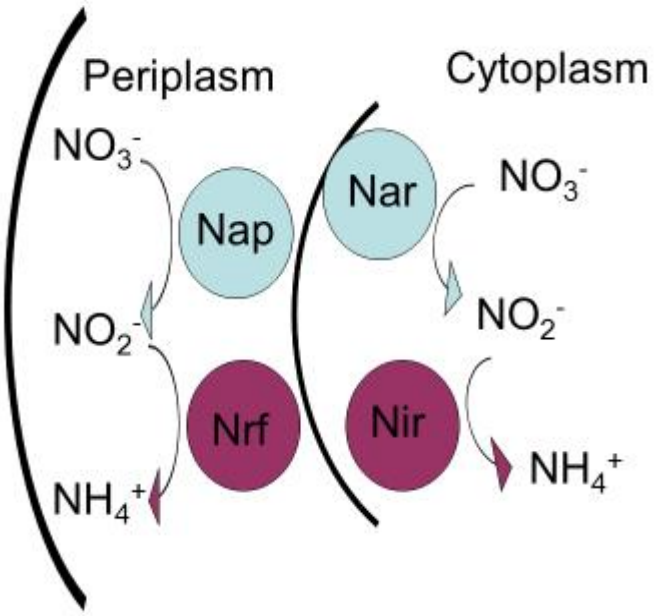

Pairing of nitrate and nitrite reductases in *E. coli* periplasm and cytoplasm

E. coli possesses two sets of paired nitrate and nitrite reductases. The *nar* operon encoded nitrate reductases located in the cytoplasm, reducing nitrate to nitrite. The generated nitrite was further reduced by the cytoplasmic nitrite reductase Nir. In the periplasm, Nap works with the cytochrome *c* nitrite reductase Nrf. Nitrate and nitrite availability modulates the transcription of the genes encoding the enzymes in this system.

Proposed mechanism of nitrite reduction by NrfA

Panel A: Electron pathway to NrfA during nitrite reduction, which is coupled to formate oxidization by the formate dehydrogenase FdhN. Electrons are transferred to NrfA from the membraneous menaquinone pool *via* membrane-associated mediator proteins, which is NrfH for *Wolinella succinogenes*, and the NrfBCD complex for *E. coli* (Hussain *et al.*, 1994; Bamford *et al*., 2002; Simon *et al.*, 2000; Simon, 2002).

Panel B: The six-electron reduction of nitrite to ammonia by cytochrome c nitrite reductase (NrfA) was proposed by Einsle *et al.* (2002). Reaction was started with the binding of substrate nitrite in place of the water molecule (reaction 1). Then the cleavage of the first N-O bond occurred and resulted in an enzyme-bound NO intermediate $\{FeNO\}^6$ (the d6 electronic configuration) (2). A further transfer of two electrons was achieved to obtain a reduced species $\{FeNO\}^8$ (the d8 electronic configuration) (3). A protonation step followed to produce Fe(II)-HNO (4), which was readily reduced by two more electrons to Fe(II)-H_2NOH (5). Oxidation of the Fe(II) ion to Fe(III) was coupled to a protonation and yielded the ammonia as the final product (6). It was released from the active site after a further protonation (7), while this cycle was closed by the one–electron reduction to the Fe(III) back to Fe(II), as the enzyme returned to its water-bound resting state (8).

Figure 1.4.

A

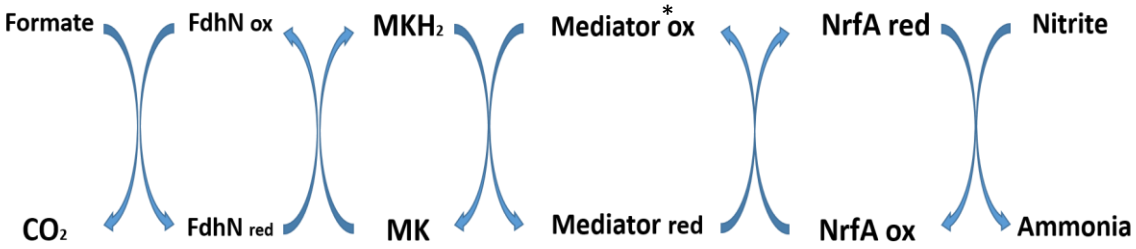

* See figure legend for detailed information about the mediator protein.

B

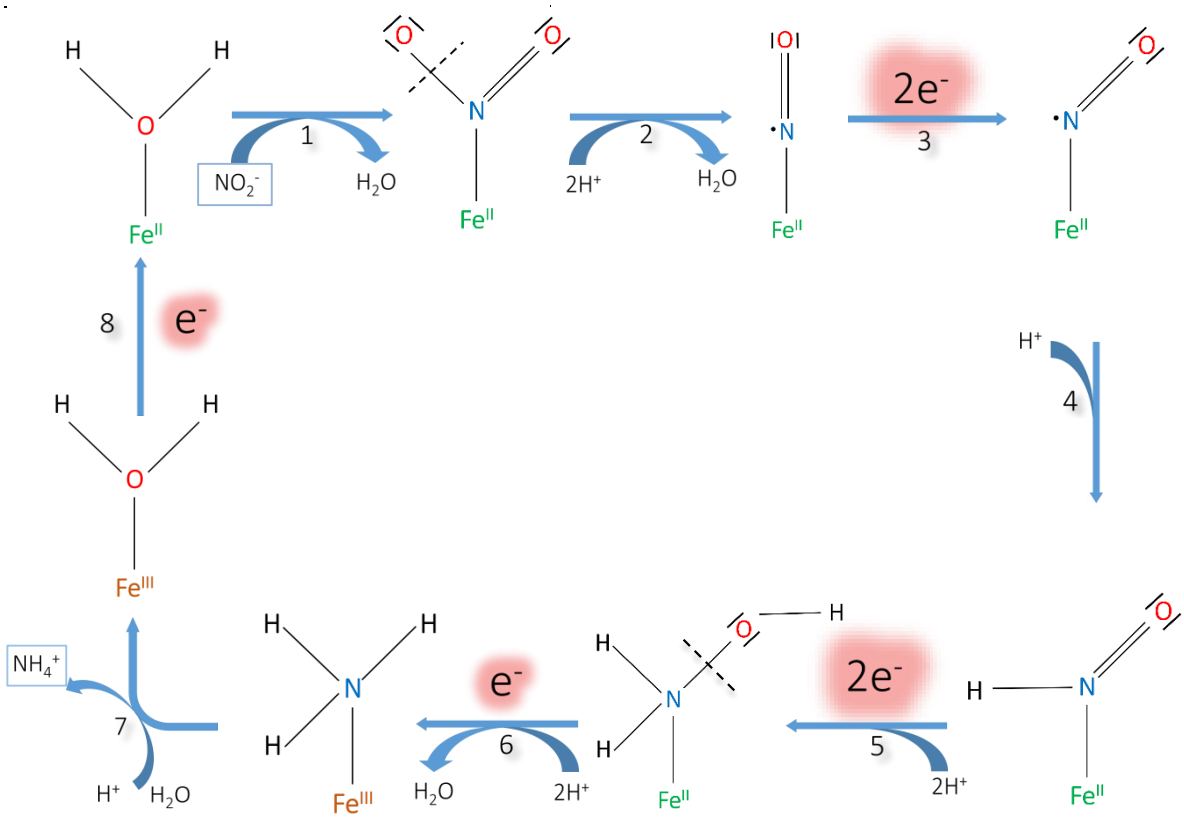

1.4. Nitric oxide (NO)

1.4.1. Nitrosative stress and the generation of NO *in vivo*

The free radical gas, nitric oxide (NO), is an important signaling molecule in biology (reviewed in Moncada *et al.*, 1991). The physiological concentration of NO in cells and tissues was considered to be 1 μM, but it might be much lower, possibly in the order of 5 nM (Halla and Garthwaiteb, 2009). NO is also important in the generation of nitrosative stress encountered by bacteria (Ji and Hollocher, 1998). Some of the nitrosative stress comes from the environment, such as from the host of microbial pathogens (Vine and Cole, 2011a). Neutrophils and activated macrophages of the mammalian immune system produce nitric oxide when infected (Fang, 2004). Reactive nitrogen species are also generated during bacterial metabolism, for example when nitrate or nitrite is reduced to ammonia. Under anaerobic conditions, NO can be generated *via* a one-electron reduction from nitrite. Not just capable of reducing nitrite to ammonia, nitrite reductases NirB and NrfA could also reduce nitrite to NO and hence contribute to the production of nitric oxide in *E. coli* (Corker and Poole, 2003; Weiss, 2006). There is a growing consensus that NarG, the cytoplasmic nitrate reductase which can reduce nitrate to nitrite, is also responsible for the most of the NO generation *in vivo* (Ji and Hollocher, 1998; Metheringham and Cole, 1997; Gilberthorpe and Poole, 2008; Vine and Cole, 2011b).

1.4.2. Damage caused by NO *in vivo*

NO does not react directly with DNA. However, NO could mediate bacterial damage by acting as a precursor for other NO-derived species. The reaction of NO and reactive oxygen species such as superoxide generates peroxynitrite, which is an extremely toxic

molecule for the bacteria. When NO reacts with oxygen in the cytoplasm, detrimental oxidised species are generated as a result. For instance, N_2O_3, a powerful nitrosating agent, is capable of damaging DNA bases and therefore leads to mutations (Spek *et al*., 2001). This type of nitrosative mutagenesis occurs when the growth conditions of bacteria are shifted from nitrate-dependent to oxygen-dependent, so that the accumulated NO might be oxidised (Weiss, 2006). NO can cause direct damage to NO sensitive targets. Nitrosylation is defined as the circumstance where NO binds to a metal centre, such as the ubiquitous Fe-S clusters found in the dehydratases, or in the transcription factors including the previously described FNR protein (reviewed in Vine and Cole, 2011a). A stable dinitrosyl-iron complex is formed in place of the Fe-S cluster after its reaction with NO (Justino *et al*., 2009). The nitrosylation of the [4Fe-4S] enzyme aconitase, which is part of the TCA cycle, and other hydratases are highly sensitive to NO, which might account for the toxicity of NO toward a variety of organisms (Gardner *et al.*, 1997).

1.4.3. Detection of NO in the cytoplasm

Several methods have been developed to detect the accumulation of NO in the bacterial cytoplasm. All of these methods employ the principle that NO changes expression of certain genes by modulating the activity of NO-sensitive transcription factors *in vivo*. NNR in *Paracoccus denitrificans* is a homologue of the FNR protein in *Escherichia coli*. It is a transcriptional factor that can respond to NO. A heterologous expression of NNR from *Paracoccus denitrificans via* an engineered *E. coli melR* promoter was used by Hutchings *et al.,* (2000) while FNR and NorR were utilized by Cruz-Ramos *et al* (2002) and Strube *et al.* (2007), respectively, to detect the accumulation of NO. In the absence

of NO, the transcription factor, NsrR, is a repressor of the *hcp* promoter. The repression is relieved when NO accumulates. For strains of *E. coli* K-12 transformed with a P*hcp::lacZ* fusion plasmid, the accumulation of NO in the cytoplasm can be detected by a β-galactosidase assay (Vine, 2011). An Oxytherm electrode unit was used to detect NO concentration in a sealed chamber where glucose, glucose oxidase and catalase were added to scavenge oxygen that would otherwise react chemically with NO (Vine, 2011).

1.4.4. Detoxification of NO in *E. coli*

Three genes, *hmp*, *nrfA* and *norV*, have been identified in *E. coli* that encode proteins that detoxify NO. Under aerobic conditions, the flavohaemoglobin, Hmp, oxidizes NO to nitrate, while under anaerobic conditions Hmp is able to reduce NO to N_2O. Hmp is considered to be much more effective in aerobic conditions (Gardner and Gardner, 2002; Poole and Hughes, 2000; Kim *et al*., 1999). NrfA is a periplasmic cytochrome *c* nitrite reductase. Its primary function is the respiratory reduction of nitrite to ammonia. It can also reduce hydroxylamine and NO when needed (Poock *et al.*, 2002). The Km of NO reduction by NrfA is estimated to be around a non-physiological concentration of 300 μM. It has been proposed that NrfA provides the first frontline defense by reducing NO in the periplasm so that there will not be a high concentration of NO diffused into the cytoplasm (van Wonderen *et al.*, 2008). The flavorubredoxin, NorV, and its associated oxidoreductase, NorW, reduce NO to N_2O (Gardner *et al.*, 2002; Gomes *et al.*, 2002, Tucker *et al.*, 2005). The transcriptional regulation of the *norVW* regulon was shown in Fig 1.5. A reverse-transcription PCR study showed that Fnr represses the transcription of the *norV* gene, as a 28-fold stimulation of transcription of *norV* was observed in an

fnr mutant (da Costa *et al.*, 2003). In addition, *norV* is upregulated by a transcriptional factor, NorR, which responds exclusively to NO (Hutchings *et al.*, 2002). An NO molecule binds reversibly to the mono-nuclear iron centre of this protein. This results in a change in the conformation of the protein and accordingly its regulation of DNA binding (D'Autréaux *et al.*, 2005).

1.5. Role of the regulatory protein NsrR in the nitrosative stress response

NsrR, originally designated as the nitrite sensitive repressor, was later realized to regulate genes involved in cell protection against nitric oxide. It is a member of the Rrf2 family of transcription factors (Rodionov *et al*., 2005). The Rrf2 family belongs to a superfamily of prokaryotic transcriptional factors that features a typical winged helix-turn-helix DNA binding motif (Aravind *et al.*, 2005). A computational bioinfomatic analysis of Rrf2 family regulators and the DNA-binding sites predicted that NsrR homologues in a variety of bacteria regulate the defense against reactive nitrogen species (RNS; Rodionov *et al*., 2005). Four promoters, *hmpA*, *ytfE*, *ygbA* and *hcp*, were predicted to be regulated by the *E. coli* NsrR in response to RNS. This prediction was confirmed by transposon insertion experiments in which the regulation of *ytfE* expression was studied. The consensus sequence of the NsrR binding site has been shown to be an inverted repeat (GATG N_{11} CATC) (Bodenmiller and Spiro, 2006). The NsrR proteins in a variety of bacteria have been shown to contain an NO-sensitive iron-sulfur cluster that was required for DNA binding activity (Isabella *et al*., 2009, Tucker *et al.*, 2008; Yukl *et al*., 2008). When exposed to NO, the iron-sulfur cluster is nitrosylated, which leads to the loss of DNA-binding activity. As a result, transcription repression is relieved to allow expression of relevant genes (Tucker *et al.*, 2008).

Figure 1.5.

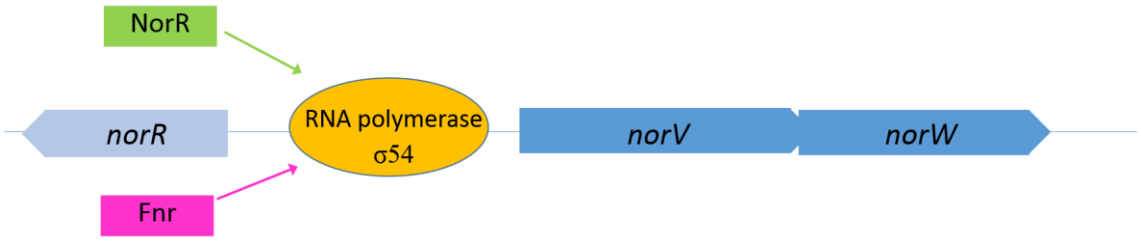

Regulation of the *norV-norW* operon

The NO reductase NorV shares the same operon with its oxidoreductase NorW. They are repressed by Fnr, and activated by NorR. Image is adapted from the Ecocyc database (www.ecocyc.org, Keseler *et al.*, 2009).

A microarray analysis showed that NsrR regulates directly or indirectly at least 30 genes, some of which are known to be involved in protection against RNS that can be generated by NO (Filenko *et al.,* 2007). NsrR recognises a target in the *nrf* promoter region. When nitric oxide is present, repressed expression of *nrf* is relieved so that it could reduce nitric oxide when required (Browning *et al.,* 2010). Other repressed genes of interest, particularly those that were suggested to be involved in nitrosative stress defense, will be illustrated below.

1.6. The di-iron protein YtfE

The gene *ytfE* was proposed to be a novel gene involved in anaerobic NO protection of *E. coli* according to a DNA microarray study (Justino *et al.,* 2005). Microarray analysis is a technique used for mapping the global gene expression profile of cells submitted to different conditions. The *E. coli* K-12 cells were first exposed to a deleterious concentration (50 μM) of NO under anaerobic conditions. Cells were collected after 15 minutes of exposure and total RNA was extracted to prepare cDNAs labeled with Cy3/Cy5 (florescent dyes) using reverse transcriptase and random primers. The cDNAs were then pooled and hybridized to the microarray chip containing known gene sequences in each spot. The chip was scanned to generate data for comparing the quantities of cDNA from the control and NO treated sample. The gene *ytfE* was found to have the highest NO transcriptional level of induction among all the genes and a severe growth impairment of a *ytfE* mutant under nitrosative stress was observed (Justino *et al*., 2005). Several studies by the same group followed on elucidating the function of YtfE in *E. coli* (Justino *et al*., 2006; Justino *et al*., 2007; Todorovic *et al*., 2008). First the phenotype study showed that the *ytfE* mutant LMS4209 grew slowly under several

anaerobic respiring conditions, such as when fumarate, DMSO, and gluconate were used as electron acceptors, even without nitrosative stress (Justino *et al*., 2006). The *ytfE* mutant LMS4209 was also sensitive to oxidative stress where hydrogen peroxide was supplemented, while plasmid encoded YtfE complemented this growth defect. Purified YtfE was shown to be able to restore the activities of aconitase B and fumarase A in a cell lysate treated with oxidative or nitrosative stress. It was proposed that YtfE protein was essential for the repair of stress-damaged Fe-S clusters (Justino *et al.*, 2007). The active centre of YtfE protein was characterised using spectroscopic techniques (Todorovic *et al*., 2008). A confocal Raman microscope was employed to show a μ-oxo-bridged di-iron centre. Spectra measured with an iron K-edge X-ray absorption spectroscopy suggested that both of the iron atoms were bound to three histidine residues each. The YtfE protein from *E. coli* belongs to a wide-spread di-nuclear iron protein family in both gram-positive and gram-negative bacteria. Because some other members also had similar functions in bacteria other than *E. coli*, it was proposed that they constitute a novel protein family RIC, for the repair of iron centres (Overton *et al.*, 2008). It was possible that YtfE functions as an enzyme for the recruitment and integration of the ferrous iron during the repair of the Fe-S centre (Justino *et al.*, 2006, Justino *et al.*, 2007). Further analysis of all genomes available showed that the *ric* gene was located near genes encoding proteins involved in oxidative and nitrosative stress (Justino *et al*., 2009). Due to the unexpected growth defect under several anaerobic respiration conditions, the *ytfE* mutant LMS4209 was later examined by a whole genome microarray (Vine *et al*., 2010). A secondary deletion of another 126 genes apart from the *ytfE* mutation was found in the LMS4209 mutant, spanning across a region containing genes essential for molybdopterin synthesis. As DMSO and nitrate

reductases are both molybdoproteins, this could explain why the mutant LMS4209 grew slowly anaerobically with DMSO or nitrate as terminal electron acceptors. The *hcp* gene was found to be among the list of the genes being deleted in LMS4209 (Vine, 2012).

1.7. Hybrid cluster protein (Hcp)

Hybrid cluster proteins (Hcp) are widely distributed in a variety of organisms from the Bacteria, Archaea and Eukarya kingdoms (Macedo *et al.,* 2003). According to a subcellular fractionation study, it is located in the cytoplasm of *D. vulgaris* (Hildenborough) (Pierik *et al.*, 1992). In the facultative anaerobe *E. coli*, the gene *hcp* was found to be on a two-gene operon with another gene *hcr* with 11 nucleotides in between. Hcr contained a [2Fe-2S] centre and FAD as cofactor. It was capable of reducing Hcp with an electron donor, such as NADH (van den Berg *et al*., 2000). Hcp has been studied extensively, due to its unique metal centre and unprecedented redox chemistry.

1.7.1. Structure of Hcp

Altogether 10 PDB files with structural models of Hcp have been deposited into the Protein Data Bank (PDB) so far, six of them were of the organism *Desulfovibrio vulgaris* and the other 4 were of *D. desulfuricans* (Table 1.2). Nine of the PDB files were released between 2000 and 2005, with only one released during 2005 and 2010. Hcp was first isolated from two strictly anaerobic sulfate-reducing bacteria: *D. vulgaris* (Hildenborough) (Hagen *et al.*, 1989, Pierik *et al.*, 1992) and *D. desulfuricans* ATCC 27774 (Moura *et al.*, 1992, van den Berg *et al.*, 1994). In *D. vulgaris* Hcp, there are eight Fe atoms in total, with Fe1 to Fe4 located in the cubane cluster and Fe5 to Fe8 in

Figure 1.6.

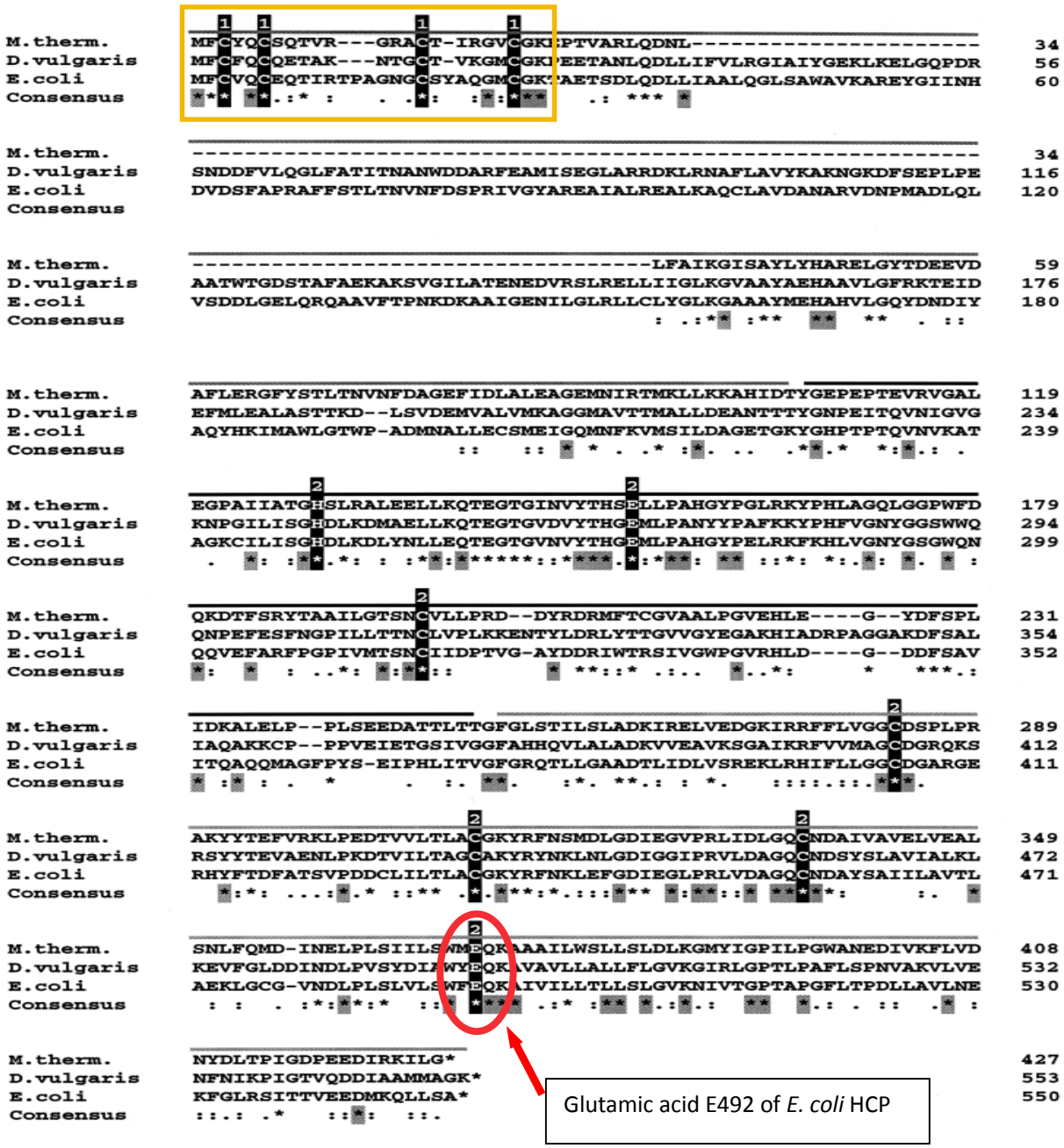

Sequence alignment of HCPs

Those four highlighted cysteine residues inside the orange box coordinate the conventional Fe-S centre at the N-terminus of HCP. The remaining 7 highlighted residues coordinate the hybrid cluster. They are four cysteines, two glutamic acids, and one histidine. Image adapted from van den Berg *et al* (2000).

Table 1.2. **PDB files deposited for structural information of Hcp protein**

PDB code	Species	Description	Resolution (Å)
1E1D	*D. vulgaris*	Structure obtained at room temperature	1.72
1E2U	*D. vulgaris*	Cryo-cooled, low temperature structure	1.60
1E9V	*D. vulgaris*	Xenon mapping of the hydrophobic cavity	1.79
1GN9	*D. desulfuricans*	Anaerobic conditions, low resolution	2.60
1GNL	*D. desulfuricans*	Anaerobic conditions	1.25
1GNT	*D. vulgaris*	Aerobic conditions	1.25
1OA0	*D. desulfuricans*	Anaerobic conditions, dithionite reduced	1.25
1OA1	*D. vulgaris*	Anaerobic conditions, dithionite reduced	1.55
1UPX	*D. desulfuricans*	Anaerobic conditions, proteins used were stored at 193 K for several months	1.25
1W9M	*D. Vulgaris*	Anaerobic conditions	1.35

Figure 1.7.

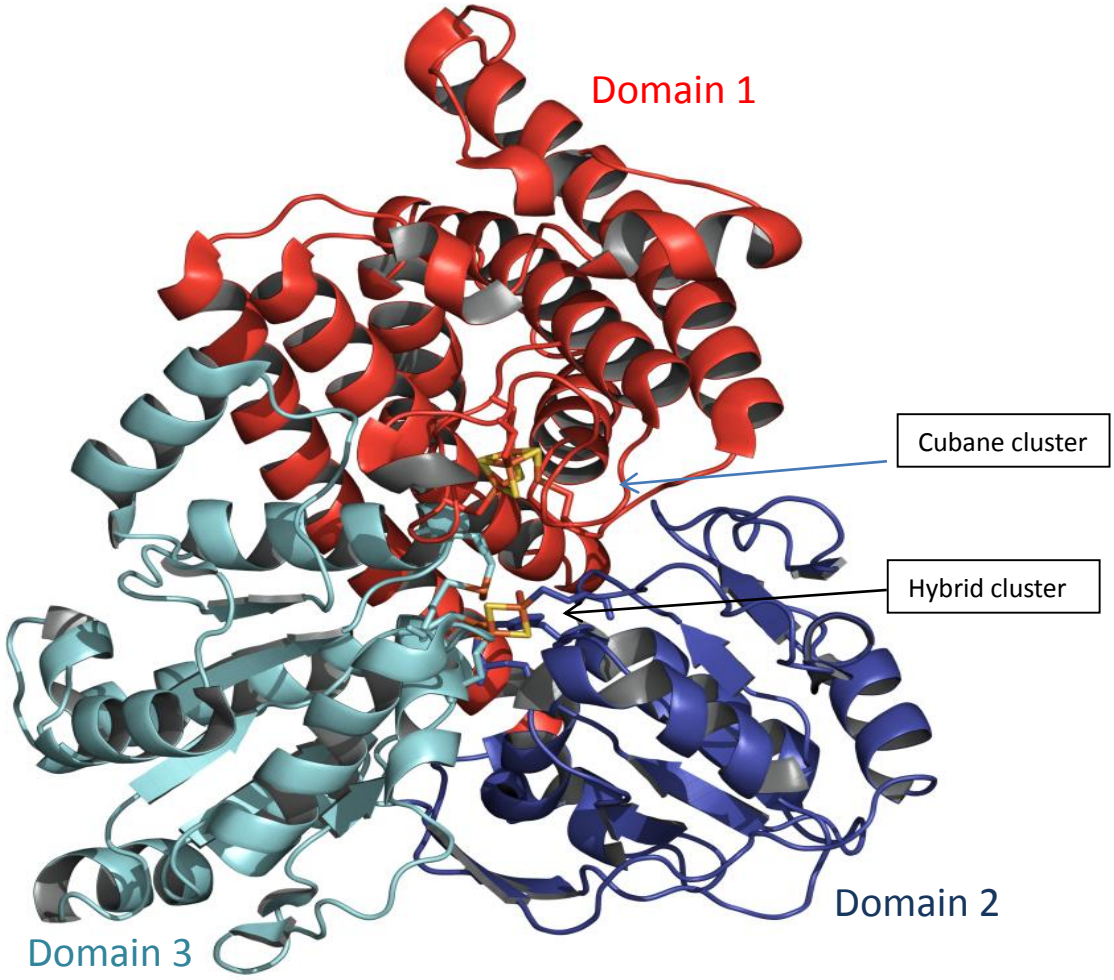

3D structure of hybrid cluster protein

Hybrid cluster protein consists of domain 1 (red), domain 2 (blue) and domain 3 (cyan). The hybrid Fe-S cluster lies at the interface of the three domains in the centre of the picture, whilst the cubane Fe-S cluster is bound near the N-terminus of domain 1. Image generated using the latest PDB file 1W9M and Pymol program. The detailed structure of each cluster will be presented in Fig 1.8.

the hybrid cluster. The Fe8 is directly coordinated by glutamic acid E494, which is one of the highly conserved residues in all Hcps (Fig 1.6, Cooper *et al.*, 2000). The corresponding glutamic acid residue number is 492 in *E. coli*. The Hcp of *D. vulgaris* consists of three domains: domain 1 with amino acid residues from 1-221, domain 2 from 222-375, and domain 3 from 376 to 553 (Fig 1.7). Hcp was formerly known as the prismane protein as it was proposed to contain a [6Fe-6S] cluster. However, an X-ray crystallography study at 1.7 Å resolution, using Hcp purified aerobically from *D. vulgaris*, showed that instead of one hexanuclear Fe cluster, Hcp contained two different Fe clusters (Arendsen *et al.*, 1998). One cluster is a regular cubane-type [4Fe-4S] cluster. The other cluster is the unique hybrid [4Fe-2S-2O] cluster — a hybrid between an iron-sulfur and an iron-oxo cluster, which is the main feature of Hcp.

The hybrid cluster has an unusual open structure, with tetrahedral arrangement between Fe5 and Fe6, and trigonal bipyramidal arrangement between Fe7 and Fe8 (Fig 1.8). Cooper *et al* (2000) deposited two PDB structure files: The structure with PDB ID number of 1E1D was obtained at room temperature, 1E2U from cryo-cooled crystal. To resolve the controversy as whether the hybrid structure was an artifact resulting from the aerobic isolation and crystallization, Hcp from *D. desulfuricans* prepared under strictly anaerobic conditions was compared with the one from *D. vulgaris* prepared aerobically, using X-ray synchrontron radiation techniques at a resolution of 1.25 Å (Macedo *et al.*, 2002; PDB ID: 1GNL and 1GNT). The hybrid clusters of anaerobically purified Hcp from *D. desulfuricans* and aerobically purified Hcp from *D. vulgaris* are shown in Fig 1.9. The overall structure of Hcp and the structure of the hybrid cluster appeared to be independent of whether Hcp was isolated aerobically or anaerobically:

A representation of the hybrid cluster structure of Hcp

Residues coordinating the four iron atoms in the hybrid cluster (4Fe-2S-3O) are shown in stick model. The circled O atom was previously designated as an unrecognized atom X by Arendsen *et al* (1998), and later modeled as an O atom since Cooper *et al* (2000). Hence sometimes the hybrid cluster is described as 4Fe-2S-2O. Sulfur 7 forms a persulfide with S_{γ} of Cys406, producing a thiocysteine moiety. Blue residues are from domain 2, and cyan residues are from domain 3. Oxygen atoms are red, sulfur atoms are yellow, and iron atoms are brown. Image generated using the latest PDB file 1W9M and Pymol program. (A) Hybrid centre shown in the same orientation as shown in Figure 1.7. (B) The orthogonal view of panel A.

Figure 1.8.

(A) Front view

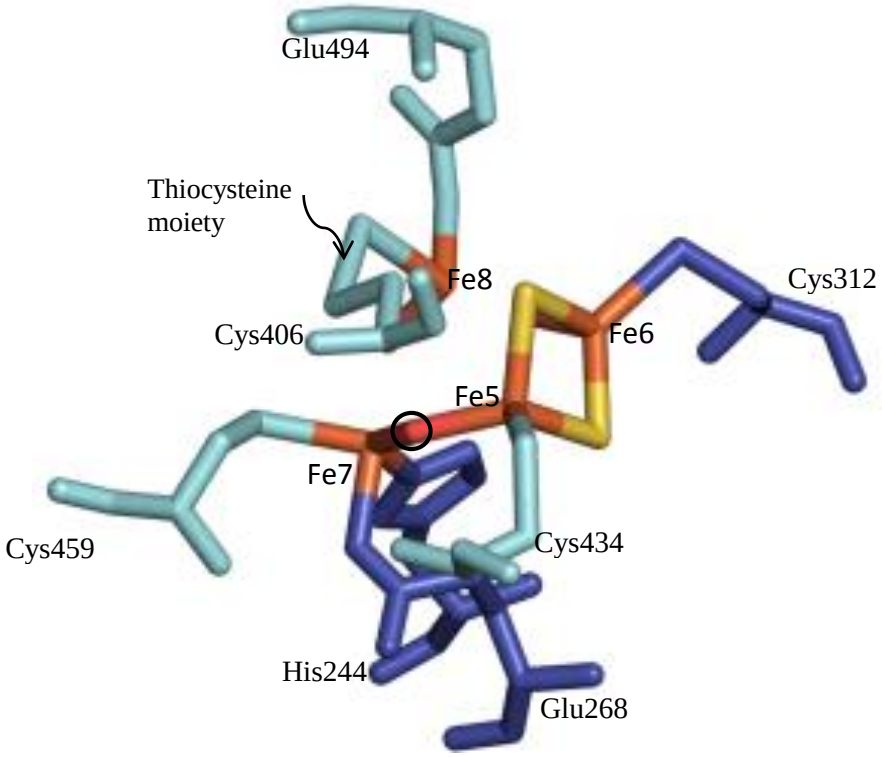

(B) Orthogonal view

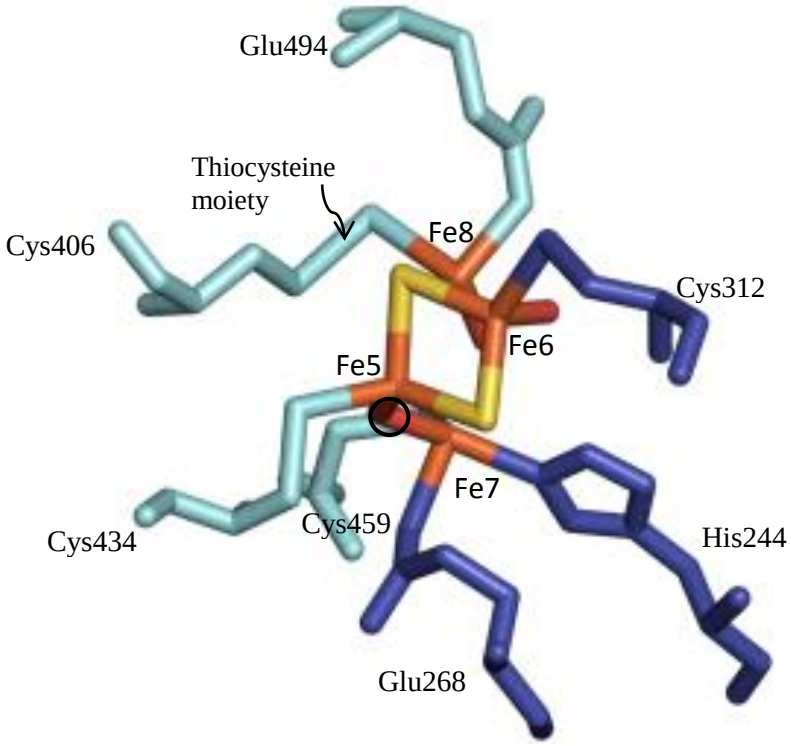

The structure of the hybrid cluster of Hcp prepared anaerobically, aerobically, and reduced with dithionite

Hcps from strict anaerobes *D. desulfuricans* and *D. vulgaris* have been isolated for X-ray crystallography study previously. The ball-and-stick model is used to present the structure data on the hybrid cluster of Hcp prepared anaerobically, aerobically, and reduced with dithione. As Hcp protein is expressed under anaerobic conditions, therefore, the anaerobically-prepared, 'as-isolated' Hcp protein structure should be of physiological relevance.

All three structures were arranged in the same orientation. Yellow spheres represents S atoms, black Fe, gray C, and red O atoms. Image was generated using Pymol program and the PDB files listed below.

A, the 'as-isolated' Hcp from *D. desulfuricans* purified anaerobically with PDB code 1GNL; B, Hcp from *D. vulgaris* purified aerobically with PDB code 1GNT; C, the dithionite-reduced Hcp from *D. desulfuricans* purrified anaerobically, with PDB code 1OA0.

Figure 1.9.

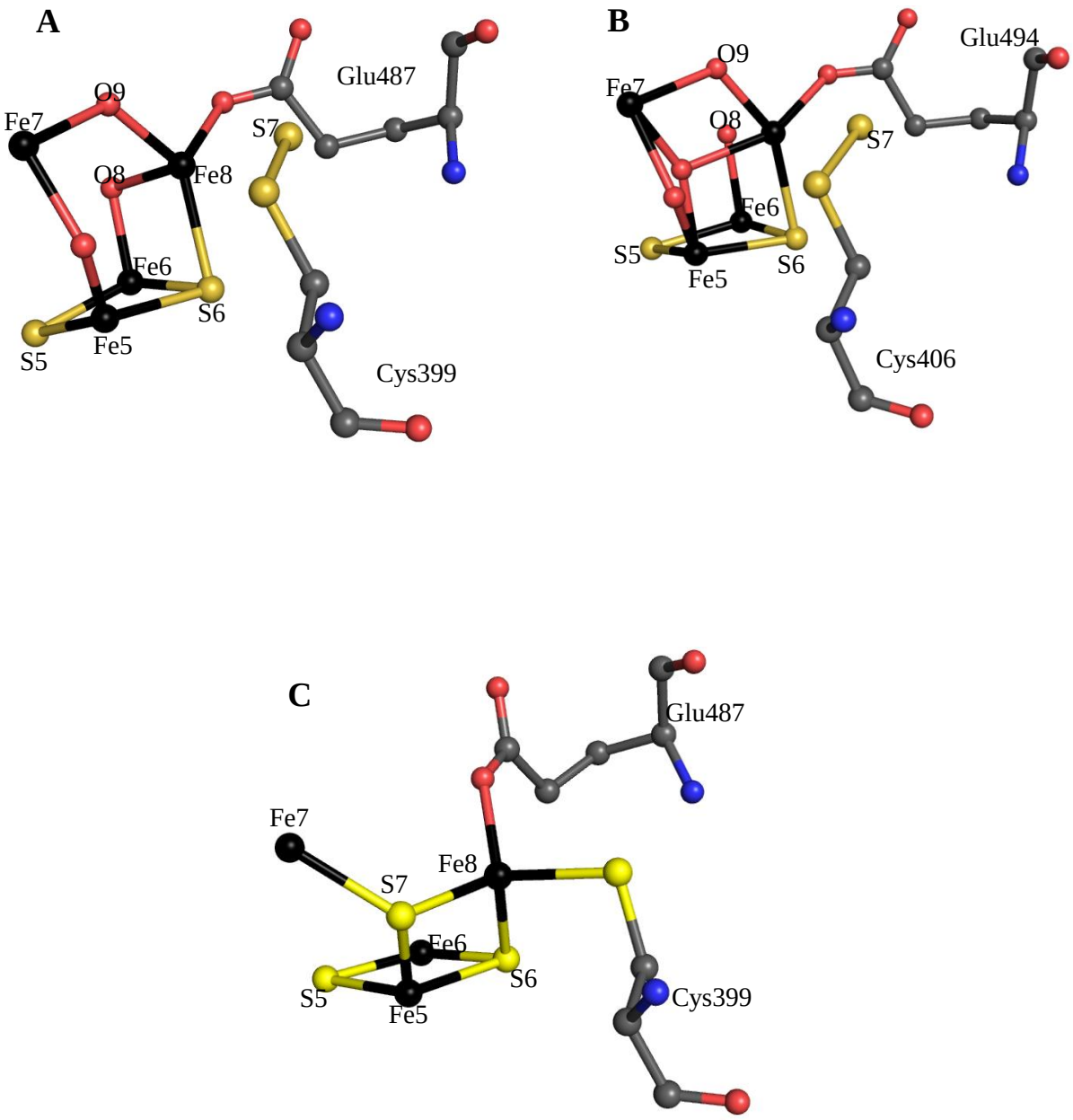
A
Glu487
O9
Fe7
S7
O8
Fe8
Fe6
S6
S5
Fe5
Cys399
B
Glu494
O9
Fe7
O8
S7
Fe6
S5
S6
Fe5
Cys406
C
Glu487
Fe7
Fe8
S7
Fe6
S6
S5
Fe5
Cys399

both structures comprise three domains and two Fe-S centres, and both oxygen and sulfur bridges were present in the hybrid cluster centres (Macedo *et al.*, 2002). It was further inferred by Aragão *et al* (2008; PDB code 1W9M) that although the overall structure of Hcp was essentially the same, the hybrid cluster was possibly in different oxidation state in the presence or absence of oxygen (Fig 1.9 A vs. B). When anaerobically prepared Hcp was further reduced with dithionite, large structural changes in the hybrid cluster were observed (Aragão *et al.,* 2003; 1OA0; Fig 1.9 C). The reduced hybrid cluster lacked the μ-bridging oxygen atoms O8 and O9 between Fe6 and Fe8 and between Fe7 and Fe8, respectively, present in the cluster before reduction.

The amino acids 139 to 553 of Hcp are 23% identical to the amino acids 150 to 637 of the homodimeric nickel-containing carbon monoxide dehydrogenase (CODH II) from the organism *Carboxydothermus hydrogenoformans* (Dobbek *et al*., 2001). CODH II is homodimeric, each containing three clusters (C, B and D). The cluster C [Ni-4Fe-4S] is coordinated by residues highly similar to thse of the hybrid cluster in Hcp, in terms of positions in the primary sequence and types of amino acids. Based on this interesting observation and previous functional studies on mutated CODH II, the ability of Hcp to reduce hydroxylamine reductase was discovered by Wolfe *et al* (2002). This will be discussed in more detail later in this thesis.

1.7.2. Regulation of Hcp

The transcription of the *hcp* gene seems to be under the control of multiple transcrptional regulators that are involved in anaerobiosis and reactive nitrogen species (RNS) response: Fnr, OxyR, NarL, and NsrR (Fig 1.10). The *E. coli* Hcp was previously

Figure 1.10.

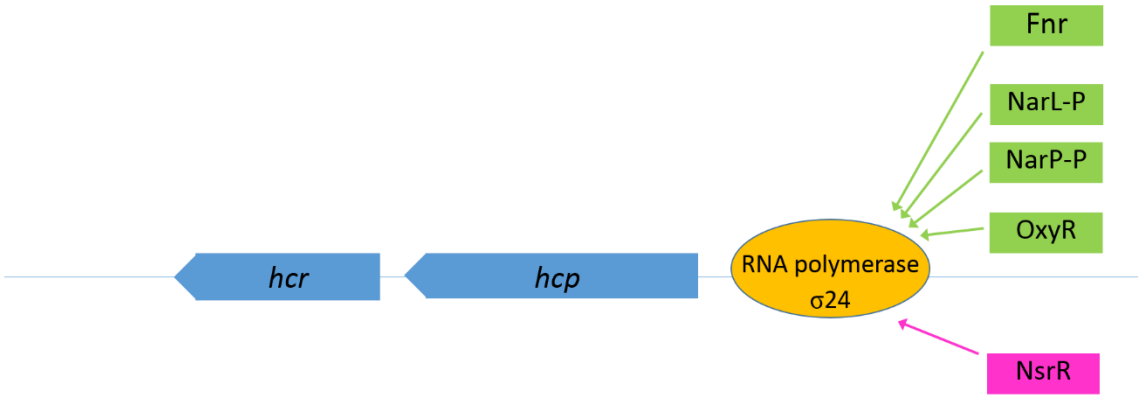

The two gene operon of *hcp-hcr* in *E. coli*

The gene hcr was found in the same operon downstream of hcp gene in *E. coli*. The hcp promoter is repressed by NsrR, activated by Fnr, phosphorylated NarL (NarP), and OxyR. Image is adapted from the Ecocyc database (www.ecocyc.org, Keseler *et al.*, 2009).

shown to be regulated by Fnr and by the nitrate/nitrite regulators NarL and NarP, using an *hcp::lacZ* fusion reporter plasmid (Filenko *et al.*, 2005). Gel retardation confirmed the binding of both FNR and NarL to the *hcp* promoter (Filenko *et al.*, 2007). Fnr was shown to be critical for the induction of *hcp* by several studies. It was shown that *hcp::lacZ* fusion could be induced by anaerobiosis alone without nitrite/nitrate, when Fnr was active, while the addition of nitrate/nitrite led to maximal activity (Chismon, 2011). In *Porphyromonas gingivalis*, *hcp* was found to be regulated by an Fnr-like regulator designated as HcpR. The induction of *hcp* by nitrite or GSNO was abolished in the HcpR mutant compared with the parental strain (Lewis *et al.*, 2012).

A microarray study of the *nsrR* regulon showed that *hcp* transcrption was repressed by NsrR by 15-fold (Filenko *et al.*, 2007). In *E. coli*, the redox-sensitive transcriptional regulator, OxyR, was reported to regulate the induction of *hcp* gene expression under oxidative stress, during exposure to hydrogen peroxide (Almeida *et al.*, 2006). However, it was reported by Seth *et al* (2012) that the treatment with hydrogen peroxide did not induce the transcription of *hcp* under either aerobic or anaerobic conditions. The electrophoretic mobility shift assay indicated that *hcp* responded to OxyR activated by nitrosylation rather than oxidation (Seth *et al.*, 2012).

1.7.3. Putative function of Hcp

At present, Hcp is annotated as a hydroxylamine reductase in online data bases such as Ecocyc and Uniprot. Catalyzing the reversible oxidation of CO to CO_2, CODH II has an active centre that is highly similar to the hybrid cluster of Hcp. Interestingly, both engineered Fe-CODH with Fe replacing the Ni in cluster C and mutant H265V CODH

with residue substitution had hydroxylamine reductase activity (Heo *et al.*, 2002). This led to the investigation of a similar hydroxylamine reductase activity for Hcp. Wolfe *et al* (2002) showed that purified Hcp can reduce hydroxylamine to ammonia, although the Km for hydroxylamine was not physiologically relevant (~25 mM at pH 7 versus ~5 mM at pH 9). *E. coli* could not grow in anaerobic culture supplemented with 1 mM hydroxylamine, while 0.5 mM hydroxylamine severally inhibited growth (Filenko, 2005). The implausibility of hydroxylamine being a natural substrate for Hcp was further evidenced by the lack of significant growth differences between an *hcp* mutant and the parent strain in media supplemented with hydroxylamine. No induction of *hcp* transcription by hydroxylamine was observed when the *hcp* promoter activity was assayed (Filenko *et al.*, 2007). In spite of the abundant structural information (with 10 PDB files deposited), the physiological functions of Hcp remain poorly understood.

1.8. Iron-sulphur proteins

Iron-sulphur proteins are prevalent in existence, characterised in containing iron-sulphur clusters. In *E. coli*, there are more than 110 proteins requiring iron-sulphur clusters to function (Py and Barras, 2010). They are introduced here because most of the proteins involved in this study are iron-sulphur proteins, including the previously described transcriptional regulators FNR and NsrR, the Hcp with debated functions, and the catalytic enzyme aconitase, which will be detailed further.

1.8.1 Structure and functions of Fe-S proteins

The Fe-S clusters are consisted of non-haem Fe and inorganic S atoms, and are coordinated to proteins by Cys residues, although alternative residues (His, Asp, Arg,

Ser, Glu) are known (Johnson *et al*., 2005; Ayala-Castro *et al*., 2008). A variety of structures of the Fe-S clusters can be formed, with the most common types being the rhombic [2Fe-2S] and cubic [4Fe-4S] cores (Roche *et al.*, 2013). In the presence of $Fe^{2+/3+}$ and S^{2-}, Fe-S clusters can be assembled spontaneously into apo-proteins *in vitro* (Malkin and Rabinowitz, 1966). However, the *in vivo* maturation process is far more complex, carefully coordinated by several synthetic pathways. At present, three pathways, namely Nif, Suf, and Isc systems, have been identified across the three kingdoms of life, with Suf and Isc being the more generalized systems existing in all prokaryotes and eukaryotes (Lill, 2011).

Due to the propensity of Fe to switch between its +2 and +3 oxidative states, the primary function of the Fe-S proteins lies in mediating biological electron transport. Common electron acceptors and donors are ferredoxins and hydrogenases. The redox potentials of the Fe-S clusters range from -500 mV to +300 mV (Table 1; Meyer, 2008).

Other functions for Fe-S proteins have also emerged in regulation and non-redox catalysis. The regulatory sensor role is connected with the labile nature of Fe-S cluster under environmental stress, such as in the presence of nitric oxide, oxygen or superoxide, or Fe deprivation (Beinert *et al.*, 1997; Kiley and Beinert, 2003). Usually it is the status of the Fe-S core that determines the activity as a regulator. As explained earlier, the oxygen sensor FNR is only active when it contains a $[4Fe\text{-}4S]^{2+}$ cluster and forms a functional dimer. In the presence of oxygen, the $[4Fe\text{-}4S]^{2+}$ centre is converted into the $[2Fe\text{-}2S]^{2+}$ cluster, causing the disassembly of the dimer and the loss of activity in FNR (Khoroshilova *et al*., 1997). In the presence of superoxide, SoxR becomes

active when the reduced form of the $[2Fe\text{-}2S]^{+}$ is oxided to the $[2Fe\text{-}2S]^{2+}$ (Ding and Demple, 1997). Nitrosylation of the Fe-S cluster in NsrR inactivates its activity to bind to the promoters and further regulate the genes involved in protection against nitrosative stress (Tucker 2008). The iron regulatory protein (IRP-1) controls the intracellular iron level at the post-transcriptional level (Rouault *et al.*, 1992). Interestingly, it was later recognized as the apo-aconitase that had lost its 4Fe-4S core at low iron concentration (Hentze and Kuhn, 1996).

1.8.2. Aconitase as a catalytic enzyme and its sensitivity to O_2 and NO

Aconitase, also known as the aconitate hydratase, is an enzyme of the citric acid cycle that catalyzes the reversible isomerization of citrate to isocitrate *via* aconitate. Two genetically distinct aconitases, AcnA and AcnB, are present in *E. coli* (Cunningham *et al.*, 1997). Phenotype and regulatory studies showed that AcnB was the major citric acid cycle enzyme, while AcnA was expressed in stationary phase and serves an auxiliary role during nutritional or oxidative stress (Gruer and Guest, 1994; Gruer *et al.*, 1997). AcnB is more sensitive to oxidation *in vivo* when compared with AcnA (Brock *et al.*, 2002, Varghese *et al.*, 2003). AcnB has a different architecture from other aconitases by containing a HEAT-like domain which is usually involved in protein-protein interaction (Williams *et al.*, 2002).

The active centre of aconitase is a [4Fe-4S] cluster. The labile Fe, unlike the other three Fe ions, is not coordinated by the cysteine residue, but instead by water molecules. This iron is prone to be released by ambient O_2, which results in the inactive form of [3Fe-4S] and the loss of aconitase activity (Gardner *et al*., 1991). This accounts for most

of the loss of activity under oxidative stress. Also, aconitases are important cellular targets of NO toxicity, although the detailed mechanism of the inactivation by NO is unclear. It was proposed by Gardner *et al* (1997) that an S-nitrosation of the active centre caused the loss of activity. Purified aconitase can be reactivated *in vitro* by the addition of Fe^{2+} and cysteine (Morrison, 1954). Furthermore, both of the O_2 and NO damaged aconitase can be reactivated *in vitro* simply by reducing ambient O_2 levels, although a much less level of reactivation was observed with the latter (Gardner *et al.*, 1991; Gardner *et al.*, 1993; Gardner *et al.*, 1997).

1.9. Aims of this work

The central theme of this thesis is to study the nitrosative stress response of the bacterium *E. coli* during anaerobic nitrate or nitrite respiration. The main specific goal was to decipher the role of the hybrid cluster protein (Hcp) under nitrosative stress. The involvement of Hcp with nitrosative stress response in *E. coli* has been a widely accepted notion, especially after the characterization of the *hcp* promoter. It is not only activated by NarL and NarP, but also repressed by NsrR (Filenko, 2005). As a result, the *hcp* gene is massively expressed in the presence of nitrate/nitrite or NO.

Four hypotheses concerning the possible function of Hcp have been investigated. The first hypothesis is that Hcp reactivates aconitase by repairing its nitrosylated [4Fe-4S] core under nitrosative stress. The second hypothesis is that Hcp interacts with aconitase to protect the labile [4Fe-4S] core from NO exposure. In the other two hypotheses a direct detoxification of NO by Hcp are postulated. One hypothesis is that Hcp acts as a buffer protein by binding NO chemically in order to reduce intracellular NO

concentration. The other hypothesis is that Hcp biochemically reacts with NO and serves as an NO reductase.

To examine the aforementioned hypotheses and to answer more detailed questions raised on the results obtained in this thesis, the objectives were as follows. First the phenotype of an *hcp* mutation in a genetic background that lacked all other known NO detoxifying enzymes was studied. A second aim was to determine whether the hybrid cluster is essential for the function and structure of Hcp. Then the effect of loss of Hcp on the activity of aconitase under conditions of nitrosative stress was be determined. As an independent approach to explore the function of Hcp, the bacterial two-hybrid system was used to identify protein interaction partners of Hcp. A critical question was whether Hcr and Hcp form an electron transfer chain for NO reduction by NADH? This required the construction and analysis of an *hcr* mutant. Finally if evidence was obtained that Hcp is able to reduce NO, the product of NO reduction would be determined.

CHAPTER 2

MATERIALS AND METHODS

2.1. Materials

2.1.1. Microorganisms, plasmids and primers

The bacterial strains, plasmids, and primers used in this study are listed in Table 2.1, 2.2 and 2.3 respectively. The plasmids and primers for the bacterial two-hybrid system are listed in section 2.3.8 of this chapter separately.

2.1.2. Media

Unless otherwise stated, the chemicals used in this work were purchased from Sigma and Difco. Lennox broth (LB) contains 20 gL^{-1} tryptone, 10 gL^{-1} yeast extract and 10 gL^{-1} NaCl. Aerobic cultures of bacteria were cultivated in LB broth unless otherwise specified. Minimal salts medium (MS) contains 4.5 gL^{-1} KH_2PO_4, 10.5 gL^{-1} K_2HPO_4, 1 gL^{-1} NH_4SO_4, 0.05 gL^{-1} $MgCl_2$, 1 µM ammonium molybdate, 1 µM sodium selenate and *E. coli* sulphur free salts (1 mL per L). The composition of *E. coli* sulphur free salts is 82 gL^{-1} $MgCl_2.7H_2O$, 10 gL^{-1} $MnCl_2.4H_2O$, 4 gL^{-1} $FeCl_2.6H_2O$, 1 gL^{-1} $CaCl_2.6H_2O$ and concentrated HCl (20 mL per L). Anaerobic cultures of bacteria were cultivated using MS medium unless otherwise specified. SOC medium contains 20 gL^{-1} tryptone, 5 gL^{-1} yeast extract, 0.58 gL^{-1} NaCl, 0.185 gL^{-1} KCl, 2.03 gL^{-1} $MgCl_2.6H_2O$, 2.46 gL^{-1} $MgSO_4.7H_2O$ and 3.6 gL^{-1} glucose, which was used during transformation procedure. Nutrient agar (NA) consists of 28 gL^{-1} NA powder. Lennox agar (LA) consists of LB medium supplemented with 1.25% (w/v) bacteriological agar. MacConkey medium with maltose contains 40 gL^{-1} MacConkey base agar (Difco Laboratories) with 1% (w/v) glucose-free maltose, which is filter-sterilized and added separately. Medium was autoclaved at 121℃ for 15 min.

Table 2.1. **Strains used in this study**

Official name	Description of genotypes	Reference
RK 4353	*ΔlacU169 araD139 rpsL gyrA*	Stewart and McGregor, 1982
JCB5210	RK 4353 *ΔnirBDC ΔnrfAB ΔnorV Δhmp::km*	Vine, PhD Thesis, 2011
JCB5257	RK 4353 Δ*nirBDC ΔnrfAB ΔnorV Δhmp::km ΔytfE::cat*	Vine, PhD Thesis, 2011
JCB5250	RK 4353 Δ*nirBDC ΔnrfAB ΔnorV Δhmp::km Δhcp::cat*	Vine, PhD Thesis, 2011
JCB5260	RK 4353 Δ*nirBDC ΔnrfAB ΔnorV Δhmp Δhcp ΔytfE::cat*	Vine, PhD Thesis, 2011
BTH101	*F- cya-99 araD139 galE15 galK16 rpsL1 (Strr) hsdR2 mcrA1 mcrB1*	D. Ladant, Institut Pasteur, Paris
JCB701	MG1655 *acnB::6* x *his*	This work
JCB5290	RK 4353 Δ*nirBDC ΔnrfAB ΔnorV Δhmp Δhcr::km*	This work
BW25113	*F^-, DE(araD-araB)567, lacZ4787(del)::rrnB-3, LAM^-, rph-1, DE(rhaD-rhaB)568, hsdR514*	Datsenko and Wanner, 2000
JW5117	BW25113 *Δhcr-773::km*	Baba *et al.*, 2006

Table 2.2. **Plasmids used in this study**

Plasmids constructed in the bacterial two hybrid system are listed in the individual section.

Plasmid name	**Description and application**	**Reference**
pCP20	Expresses the Flp recombinase gene (*exo*). Cm^R and Amp^R	Datsenko and Wanner, 2000
pACYC184	Low copy number plasmid, 10-15 copies/cell (Fig 2.1). Cm^R and Tet^R	ATCC 37033
pJW11	Derivative of plasmid pACYC184. Encodes Hcp protein under the control of the *hcp* promotor. Cm^R	This work
pJW111	Derivative of plasmid pJW11. Residue No. 492 of Hcp was mutated from glutamic acid to aspartic acid. Cm^R	This work
pJW112	Derivative of plasmid pJW11. Residue No. 492 of Hcp was mutated from glutamic acid to alanine. Cm^R	This work
pJW113	Derivative of plasmid pJW11. Residue No. 492 of Hcp was mutated from glutamic acid to valine. Cm^R	This work
pJW114	Derivative of plasmid pJW11. Residue No. 492 of Hcp was mutated from glutamic acid to glycine. Cm^R	This work
pJW12	Derivative of plasmid pACYC184. Encodes Hcp protein under the control of the *hcp* promotor CmR	This work
pET28a	Protein expression vector (Fig 2.2). Km^R	Novagen
pET-HCP	Derivative of plasmid pET28a. Encodes Hcp protein with an N-terminus His-tag under the control of T7 promoter. Km^R	Almedia *et al.*, 2006

pET-HCP E492D	Derivative of plasmid pET-HCP. Residue No. 492 of Hcp was mutated from glutamic acid to aspartic acid. Km^R	This work
pET-HCP E492A	Derivative of plasmid pET-HCP. Residue No. 492 of Hcp was mutated from glutamic acid to alanine. Km^R	This work
pET-HCP E492V	Derivative of plasmid pET-HCP. Residue No. 492 of Hcp was mutated from glutamic acid to valine. Km^R	This work
pET-HCP E492G	Derivative of plasmid pET-HCP. Residue No. 492 of Hcp was mutated from glutamic acid to glycine. Km^R	This work
pUT-E492D	Derivative of plasmid pUT18C-Hcp. Residue No. 492 of Hcp was mutated from glutamic acid to aspartic acid. Km^R	This work
pUT-E492A	Derivative of plasmid pUT18C-Hcp. Residue No. 492 of Hcp was mutated from glutamic acid to alanine. Km^R	This work
pUT-E492V	Derivative of plasmid pUT18C-Hcp. Residue No. 492 of Hcp was mutated from glutamic acid to valine. Km^R	This work
pUT-E492G	Derivative of plasmid pUT18C-Hcp. Residue No. 492 of Hcp was mutated from glutamic acid to glycine. Km^R	This work
pJW21	Derivative of plasmid pET28a. Encodes Hcr protein with an N-terminus His-tag under the control of T7 promoter. Km^R	This work
pJW22	Derivative of plasmid pET28a. Encodes Hcp with an N-terminus His-tag and Hcr protein without any tag, under the control of T7 promoter. Km^R	This work

Table 2.3. **primers used in this study**

Primers used in the bacterial two hybrid system are listed in the individual section.

Primer name	**Sequence (5'-3')**	**Description and application**
AcnB fwd checking	ATCCTGTGTGCTCCGAACGACCCGGATGAC	Homologous to the regions flanking the modified fragment on *E. coli* chromosome. Used for checking the recombinants of JCB701.
AcnB rev checking	ACAGGCTTTCTTCGTCGTAGTAGTTCATCC	
T7 promoter	TAATACGACTCACTATAGGG	Anneals to the T7 promoter and terminor region of the pET plasmids. Used for checking cloned gene sequence.
T7 terminator	GCTAGTTATTGCTCAGCGG	
Hcp fwd 1	CGCCAACCCAGGTCAACG	Forward primer that anneals within the *hcp* gene and used to check site-directed mutagenesis mutants
Hcp rev 2	CCACTTGCTGATTCTGCCAGC	Reverse primer that anneals within the *hcp* gene.
HCP SEQ 1	CTCCGGCAGGAAACGGCTG	Forward primers that anneals to the sequence within the *hcp* gene.
HCP SEQ 2	ATCGTCATTCTGCTGACGC	
Hcr genome rev checking	CCAGATGCGTTTCACCCC	Homologous to the downstream sequence of the *hcr* gene on *E. coli* chromosome.
Complementation		
Hcp184fwd HindIII	ATATAAAGCTTCCGGTATTTTATTGACCG	Cloning of the *hcp* or *hcp-hcr* genes with the *hcp* promoter in vector pACYC184 for complementation of *hcp* mutation

Hcr184rev BamHI	ATATAGGATCCTTATGCGAGAACCAAATCCCC	Use with the forward primer for the construction of pJW11
Site-directed mutagenesis		**Description**
hcpE492X fwd	GCTGGTGCTCTCCTGGTTTGNCCAGAAAGCGATCGTCATTCTGC	Primers used in site-directed mutagenesis reaction. Designed to change the codon of Hcp E492 from GAA to GNC
hcpE492X rev	GCAGAATGACGATCGCTTTCTGGNCAAACCAGGAGAGCACCAGC	
Protein expression		
pet28a Hcp forward	ATATACCATATGATCATGTTTTGTGTGC	Cloning of the *hcp* or *hcp-hcr* genes in expression vector pET28a
pET28a Hcr forward	ATATACCATATGTCGATGACGATGC	Cloning of the *hcr* gene in expression vector pET28a
pET28a Hcr Reverse	TATATAAGCTTGAATTCTTATGCGAGAACCAAATCC	Use in conjunction with pET28a Hcp forward or pET28a Hcr forward primer to construct the plasmids pJW21 or pJW22

Figure 2.1.

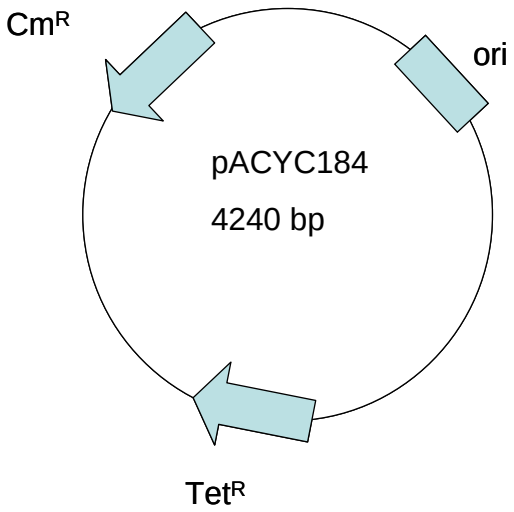

Plasmid map of vector pACYC184

Plasmid pACYC184 has a low copy number of 10-12 /cell. The replication system of p15A requires DNA polymerase I (Chang and Cohen, 1978). There are two antibiotic resistance markers: chloramphenicol (Cm^R) and tetracycline (Tet^R). Endonuclease cleavage sites are present in the two antibiotic resistance genes. Insertional inactivation of either Cm^R or Tet^R can be employed during cloning.

Figure 2.2.

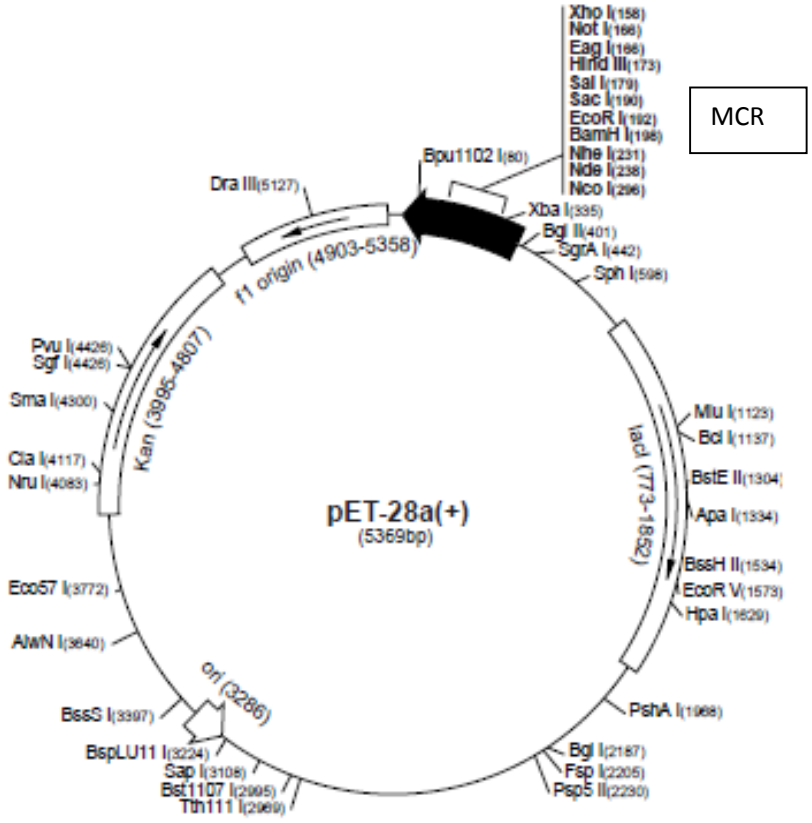

Plasmid map of vector pET28a

The pET expression system is the most commonly used bacterial system for the over-expression of genes of interest. pET-28a vector carrys an N-terminal 6xHis Tag and an optional C-terminal 6xHis Tag sequence for subsequent IMAC-based purification. Unique endonuclease cleavage sites are shown on the circle map. The gene is cloned within the multiple cloning region (MCR), and then expressed under the control of a bacteriophage T7 promoter. *E. coli* BL21(DE3), which contains the gene for T7 RNA polymerase under control of the *E. coli lacZ* promoter, was used as a host for this vector. Image is from Novagen.

2.1.3. Growth of strains

For aerobic cultivation, a flask of a volume 10 times of that of the culture was used to ensure sufficient aeration. A single colony of bacteria was inoculated from an agar plate into a flask containing sterile LB medium and aerated at 250 rpm, 37℃ overnight unless otherwise stated. For anaerobic cultivation, sealable containers with corresponding size filled with MS medium were used for anaerobic cultivation. Cultures were left statically either at 30 or 37℃ overnight unless otherwise stated.

2.1.4. Antibiotics

The working concentrations of ampicillin and kanamycin used in selective medium were 100 μg/mL and 50 μg/mL respectively. The stock solution (both of 100 mg/mL) was prepared by dissolving 1 g of sodium salt of ampicillin or kanamycin in 10 mL distilled water and filtering through a 0.2 μm sized filter membrane for sterilization. The stock solution was added at an appropriate volume ratio to the liquid medium, or sterilized NA medium cooled down to 45℃ for the preparation of antibiotic plates. The working concentration of chloramphenicol used for selective purpose was 50 μg/mL. The stock solution (50 mg/mL) was prepared in the same way as described above except that the solid chloramphenicol was dissolved in 100% (v/v) ethanol. All of the antibiotic stock solutions were kept in the freezer. Antibiotic plates were kept in cold room at 4℃ and used within two weeks.

2.1.5. Buffers and solutions

Buffers and solutions used in this work are listed in Table 2.4.

Table 2.4. **Buffers and solutions used in this work**

Name	Composition
General buffers.	
Tris-EDTA buffer (TE, pH 8.0).	10 mM Tris-HCl and 1 mM EDTA.
Phosphate buffer (50 mM, pH 7.5).	7.26 gL^{-1} K_2HPO_4 and 1.13 gL^{-1} KH_2PO_4.
Buffers for making competent *E. coli* cells.	
TFB 1.	100 mM RbCl, 50 mM $MnCl_2$, 30 mM potassium acetate, 10 mM $CaCl_2$ and 15% (v/v) glycerol.
Buffers for agarose gel electrophoresis.	
5xTBE.	0.445 M Tris-HCl, 0.445 M boric acid and 0.01 M EDTA (pH 8).
Sample buffer.	TE supplemented with 0.025% w/v bromophenol blue and 10% v/v glycerol.
Buffers and solutions for β-galactosidase assays.	
Z buffer.	0.75 gL^{-1} KCl, 0.25 gL^{-1} $MgSO_4.7H_2O$, 8.55 gL^{-1} Na_2HPO_4, 4.87 gL^{-1} $NaH_2PO_4.2H_2O$ and β-mercaptoethanol (2.7 mL per L).
ortho-nitrophenyl β–D-galactopyranoside (ONPG, 13 mM)	0.032g ONPG in 1 x A (10 mL).
Buffers and solutions for aconitase activity assays.	
Aconitase assay buffer.	50 mM Tris-HCl and 0.6 mM $MnCl_2$, pH7.4.
Buffers and solutions for Lowry protein assays.	
Folin A solution.	2% (w/v) Na_2CO_3 in 0.1 M NaOH.
Folin B solution.	Add 1 mL of 1% (w/v) CuSO4 and 1 mL of 2% (w/v) Sodium potassium tartrate to 100 mL of Folin A solution.

Buffers for His-tagged protein purification.	
Buffer A.	50 mM Tris-HCl, 250 mM NaCl, 5% (v/v) Glycerol, and 10 mM Imidazole, pH 7.0.
Buffer B.	50 mM Tris-HCl, 250 mM NaCl, 5% (v/v) Glycerol, and 500 mM Imidazole, pH 7.0.
Buffers for polyacrylamide gel electrophoresis.	
20% Sodium dodecyl sulphate (SDS)	20 g SDS in 100 mL distilled water.
Stock resolving gel buffer. 0.75 M Tris/HCl, pH 8.3.	90.86 gL^{-1} Tris hydroxymethyl methylamine, pH to 8.3.
Stock stacking gel buffer. 1.25 M Tris/HCl, pH 6.8.	151.46 gL^{-1} Tris hydroxymethyl methylamine, pH to 6.8.
Stock electrode buffer.	150 gL^{-1} glycine and 30 gL^{-1} Tris hydroxymethyl methylamine.
Working electrode buffer.	1:10 dilution of stock electrode buffer supplemented with 0.1% SDS.
0.2% Coomassie brilliant blue.	2 gL^{-1} Coomassie brilliant blue dissolved in 400 mL distilled water, 500 mL methanol and 100 mL glacial acetic acid.
Fast destain.	40% (v/v) methanol, 10% (v/v) acetic acid, 50% (v/v) distilled water.
Slow destain.	10% (v/v) methanol, 10% (v/v) acetic acid, 80% (v/v) distilled water.
Shrink solution.	45% (v/v) methanol, 5% (v/v) glycerol, 50% (v/v) distilled water.
Sample buffer	0.125 M Tris/HCl, pH 6.8 supplemented with 20 gL^{-1} SDS, 50 mgL^{-1} bromophenol blue and 20% (v/v) glycerol. Supplement each 1 mL with 87 µL β-mercaptoethanol immediately before use.
30% (w/v) acrylamide solution.	30% (w/v) acrylamide/methylene bisacrylamide solution (37.5:1 ratio). Purchased as 'Protogel', National Diagnostics.

2.2. DNA techniques

2.2.1. Purification of DNA

The size of DNA used in this work ranges from 100 bp to 10 kb from enzymic reactions and PCR, the protocol using a Bioline PCR purification kit was applied. Bioline PCR purification and gel extraction kit was used to purify DNA from PCR reactions, enzyme digestion and dephosphorylation reactions. Under high salt and appropriate pH, the silica-gel membrane in the spin-column absorbs the DNA while allowing DNA polymerase and endonuclease to pass through. The bound pure DNA could then be eluted from the membrane using low-salt solution solutions.

2.2.2. Restriction digestion of DNA fragments

The following components were added into one tube to set up a restriction digestion: 1 units of the restriction endonuclease, 2 µL of restriction digestion buffer (10x), 5 µL of plasmid DNA (150 ng/µL) and appropriate amount of water to the final volume of 20 µL. One unit of a restriction endonuclease is defined as the amount of the enzyme that cuts 1 µg of DNA in 1 hour. The tube containing the digestion reaction was incubated at the optimal temperature for the specific restriction endonuclease, and then purified using a Bioline PCR purification kit. Alternatively, the fragments could be separated by DNA gel electrophoresis and purified using a gel extraction kit.

2.2.3. Dephosphorylation of a vector DNA

The calf intestinal alkaline phosphatase (CIAP) cleaves terminal 5' phosphate groups from linear DNA molecules. After the DNA had been digested with appropriate restriction endonucleases, to prevent recircularisation of the vector plasmid in

subsequent ligation, the tube containing digestion reaction was treated with 5 units of CIAP at 37℃ for 1 hour.

2.2.4. Ligation reaction

In ligation reactions, vector and insert DNA fragments were ligated *via* the formation of phosphodiester bonds between 5' phosphate groups and 3' hydroxyl groups between DNA fragments. This reaction was catalyzed by the T4 DNA ligase. The vector DNA fragment was usually extracted from agarose gel after DNA gel electrophoresis. The insert was generated by a PCR reaction. After digestion reaction, it was then purified directly using Bioline PCR purification kit. To set up a 20 µL ligation reaction, 100 ng of the insert DNA fragment, 50 ng of dephosphorylated vector DNA, 2 µL of ligase buffer (10x), 1 unit of T4 DNA ligase and appropriate amount of water were added into a single tube. The reaction tube was incubated overnight at 25℃.

2.2.5. Preparation of competent cells

A single colony of bacteria from a fresh agar plate less than 3 weeks old was inoculated into 2 mL of LB containing an appropriate concentration of the relevant selective antibiotics, and the culture was aerated at 37ºC overnight. The buffers used were taken out from either coldroom or freezer and precooled on ice. The overnight culture (0.5 µL) was added to 50 mL of prewarmed LB medium supplemented with relevant antibiotics in a 500 mL conical flask, and the culture was aerated at 37ºC until an OD_{650} of 0.5 was reached. The flask was put on ice for 5 minutes to cool down the culture. The contents ware then transferred to a 50 mL sterile Corning centrifuge tube for centrifugation. In a precooled centrifuge with temperature set at 4ºC, cells were harvested at a low speed of

4800g for 5 min. The supernatant was discarded carefully and the bacteria was resuspended gently in 15 mL of ice-cold, sterile TFB1 buffer. The tube was kept on ice for an additional 90 minutes. The cells were collected again *via* centrifugation with the same settings as above mentioned. Supernatant was discarded and 2 mL of ice-cold, sterile buffer containing 0.1 M $CaCl_2$ and 15% (v/v) glycerol was used to resuspend the pellet. Resuspension was divided into aliquots of 50 µL in sterile 1.5 mL Eppendorf tubes and put into the -80ºC immediately afterwards.

2.2.6. Transformation with plasmid DNA

Plasmid DNA (5 to 50 ng) was added to the 1.5 mL micro centrifuge tube containing 50 µL of competent cells and they were mixed gently by pipetting up and down. After incubating on ice for 20 minutes, the tube was transferred to a 42ºC heating block for 1 minute. Immediately after this, 0.5 mL LB or SOC medium broth was added into the tube to resuspend the cells. To allow recovery of bacteria, the resuspension was transferred to a sterile test tube and aerated at 37ºC or 30ºC for one or two hours. 100 µL of the culture was plated onto a nutrient agar plate with supplemented relevant selective antibiotics. The plates were incubated at 37ºC or 30ºC overnight.

2.2.7. Gene doctoring

Gene doctoring is a homologous recombination technique for making chromosomal modifications in *Escherichia coli*, primarily for the coupling of genes to epitope tags (Lee *et al.*, 2009). It could also be used for deletion of genes. A λ-red recombinase system is used to facilitate the recombination of target DNA into the chromosome with three proteins, Gam, Exo and Bet: Gam protects linear double stranded DNA from

degradation; Exo generates single stranded DNA overhangs; Bet catalyses the recombination of the Exo generated product. In gene doctoring, two plasmids are used: the donor plasmid carries a linear double stranded homologous DNA target flanked by two I-SceI recognition sites, so that the target DNA fragment to be recombineered to the chromosome will be released *in vivo* once being cleaved by I-SceI meganuclease; the recombineering plasmid carries the λ-red and I-SceI endonuclease genes, under the control of an *araBAD* promoter.

In practice, these two plasmids, *acnB* pDOC-H (donor plasmid) and pACBSCE (recombineering plasmid) were co-transformed into the recipient *E. col*i competent cells of MG1655. The co-transformants were selected using LB agar plates containing 35 μg/mL chloramphenicol (for pACBSCE), 100 μg/mL ampicillin and 50 μg/mL kanamycin (both for *acnB* pDOC-H). As a functional *sacB* gene on the donor plasmid would render the host bacteria unable to grow on medium supplemented with 5% (w/v) sucrose, sucrose sensitive colonies were screened *via* patching the cotransformants from plates without sucrose to plates with the addition of sucrose. A single fresh sucrose sensitive cotransformant was selected and inoculated to LB liquid medium containing the above mentioned three antibiotics and 0.5% (w/v) glucose. Cultures were aerated at 37℃ for 2 hours. Cells were harvested *via* centrifugation and resuspended using 1 mL LB with the addition of 0.5% (w/v) L-arabinose. The resuspension was aerated at 37℃ until turbid. Dilutions of culture (120 μL) were plated on to LB agar plates containing 5% (w/v) sucrose and 50 μg/mL kanamycin and incubated at 30℃overnight. The addition of sucrose was for counter-selecting the colonies still harboring the donor plasmid with functional *sacB* gene.

Colonies were then patched on to LB plates with 100 µL ampicillin and LB plates with 35 µL chloramphenicol. Only colonies sensitive to both ampicillin and chloramphenicol were selected and marked as recombinant candidates. For schematic diagram of the gene doctoring recombineering protocol see Fig 2.3. Recombination was further checked by PCR and sequencing, using checking primers annealing to the chromosomal DNA flanking the modified region.

2.2.8. Site-directed mutagenesis

Site-specific mutations was made in double-stranded plasmids using QuikChange site-directed mutagenesis kit (Stratagene). The DNA template was modified by point mutations, resulting in amino acid substitution, insertion or deletion. A double stranded plasmid was used with two complementary synthetic oligonucleotide primers that anneal to opposite strands of the vector (Table 2.2 & 2.3). The two primers contained mutations at a target site GAA of the *hcp* gene. The bases coding for this region were replaced by GNC representing a random selection of bases at N. The primers used were of a high purity grade for increased mutation efficiency. Usually they were purified either by fast performance liquid chromatography (FPLC) or by polyacrylamide gel electrophoresis (PAGE).

The procedure was depicted in Fig 2.4. A high-fidelity, proof-reading Pfu Turbo DNA polymerase was added along with the plasmid and primers for temperature cyclings, during which primers were extended from 5' to 3' around the melted single-stranded plasmid DNA. The incorporation of the oligonucleotide primers generated a mutated

Figure 2.3.

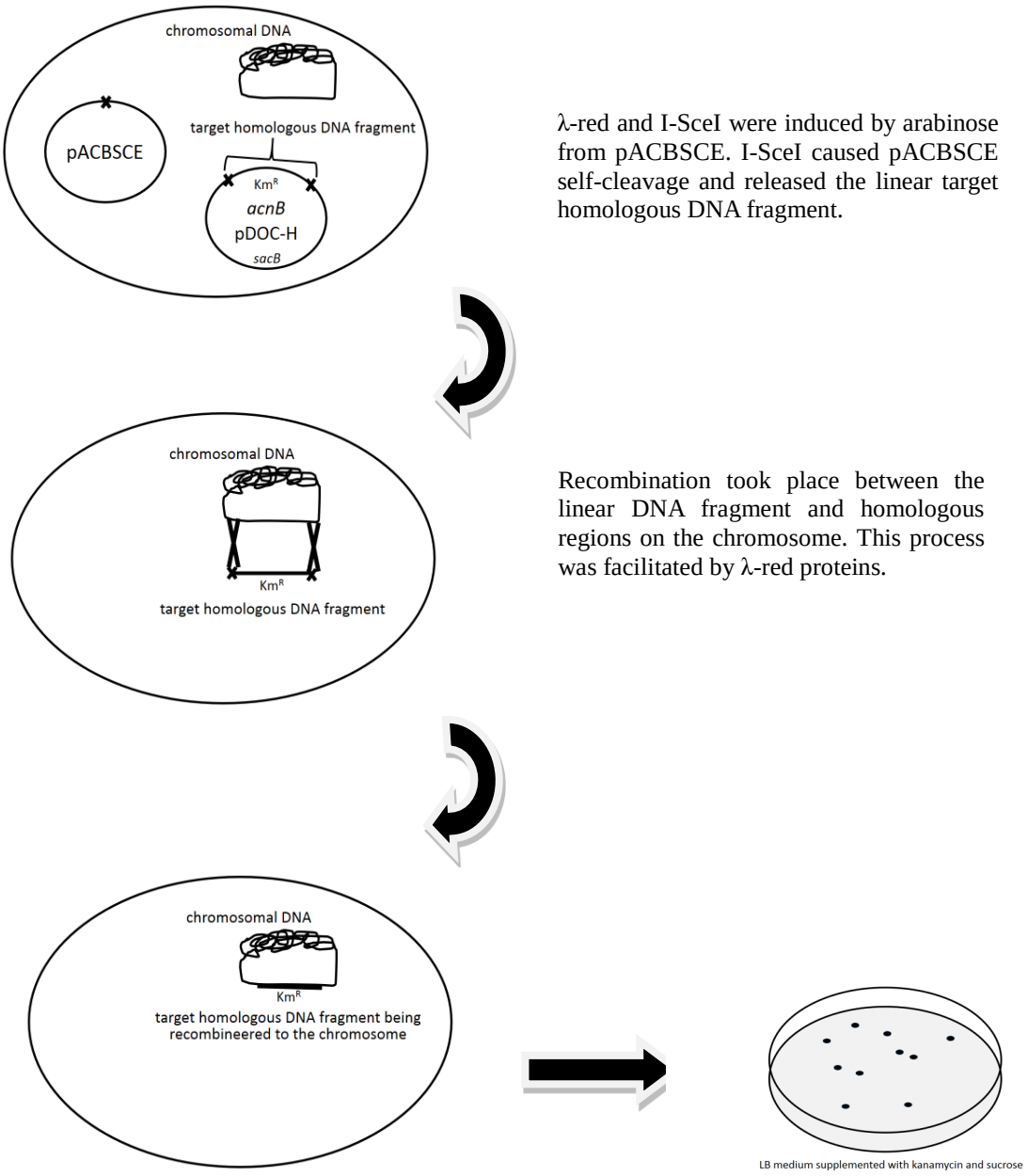

Schematic diagram of gene doctoring recombineering

The donor plasmid *acnB* pDOC-H and recombineering plasmid pACBSCE were co-transfromed into the cell. The expression of λ-red proteins and I-SceI were promoted from plasmid pACBSCE by arabinose induction on the *araBAD* promoter. A linear DNA fragment was excised from donor plasmid by I-SceI and recombineered to the chromosome. Recombinants were screened with sucrose and kanamycin.

Diagram of site-directed mutagenesis

Parent plasmid was extracted and used as template in mutagenesis reactions. Synthetic oligonucleotides primers (orange lines) containing desired mutations anneal to the target site on the template (blue stars).

Figure 2.4.

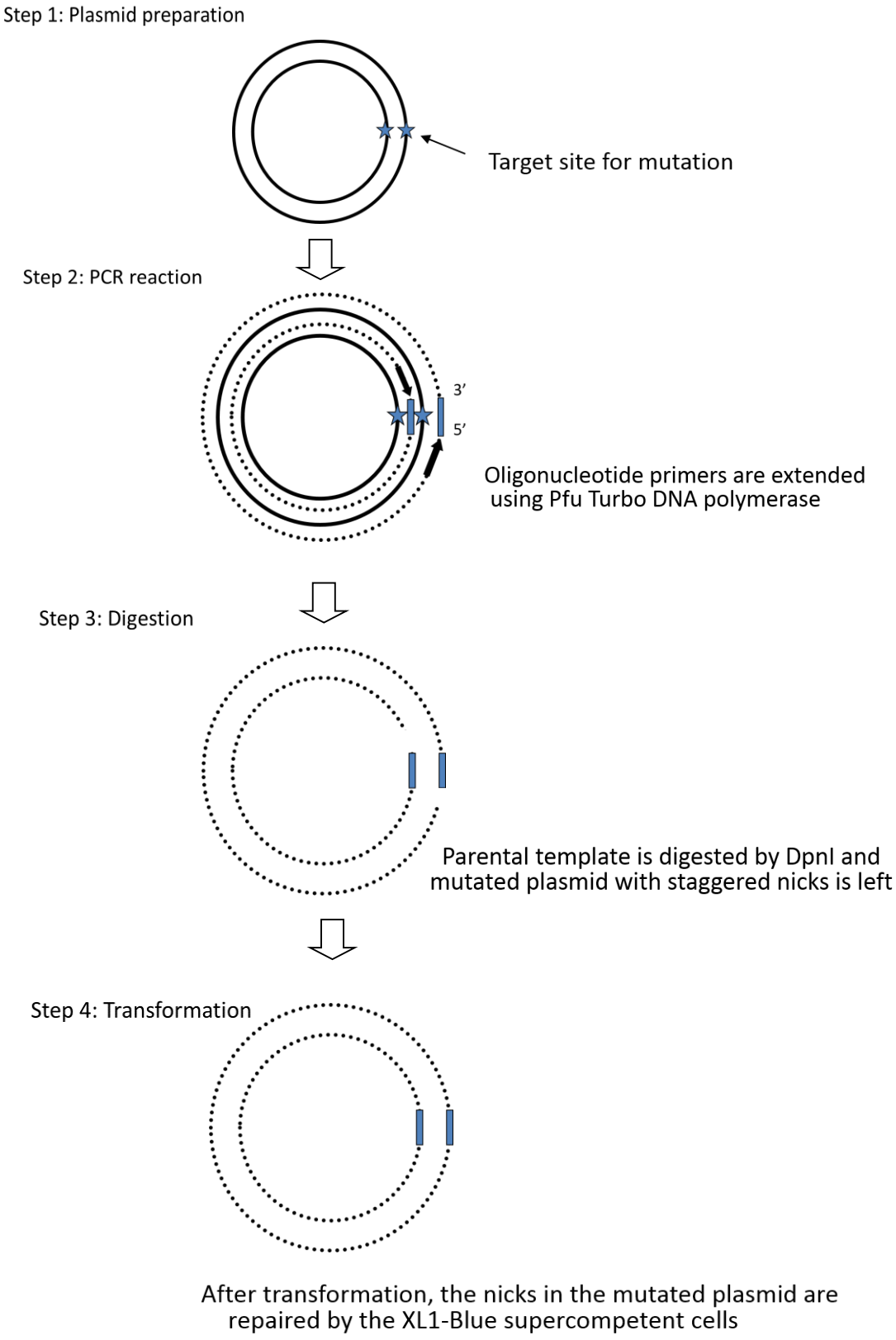
Step 1: Plasmid preparation
Target site for mutation
Step 2: PCR reaction
3′
5′
Oligonucleotide primers are extended using Pfu Turbo DNA polymerase
Step 3: Digestion
Parental template is digested by DpnI and mutated plasmid with staggered nicks is left
Step 4: Transformation
After transformation, the nicks in the mutated plasmid are repaired by the XL1-Blue supercompetent cells

plasmid. Following the temperature cycling reaction, the reaction tubes were added DpnI and incubated at 37˚C for 1 hour. DpnI digested the methylated parental plasmid template extracted from *E. coli*, while leaving the newly synthesized mutation-containing DNA product intact. After the digestion of DpnI, the mixture in the tube was cleaned with the resin provided in the kit, and a small aliquot was transformed or electroporated into XL1-Blue supercompetent cells. Transformants were selected and purified on nutrient agar plates supplemented with appropriate antibiotics, depending on the antibiotic resistance of the plasmid template. Plasmids were extracted and further sequenced to select desired mutation.

2.3. Bacterial and biochemical methods

2.3.1. Bacteriophage P1 transduction

The bacteriophage P1 preparation and transduction are as described in Vine, 2012.

2.3.2. Preparation of cell-free extracts

Cell breakage was achieved by sonication. Glass vessels with cell suspension were placed on ice during sonication. The sonicator was tuned with a microtip (Misonix XL2020 Sonicator). Each sample was treated with 4 minutes of sonication in total. The process was interrupted every 30 seconds to ensure that the sample was kept cold throughout. After sonication, samples were centrifuged in a cold room or in centrifuge with a cooling function and supernatants were collected.

2.3.3. Aconitase activity assay

Strains from fresh NA plates were inoculated into 10 mL LB in 50 mL conical flasks

and were aerated at 37℃ for 12 h. Then they were transferred to MS medium to a total volume of 100 mL and grown overnight anaerobically to allow the bacteria to adapt from aerobic metabolism to anaerobic metabolism. Finally the 100 mL cultures were inoculated to MS medium up to a total volume of 1 L. Cells were collected and resuspended in 1 mL aconitase assay buffer for sonication treatment.

Aconitase activity in cell-free extracts was assayed by following absorbance at 340 nm at 25℃ in a 1.0-mL reaction mixture containing 50 mM Tris-HCl, pH 7.4, 30 mM sodium citrate, 0.6 mM $MnCl_2$, 0.2 mM $NADP^+$. One unit will convert 1.0 μmole of citrate to isocitrate per minute at pH 7.4 at 37℃. At least two independent experiments were completed unless otherwise specified. Standard deviations were represented by error bars.

$$\text{Units/mL enzyme} = \frac{(\Delta A_{340nm}/\text{min Test} - \Delta A_{340nm}/\text{min Blank})*(df)*(1)}{(V)*(6.22)}$$

Where

df = dilution factor

1 = Total volume (mL) of assay

V = Volume (mL) of enzyme used

6.22 = Millimolar extinction coefficient of NADPH at 340 nm

2.3.4. Lowry protein assay

The method developed by Lowry *et al* (1951) was used to determine the protein concentration. Under alkaline conditions, cupric ions (Cu^{2+}) chelate with the peptide nitrogens, which results in the reduction of cupric ions (Cu^{2+}) to cuprous ions (Cu^+). A

subsequent reduction of the Folin phenol reagent by the cuprous ions (Cu^{+}) forms a blue coloured product, allowing colorimetric quantification at 750 nm. This assay is sensitive to pH changes and the pH should be maintained at 10 – 10.5. Also a variety of compounds will interfere with the procedure. Assay tubes need to be clean and three replicas are included for each sample.

Samples (50 µL) were pipetted into the tubes containing 550 µL of distilled water. Bovine serum albumin (1 mg/mL) was included as the standard while distilled water was used as blank. Next 3 mL of Folin B solution was added to each tube followed by vortex. Ten minutes after the addition of Folin B solution, 0.3 mL of 58.8% (w/v) Folin-Ciocalteu reagent was added to each tube. The tubes were vortexed and left for 30 minutes to allow the blue colour to develop. The OD of the mixture in each tube was measured at 750 nm. The OD measured for each sample was compared to that of the standard for the final quantification of protein concentration. In aconitase assay, the measured protein concentration was used to normalize the enzyme activity for the specific enzyme activity.

Normalised enzyme activity:

$$\text{Units/mg enzyme activity} = \frac{\text{Units/mL enzyme activity}}{\text{mg protein/mL enzyme}}$$

2.3.5. ß-galactosidase activity assay

The ß-galactosidase activity was assayed as described in Vine, 2012.

2.3.6. Spot test for the detection of nitrite

Nitrite reacts with sulphanilamide under acidic conditions. The product of the reaction

could further react with N-napthylethylene diamine dihydrochloride to form an azo derivative dye. In practice, samples were mixed with equal volumes of 1% (w/v) sulphanilamide in 1M HCl and N-napthylethylene diamine dihydrochloride. The mixture was transferred to a white background. The appearance of pink colour indicates the presence of nitrite in sample. This colorimetric method was only used for qualitative purposes in this study.

2.3.7. Preparation of nitric oxide saturated water (NOSW)

A vial of 5 mL sterile distilled water (pH = 3, adjusted by HCl) was sealed with a turnover rubber stopper (Fisher Scientific, Leicestershire, UK), which was pierced through by two needles of different lengths to allow the gas to sparge through the water. The longer needle was the inlet for the gas, the tip of which was submersed beneath the surface of water. The shorter needle was the outlet with the tip kept in the headspace. As nitric oxide is unstable in the presence of oxygen, dissolved oxygen needs to be removed from the water *via* sparging gaseous nitrogen before nitric oxide should be applied. A three way silicone tube was used to attach the nitrogen cylinder, nitric oxide cylinder and the vial. The water was first bubbled with gaseous nitrogen for 30 minutes, then saturated with nitric oxide for 30 minutes. The concentration of nitric oxide in the water prepared as described above is 2 mM. When needed, NOSW was taken from the vial with a needle and a gas tight syringe.

2.3.8. Bacterial two-hybrid system detecting protein interactions

The bacterial two-hybrid system employed in this work is a technique that detects protein-protein interactions *in vivo* (Karimova *et al.,* 1998, Karimova *et al.,* 2000; Fig

2.5). It is based on the interaction-mediated reconstitution of the adenylate cyclase (Cya) activity in *E. coli*. Two complementary fragments from the catalytic domain of Cya from *Bordetella pertussis*, T25 and T18, were fused to putative interacting proteins or polypeptides. If a pair of proteins interact and come physically close to each other, T25 and T18 reconstitute functional complementation, which results in cAMP production from ATP. The synthesized cAMP binds to the catabolite activator protein, CAP, forming a cAMP/CAP complex. It is a pleotropic regulator of a number of genes including *lac* and *mal*. As a result, bacteria become able to use maltose or lactose as the unique carbon source. Also, LacZ production can also be monitored as an indicator of protein-protein interactions.

The genes encoding the two putative interacting protein pairs, X and Y, were amplified from the chromosome of MG1655 by PCR, and cloned into pKT25 and pUT18 (or pUT18C). For plasmid descriptions see Fig 2.6, 2.7 and 2.8. The plasmid constructs were sequenced to ensure that cloned genes were in frame with the T25 and T18 fragment open reading frames. The plasmids were amplified using an *E. coli* strain DH5 at 30˚C. A non-reverting *cya* mutant of *E. coli* strain, BTH101, was made into competent cells and transformed with the low-copy number plasmid pKT25 construct. Kanamycin resistance was the selection marker of the transformants, which were then made into competent cells again for the transformation of the high copy-number plasmid pUT18 (or pUT18C) construct. Co-transformants were plated on MacConkey base medium supplemented with maltose, kanamycin and ampicillin. A single colony was picked to inoculate a 4 mL liquid LB medium in 100 mL shake flask, aerated overnight at 37˚C. Then the culture was transferred to a 100 mL flask containing 94 mL

Figure 2.5.

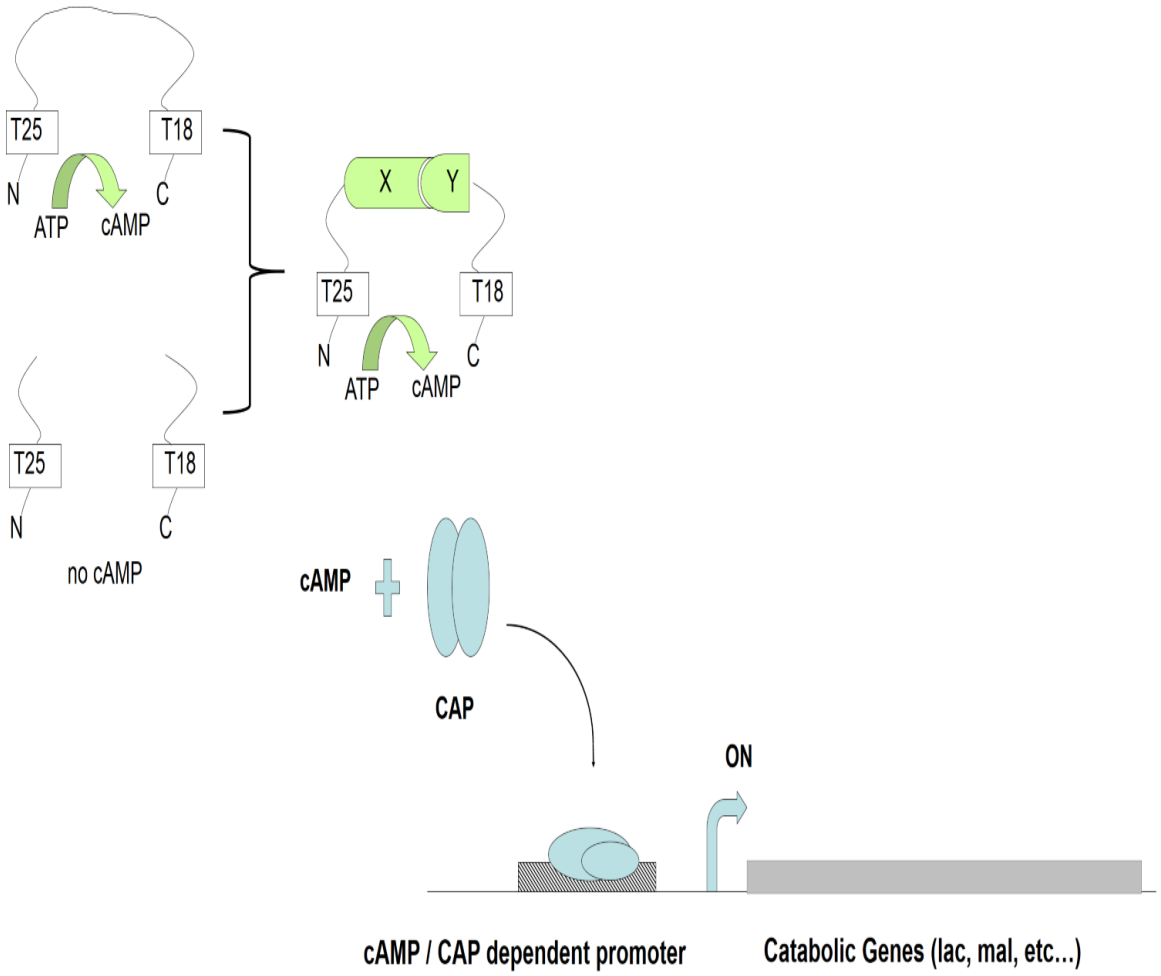

Principle of the bacterial two-hybrid system

Two complementary fragments from the catalytic domain of adenylate cyclase (Cya) from *Bordetella pertussis*, T25 and T18, reconstitute Cya activity if they are brought together. When they are fused to interacting polypeptides, X and Y, heterodimerization of the two chimeric proteins leads to functional complementation between T18 and T25. As a result, ATP could be converted to cAMP, which binds to the catabolic activator protein, CAP. The cAMP/CAP complex activates the transcription of several resident genes, such as *lac* and *mal*. Reference is from Karimova *et al.*, 2000.

Table 2.5. **Plasmids used and constructed in the bacterial two hybrid system**

Plasmid name	Description and application	Reference
pKT25	Vector used in the bacterial two hybrid system (Fig 2.6).	D. Ladant, Institut Pasteur, Paris, France
pUT18	Vector used in the bacterial two hybrid system (Fig 2.7).	D. Ladant, Institut Pasteur, Paris, France
pUT18C	Vector used in the bacterial two hybrid system (Fig 2.8).	D. Ladant, Institut Pasteur, Paris, France
pKT25-Zip	pKT25 derivative encoding the leucine zipper of GCN4. Km^R	D. Ladant, Institut Pasteur, Paris, France
pUT18-Zip	pUT18 derivative encoding the leucine zipper of GCN4. Amp^R	D. Ladant, Institut Pasteur, Paris, France
pGS1711	pKT25 derivative encoding T25-AcnB. Km^R	Tang *et al.*, 2005
pGS1715	pUT18C derivative encoding T18 Cya fragment fused to AcnB T18-AcnB. Amp^R	Tang *et al.*, 2005
pKT25-Hcp	pKT25 derivative encoding T25-Hcp. Km^R	This work
pUT18-Hcp	pUT18 derivative encoding Hcp-T18. Amp^R	This work
pUT18C-Hcp	pUT18C derivative encoding T18-Hcp. Amp^R	This work
pKT25-Hcr	pKT25 derivative encoding T25-Hcr. Km^R	This work
pUT18-Hcr	pUT18 derivative encoding Hcr-T18. Amp^R	This work
pUT18C-Hcr	pUT18C derivative encoding T18-Hcr. Amp^R	This work
pKT25-YtfE	pKT25 derivative encoding T25-YtfE. Km^R	This work
pUT18-YtfE	pUT18 derivative encoding YtfE-T18. Amp^R	This work
pUT18C-YtfE	pUT18C derivative encoding T18-YtfE. Amp^R	This work
pKT25-NsrR	pKT25 derivative encoding T25-NsrR. Km^R	This work
pUT18-NsrR	pUT18 derivative encoding NsrR-T18. Amp^R	This work
pUT18C-NsrR	pUT18C derivative encoding T18-NsrR. Amp^R	This work

Table 2.6. **primers used in the bacterial two hybrid system**

Primer name	**Sequence (5'-3')**	**Description and application**
Checking primers		**Used in sequencing**
pKT25 fwd checking	GACGGCGGATATCGACATGTTCG	Anneals to ~100bps upstream and downstream of the multiple cloning sites of pKT25 vector
pKT25 rev checking	GGGCCTCTTCGCTATTACGCC	
pUT18 fwd checking	AGCGCAACGCAATTAATGTGAGTTAGC	Anneals to ~100bps upstream and downstream of the multiple cloning sites of pUT18 vector
pUT18 rev checking	CCACTGCGGAACGGGC	
pUT18C fwd checking	GGCGTGCCGAGCGG	Anneals to ~100bps upstream and downstream of the multiple cloning sites of pUT18C vector
pUT18C rev checking	GGGAGCAGACAAGCCCG	
Cloning primers		**Anneals at the beginning (fwd) or end (rev) of the gene described**
Hcp pKT25 fwd PstI	ATATATGCTGCAGGGTTTTGTGTGCAATGTGAACAAACTATCC	*hcp*
Hcp pUT18 fwd PstI	ATATATATCTGCAGGTTTTGTGTGCAATGTGAACAAACTATCC	*hcp*
Hcp pKT25 pUT18 rev	ATATATGGGATCCTCCGCGCTCAACAGTTGC	*hcp*
Hcr pKT25 fwd PstI	ATATATGCTGCAGGGACGATGCCAACGAATCAATGC	*hcr*
Hcr pUT18 fwd PstI	ATATATATCTGCAGGACGATGCCAACGAA	*hcr*

	TCAATGC	
Hcr pKT25 pUT18 rev	ATATATGGGATCCTCTGCGAGAACCAAATCC	*hcr*
YtfE pKT25 fwd PstI	ATATATGCTGCAGGGGCTTATCGCGACCAACCTTTAGGTG	*ytfE*
YtfE pUT18 fwd PstI	ATATATATCTGCAGGGCTTATCGCGACCAACCTTTAGGTG	*ytfE*
YtfE pKT25 pUT18 rev	ATATATGGGATCCTCCTCACCCGCCAGCGC	*ytfE*
NsrR pKT25 fwd PstI	ATATATGCTGCAGGGCAGTTAACGAGTTTCACTGATTACGG	*nsrR*
NsrR pUT18 fwd PstI	ATATATATCTGCAGGCAGTTAACGAGTTTCACTGATTACGG	*nsrR*
NsrR pKT25 pUT18 rev	ATATATGGGATCCTCCTCCACCAGCAATAATTTATAAAGCGG	*nsrR*

Figure 2.6.

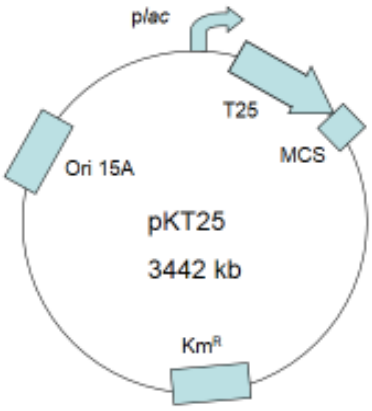

Plasmid map of vector pKT25

Vector pKT25 is derived from the low copy-number plasmid pSU40 with a selectable marker of kanamycin resistance. T25 fragment corresponds to the first 224 amino acids of adenylate cyclase (Cya) from *B. pertussis*. A multiple cloning site (MCS) was inserted at the 3'- end of T25 so that fusions constructed would be at the C-terminal end of the T25 polypeptide.

Figure 2.7.

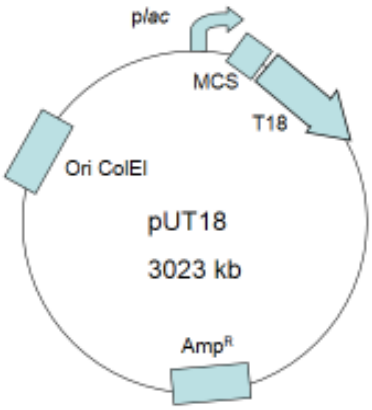

Plasmid map of vector pUT18

Vector pUT18 is a derivative of the high copy number vector pUC19 with a selectable marker of ampicillin resistance. It is designed to create fusion proteins in which a heterologous polypeptide would be fused to the N-terminal end of T18, as the multiple cloning site (MCS) was inserted at the 5'- end of T18. The encoded T18 framment corresponds to amino acids 225 to 399 of adenylate cyclase (Cya) from *B. pertussis*.

Figure 2.8.

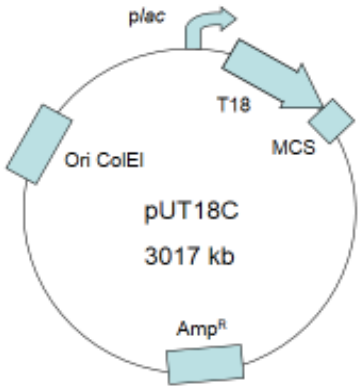

Plasmid map of vector pUT18C

Vector pUT18C is also a derivative of the high copy number vector pUC19 with a selectable marker of ampicillin resistance. T18 fragment of this vector is the same as that of pUT18. It is designed to create fusion proteins in which a heterologous polypeptide would be fused to the C-terminal end of T18, as the multiple cloning site (MCS) was inserted at the 3'- end of T18.

LB supplemented with antibiotics and left statically at 37˚C for 4 hours. Samples were taken to measure the β-galactosidase activity.

2.3.9. Circular dichroism spectroscopy

Circular dichroism spectroscopy (CD) is a technique frequently used for the investigation of protein secondary structures. In principle, the chirality of the secondary structural motifs, such as α-helices and ß-sheets, is utilized to distinguish different absorptions in circularly polarized light. A Jasco J715 spectropolarimeter was used to measure the CD spectra. The blank was measured using a cuvette with a 2 mm light path, containing 600 µL of 0.01 M phosphate buffer. Purified proteins were concentrated to above 5 mg/mL, and then an appropriate amount was added into the same cuvette to give a final concentration of 0.02 mg/mL. Spectra were averaged over 16 scans. The final spectrum was obtained by subtracting the sample spectrum with the buffer spectrum. The data were submitted to the web server DichroWeb for analysis (Whitmore and Wallace, 2004). The deconvolution algorithm used was CDSSTR developed by Compton and Johnson (1986). It requires a reference data set of known secondary structures to compare with the tested protein structure. The reference data set 4 optimal for a wavelength of 190 to 240 nm was used in this study (Sreerama *et al.*, 2000).

2.3.10. The automatic sampling and gas analysis system

This automatic sampling and gas analysis system was assembled by Molstad *et al* (2007), from the Norwegian University of Life Sciences. It was primarily designed to analyse gas production and consumption profiles of denitrifying bacteria (O_2, NO, N_2O

and N_2).

2.3.10.1 System set-up and NO preparation

In this work, this automated robotic system was employed to investigate the NO reduction of an *E. coli hcp* mutant. Altogether 28 positions were available in the rack to accommodate serum flasks (120 mL total volume) containing 50 mL sterile minimal salt medium each. The rack was placed in a thermal water bath with temperature set at 30ºC. Headspace gas of each flask was periodically sampled by a Gilson Model 222 (Gilson, leBel, France) autosampler, which was controlled by a Python program installed on the computer. The gas sample was then pumped to gas analyzers by a Gilson Minipuls 3 peristaltic pump (Fig 2.9). An equal volume of helium gas was pumped down into the headspace to keep the pressure in the vial. The direction, speed and timing of the pumping were also controlled by the injection program written in Python language. The gas analyzers consisted of two parts: a chemoluminescence NO analyzer dedicated to detect NO and a Varian CP4900 microGC for all the other gases such as O_2, N_2O, N_2 and CO_2 etc. Calibration was routinely done by injecting gas standards of known concentration to generate a digital signal corresponding to the known concentration, which was then in turn compared to the signal obtained for each sample to determine the actual concentration in question.

After autoclaving and before inoculation, all flasks were treated with repeated cycles of evacuation and He washing to remove the oxygen inside the vial using the He washing device (Molstad *et al.,* 2007). Then an inoculum of different strains was injected into each vial. The desired concentration of gaseous NO was added into the headspace using

a gastight syringe. The automatic sampling system was controlled by a Python program, which determined the time of sampling and the position of the vial to be sampled. After each gas sample was analysed by GC and the NO analyser, the data generated would be amended to an Excel spreadsheet after a sorting routine, linking each chromatogram to each vial.

The injected gaseous NO was generated *via* the reduction of nitrite as described in equation: $I^- + NO_2^- + 2H^+ \rightarrow NO + ½\ I_2 + H_2O$. Four separate vials (120 mL) were prepared each containing one of the followings: 50 mg NaI, 50 mL 50% (v/v) acetic acid, 50 mL 0.3 M KNO_2, 20 mL 10 M KOH. Vials were sealed with septa and treated with evacuation and He washing cycles. Then 5 mL 50% (v/v) acetic acid and 1 mL 0.3 M KNO_2 were drawn and injected into the vial containing NaI, which was then left at room temperature for 2 hours to allow reaction to complete. To neutralize the excessive acetic acid in the vial, 6 mL 10 M KOH was drawn and injected into the reaction vial. The expected yield of NO in vial was around 10000 ppm.

2.3.10.2. Preparation of inoculum and experimental design

The NO reduction experiment on the robot was to be conducted anaerobically, therefore the vials installed on the robot were pre-washed with Helium gas to remove oxygen, and the inoculum to be used was also prepared anaerobically. Two steps were involved for the anaerobic inoculum preparation. First a conical flask containing 10 mL LB was inoculated with a single colony from plate and aerated at 30˚C for 12 hours. Then 10 µL of the aerobic culture was injected into a sealed anaerobic vial pre-washed with helium gas and incubated at 30˚C till mid-exponential phase, to allow the bacteria to adapt to

anaerobic conditions prior to the robotic experiment. The anaerobic inoculum was transferred using a gas-tight syringe and injected into the anaerobic vials installed on the robot. The amount of inoculum was adjusted to make the starting OD_{650} of all experiments between 0.01 and 0.02, and the temperature used for growing anaerobic seed culture and in the robotic experiment was 30˚C, unless otherwise specified.

Gas standards were measured in each experiment to calibrate gas readings. An automatic sampler collected gas sample from the headspace of a vial under the control of the Python program, which required an input for the number of vials (N) included in each sampling cycle. This enabled the automatic sampler to continuously go to the next vial in a loop of 1 to N once it was triggered each time. The process of one complete gas analysis for a single vial took 6.19 minutes (See Fig 2.9. for graphic depiction of the setup). The next vial would be analyzed in the same way immediately after the previous analysis had finished. Regarding the sampling frequency of one particular vial on the robot, it depended on how many vials were included in one cycle, such as, the first vial would be sampled again after the analysis of the vial number N had finished. To increase the frequency of data collection for each vial, only four vials, hence four positions on the rack of robot were used during each cycle, although 28 positions were available in total. Subsequent new cycles of experiments were conducted for replicas, also with four vials each cycle. The sampling frequency of one particular vial would be approximately 25 minutes (6.19 * 4 = 24.76 minutes).

The anaerobic vials used in the experiment were all of the same size, with a fixed volume of 120 mL containing 50 mL culture, which left a 70 mL volume for gas. Each

Figure 2.9.

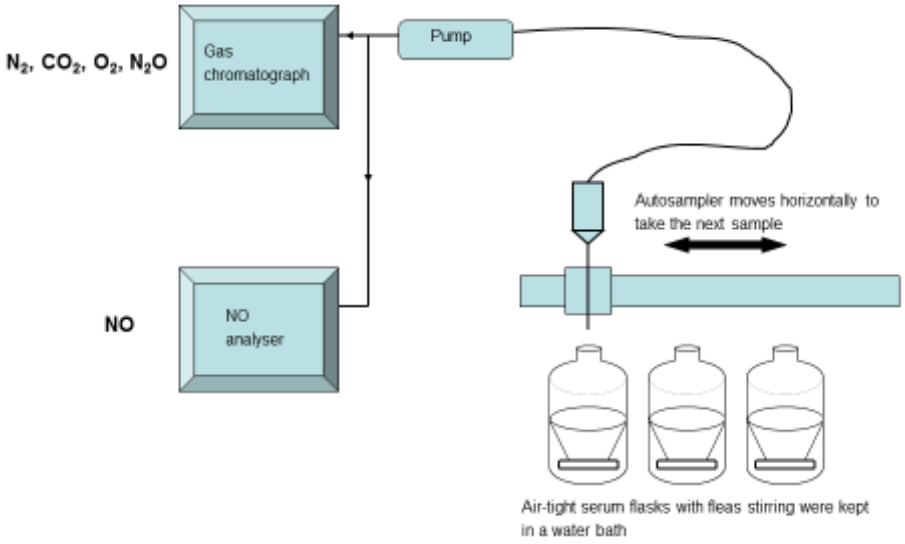

The automatic sampling and gas analysis system

This system allows real time monitoring of gas concentration in vials. The vials were sealed with septa and were washed with helium gas. Different strains were raised in parallel and inoculated into the anaerobic vials *via* syringe injection. Fleas were constantly stirring to ensure equilibrium between gas and liquid phase. The autosampler and pump were controlled by a Python program on the computer for periodical samplings. The gas samples were then analyzed by a gas chromatograph and a NO analyser.

time a fixed amount of gas sample was drawn every 25 minutes for analysis, the same amount of helium gas was injected back into the vial to keep in the vial a constant gas pressure. The average of dilution to the headspace gas caused by each sampling should be 1.6%, according to repeated samplings to a vial filled with air (Molstad *et al.*, 2007). Fig 2.10 showed theoretical decline of NO concentration simply caused by dilution at 1.6% each time. The actual dilution rate appears to vary slightly between experiments. To calculate the actual rate after deduction of the rate of dilution from the total rate, control vial without bacteria was included for each NO concentration used for measuring the dilution rate.

Other vials were inoculated with different strains to measure the NO reduction rate of each strain. For the four vials in the first run, three of them were inoculated with RK4353, JCB5210, JCB5250 respectively, while the last one being the control vial without inoculation. The same amount of NO, 1000 nmol NO in total in vial (344 ppmv) generating 620 nM NO in liquid phase (according to Henry's law), was injected into each vial, 6 minutes before the first sampling of each vial. In practice, NO was added to the next vial while the current vial was being sampled by the autosampler, as the next vial will be sampled by the autosampler in 6.19 minutes. The NO and other gas concentration was determined every 25 minutes for each vial until NO concentration in each vials had gone down to detection limit (0.2 ppmv). Then the current cycle would be terminated and a new cycle would begin. In subsequent runs, experiments using same strains under same NO concentration were repeated. According to the NO tolerance of each strain, additional experiments were also completed using adjusted different starting concentrations of NO — higher concentrations for RK4353 and lower

Figure 2.10.

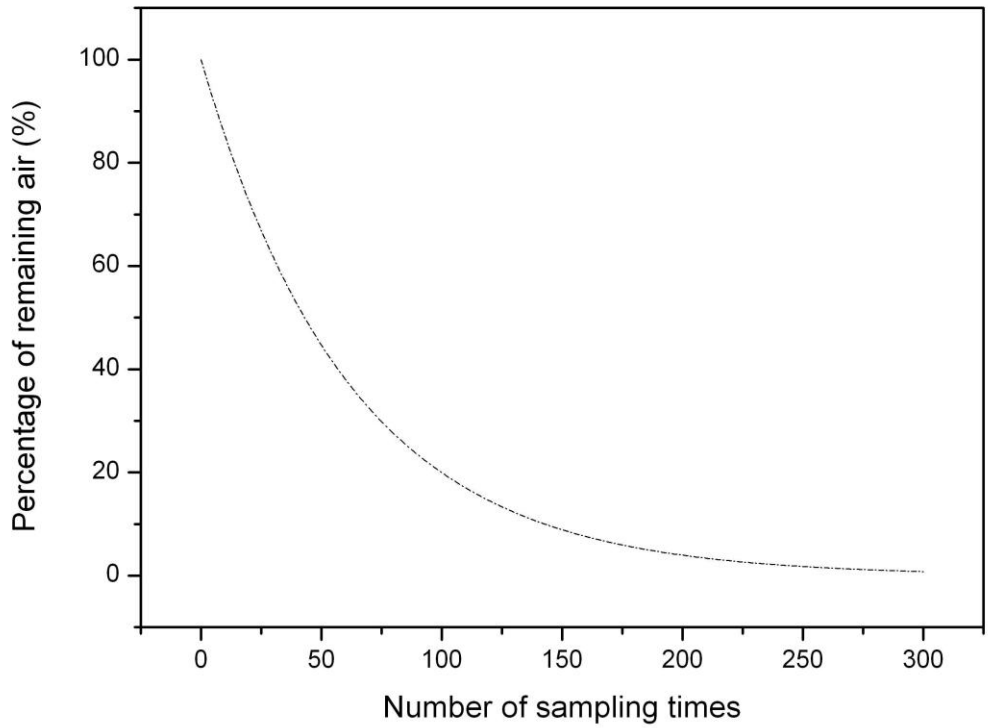

Theoretical decline of gas concentration due to sampling alone

The dashed line shows the decrease of sample concentration at a dilution rate of 1.6% each time. A vial was filled with air for analysis of dilution effect. After each time of sampling, air concentration in vial will be reduced to 98.4% of that before sampling. Starting from 100%, the air concentration approaches to zero after the removal of 300 samples.

concentrations for JCB5210 and JCB5250. The NO concentration changed over time for each strain will be presented in its own section. NO reduction rate will be analyzed against NO concentration for kinetic characterization of each strain.

The cell density is required to calculate the specific rate of NO reduction. However, the sample volume each time used for OD determination is much higher than that required for gas sampling. The loss of sample volume would reduce the pressure inside the vial. During the design of the robot, the loss of gas sample was taken into consideration *via* injecting back same volume of helium gas after each sampling. However, OD measurement was not a feature built into the robot system, therefore had to be done manually. For OD determination, 1 mL liquid culture was drawn from the 50 mL liquid culture and thus lost. To keep the volume percentage of gas and liquid constant for each vial, continuous sampling of liquid culture should be avoided. Therefore, liquid samples were only taken twice, one at the beginning and the other at the end to determine the optical density. The change of biomass in liquid medium during cultivation in between of these two sampling points was deduced from the rate of CO_2 emission. This is because in a test run with all the strains used in this robotic experiment, including RK4353, JCB5210, JCB5250 and JCB5290, it was observed in the gas profiles over time that the CO_2 concentration was incremented exponentially, in the same pattern with bacterial growth. The positive correlation between CO_2 emission and bacterial growth was therefore described using a linear model. As CO_2 concentration can be measured for each gas sample automatically, the biomass at each time point (represented by OD_t) can be calculated from the reading of CO_2 concentration as shown in the equation below. The conversion factor from OD to dry cell weight is 0.4 at 650 nm.

The estimated biomass (OD_t) at a certain time point t was calculated using the equation:

$$Od_t = OD_0 + \frac{[CO_2]_t - [CO_2]_0}{[CO_2]_f - [CO_2]_0} \times (OD_f - OD_0)$$

Where:

OD_t = estimated optimal density (OD) at time t;

$[CO_2]_t$ = concentration of CO_2 at time t;

OD_o = measured initial OD at time 0;

$[CO_2]_0$ = concentration of CO_2 at time 0;

OD_f = measured final OD at the last data point;

$[CO_2]_t$ = final concentration of CO_2 at the last data point;

To check that this equation based on a simple linear model is empirically correct to describe the growth under experiment conditions, separate growth experiments were set up in parallel by adding four extra vials with the same amount of inoculum for each strain. In Fig 2.11, the anaerobic growth of the quadruple mutant strain JCB5210 with or without NO was shown as an example. Liquid samples were drawn from these parallel vials in different time points and were compared with the estimated optical density calculated using the equation shown above. The blue line shows the CO_2 concentrations at each gas sampling points. The estimated OD agrees with the actual OD of the data points measured in those four separate vials, as shown by the comparison between the red line of estimated values and four different symbols of actual determined values. This was also observed for other strains under the conditions tested in this robotic experiment.

Positive correlation of CO_2 emission and biomass accumulation under conditions used in the robotic experiments

The CO_2 concentration in gas samples during bacterial growth was shown as the blue line. The biomass was determined from the optical density of the liquid culture at 650 nm. To avoid loss of liquid medium caused by sampling, the optical density of the vial under study was measured twice at the beginning and end of experiment, shown as the red diamonds. The red line connecting these two points represents calculated OD values based on a positive linear correlation of CO_2 concentration in the gas phase. For evaluation purposes, four separate vials were used as replicas for actual measurements of OD readings, labelled as +, x, ○, and Δ respectively.

Panel A shows the anaerobic growth of JCB5210 without NO addition;

Panel B shows the anaerobic growth of JCB5210 supplemented with 1000 nmol of NO in the headspace.

Figure 2.11.

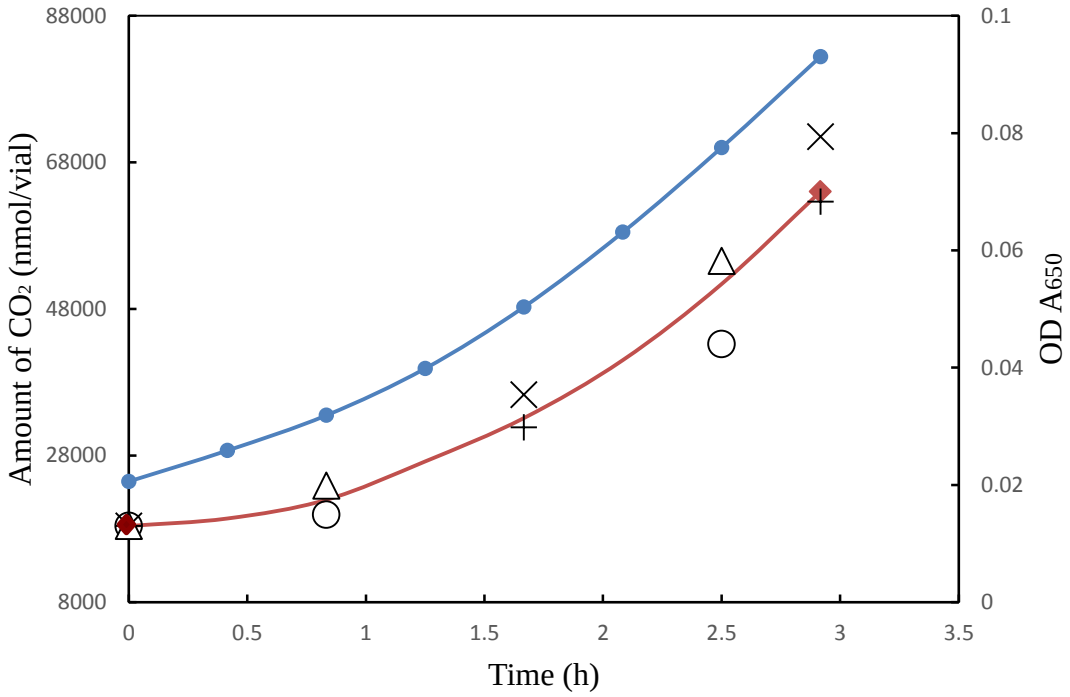
88000
68000
48000
28000
8000
0.1
0.08
0.06
0.04
0.02
0
0
0.5
1
1.5
2
2.5
3
3.5
Amount of CO2 (nmol/vial)
OD A650
Time (h)

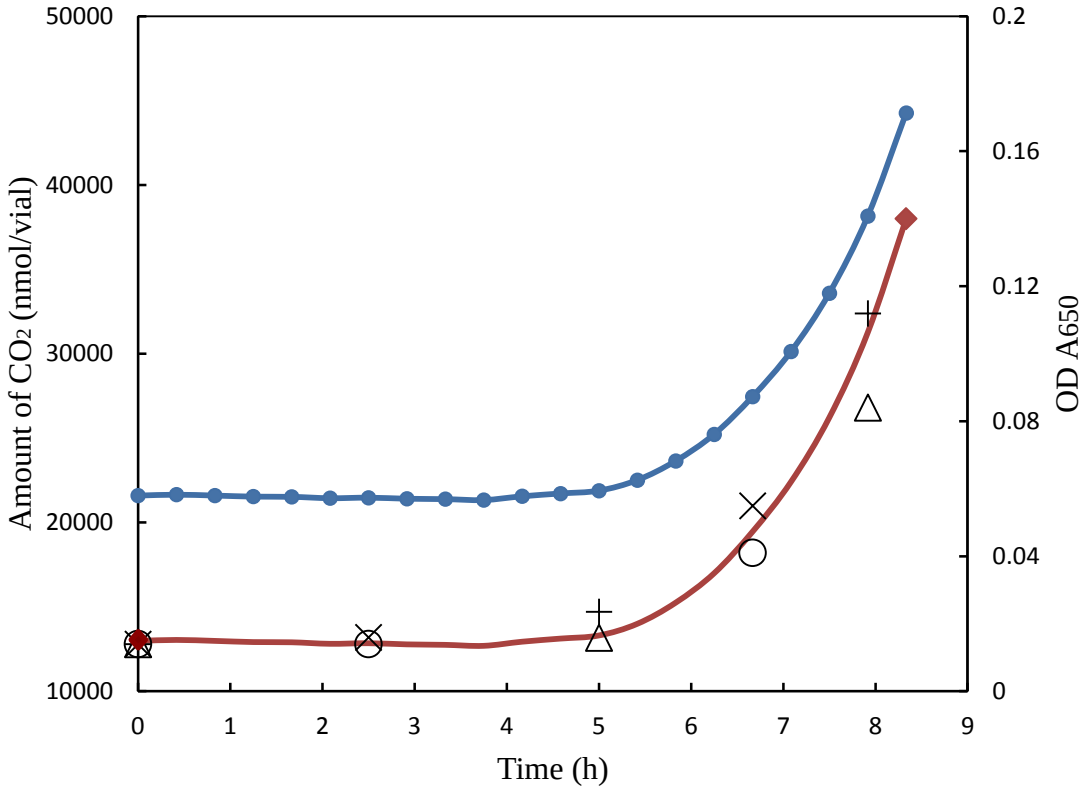
50000
40000
30000
20000
10000
0.2
0.16
0.12
0.08
0.04
0
0
1
2
3
4
5
6
7
8
9
Amount of CO2 (nmol/vial)
OD A650
Time (h)

2.3.11. NO electrode assay

To measure the rate of NO consumption in the liquid phase within the range of 0.4 to 5 μM, an NO electrode sensor (2-mm diameter Precision Instruments ISO NOP) was used in combination of a modified Clark-type electrode chamber with a 2 mL working volume (Fig 2. 12). Gastight syringes were used to deliver reagents into the electrode chamber through the hole in the centre of the lid. Prior to NO addition, oxygen was removed by adding 4 Units/mL of glucose oxidase, 20 Units/mL of catalase and 16 mM of glucose into the reaction chamber. Then electrode was calibrated according to manufacturer's manual. For calibration, gaseous NO was generated using the following reaction: $2KNO_2+2KI+2H_2SO_4 \rightarrow 2NO+ I_2+2H_2O+2K_2SO_4$. The electrode was put into a 20mL glass vial containing 20 mL of 0.1 M H_2SO_4 and 0.33 g KI (0.1 M), with the tip immersed 3 mm into the solution. When the reading on the indicator stabilised at the baseline level, known aliquots of 50 μM KNO_2 were added into the glass vial. A magnetic stirring bar should be used during calibration. As stated in the equation, the concentration of NO produced should equal to the final concentration of KNO_2 in the 20 mL reaction (Fig 2.13). For the experiment, propyl-nonoate aliquots (0.5 μM) were used to generate NO. Purified proteins were added after the NO trace stablized at the plateau for the determination of reduction rate.

2.4. Protein techniques

2.4.1. Purification of His-tagged proteins by affinity chromatography

The system of the AKTA purifier was prewashed with distilled water twice. Then the His-trap column was installed and the system was washed with Buffer A twice.

Figure 2.12.

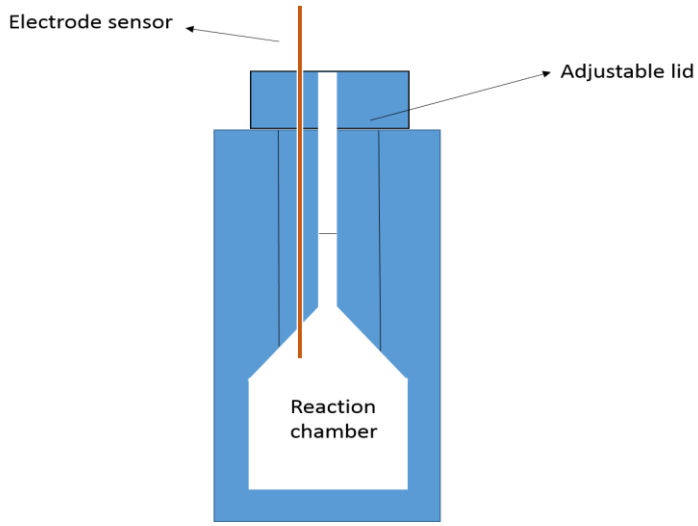

Set up of the NO electrode

An NO electrode (2-mm diameter Precision Instruments ISO NOP) was used in combination of a modified Clark-type electrode chamber, where anaerobic reactions could take place. The electrode chamber was sealed with the lid containing a long and narrow hole in the middle, allowing reagents to be added *via* gas tight syringes. Prior to NO addition, oxygen was removed by adding 4 Units/mL of glucose oxidase, 20 Units/mL of catalase and 16 mM of glucose into the reaction chamber. The electrode was calibrated by known concentrations of NO generated from chemical nitrite reduction. During usage, a tiny magnetic stirring bar was used inside the electrode chamber to ensure effective mixture of all components.

Figure 2.13.

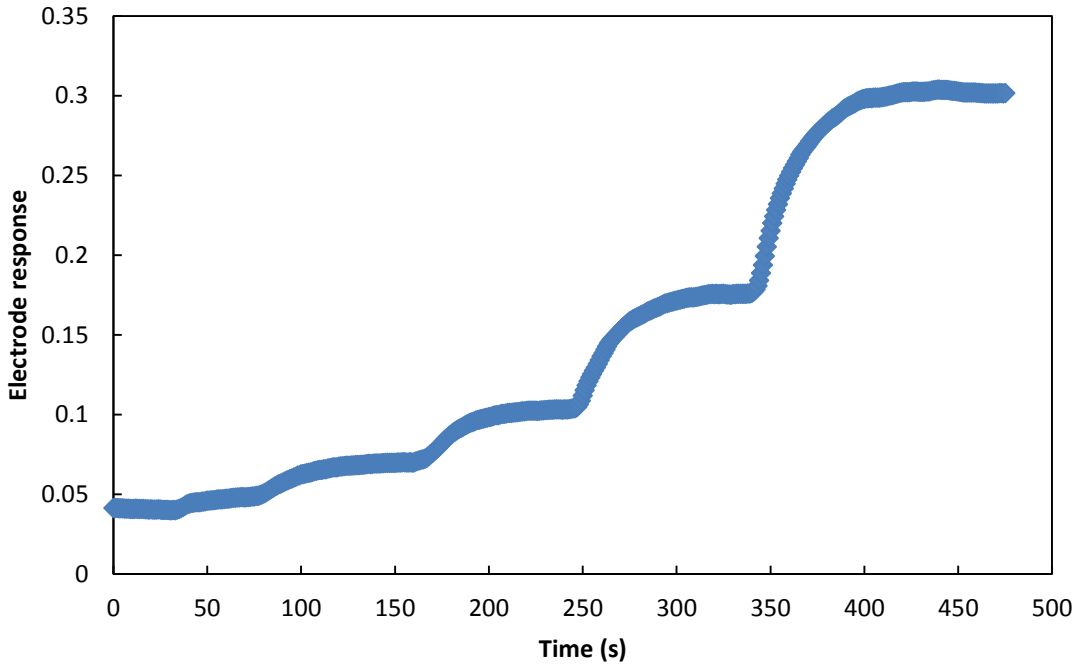

Calibration curve of NO electrode

This graph shows a typical NO calibration curve. NO was generated by adding doses of KNO_2 into an acidic and reductive solution containing H_2SO_4 and KI in a glass vial. The amount of NO equals stoichiometrically to that of KNO_2. In this calibration, the amount of the KNO_2 solution doubled each time, and the NO electrode responded accordingly.

Meanwhile, the cell suspension was sonicated and centrifuged at 39,000 rpm for 1 hour. Supernatant was filtered and loaded onto the His-trap column, which was washed with 20 column volumes of Buffer A to remove unbound proteins. The bound proteins were eluted with a gradient wash (0 to 100% of Buffer B in Buffer A). Fractions containing desired protein were pooled and protein purity was analyzed *via* SDS-PAGE as described. The protein sample was concentrated using Vivaspin protein concentrator, divided into 200 µL aliquots and stored in -80ºC.

2.4.2. SDS polyacrylamide gel electrophoresis (SDS-PAGE) of proteins

The loading dye was prepared by adding sample buffer with β-mercaptoethanol as described in table 2.4. Cells harvested from culture or purified protein fractions were resuspended in loading dye and boiled at 100ºC for 10 minutes. After the samples had cooled to room temperature, 10 µL of each sample was loaded onto the SDS-PAGE gel (15% w/v polyacrylamide gels). The gel apparatus was supplied with 200V until the bands from the protein marker were well separated. Gels were stained in Coomassie blue staining buffer for 1 hour, and then de-stained overnight on a rocking platform. The gel was scanned by Syngene scanner and analysed by Genesys software.

2.5. Computer programs

Data were analysed using statistics package R for data modeling. Sequencing data was visualized using Chromas. Protein structure was displayed using Pymol.

CHAPTER 3

Identification of the physiological role of Hcp in protecting *E. coli* mutants from nitrosative stress

3.1. Introduction

Genes that are massively upregulated by NO *in vivo* due to the relief of NsrR repression include *hcp* and *ytfE* that are the foci of the work of this chapter. It was reported previously by Justino *et al.* (2006) that the *ytfE* mutant they had constructed was very sensitive to nitrosative stress. However, the mutant LMS4209 used for that study was not only a *ytfE* mutant, but also had a secondary deletion of another 126 genes in the chromosome, including the gene *hcp*. The phenotypes of *ytfE* or *hcp* mutants will be re-evaluated in this chapter. The effects of mutations in these genes on the growth under nitrosative stress will be reported. The starting point for these experiments was a quadruple mutant strain JCB5210, constructed by Dr Claire Vine, that is defective in *nirBDC*, *nrfAB*, *norV* and *hmp*. These genes are either known or believed to encode proteins that can metabolise, and hence detoxify, NO. Three derivatives of this strain had also been constructed by Dr Vine that were Hcp^+ $YtfE^-$, Hcp^- $YtfE^+$, or Hcp^- $YtfE^-$: these are strains JCB5257, JCB5250, and JCB5260, respectively. This provided a set of four isogenic strains with every combination of *hcp* and *ytfE* genes in a host strain that was expected to be sensitive to nitrosative stress. These strains were grown anaerobically in MS medium that was either unsupplemeneted, or supplemented with either NO-saturated water (NOSW), nitrite or nitrate, and the growth of the four strains was compared. It was found in this phenotypic study that *hcp* strains JCB5250 and JCB5260 were sensitive to nitrosative stress. Complementation using plasmid pJW11 encoding native Hcp protein confirmed that the sensitivity was caused by loss of Hcp. The plasmid pJW11 was further used as a template in mutagenesis reactions to study the effect of disruption of the hybrid cluster centre on the function of Hcp.

So far there is no available X-ray crystallography study on Hcp from *E. coli*. However, sequence alignment of Hcps found in different microorganisms showed that the residues coordinating the two Fe-S centres of Hcp are highly conserved (Fig 1.6). The unique hybrid cluster is speculated to be the active centre of Hcp, though this is not yet proved by any direct experimental evidence. According to the structural study of Hcp from *D. vulgaris* (Cooper *et al.*, 2000, 1E1D), the Fe8 from the hybrid cluster is directly coordinated by glutamic acid E494, the equivalent of which is E492 in Hcp from *E. coli*. In this study, this residue will be replaced by different amino acids to generate Hcp mutants (referred to as E492X mutants) with malfunctioning hybrid clusters. In this chapter, two plasmids will be used as the templates in site-directed mutagenesis reactions to serve different purposes. First the aforementioned plasmid pJW11 was mutated and used in a complementation experiment to examine whether the *hcp* mutant strain JCB5250 is protected by the Hcp E492X mutants under nitrosative stress. Second the protein expression vector pET-HCP will be modified to overexpress Hcp E492X mutants, which will be studied using circular dichroism spectroscopy to check whether they are still properly folded.

In this study, the activity of aconitase was measured as an indicator of intracellular nitrosative stress within the isogenic mutants. Aconitase was shown to be very sensitive to NO toxicity due to its Fe-S centre (Gardner *et al.*, 1997). In order to compare the effect of the *ytfE* and *hcp* mutations on aconitase activity under nitrosative stress conditions, aconitase activity was assayed in anaerobic cultures of the four isogenic strains that had been grown in the presence or absence of nitrate or NOSW. It was found that aconitase was inactivated in *hcp* mutant under nitrosative stress conditions.

Whether Hcp directly repaired aconitase was further assessed *in vitro* using purified Hcp and aconitase. A strain was constructed with a 6xhistidine tag attached to the aconitase B in the genome, which enabled affinity purification of aconitase B from the cell extract. The activity of purified aconitase B in the presence of NO, with or without purified Hcp was determined.

3.2. Effect of nitric oxide on anaerobic growth of strains defective in previously characterized NO reductases

The concentration of nitric oxide used was optimized with the quadruple mutant strain JCB5210 and one of its derivatives, JCB5250, which is further defective in *hcp* (Fig 3.1). When a high nitric oxide concentration of 5 µM was employed, both of the strains ceased to grow after inoculation. An intermediate concentration of 1 µM was adopted for further investigation, since the phenotypes of the above two strains were different with the same imposed stress level. The four isogenic strains with different combinations of *hcp* or *ytfE* mutations were inoculated into 20 mL LB medium and grown aerobically overnight. Appropriate volumes of the overnight cultures were used to inoculate 100 mL MS medium with a starting OD of around 0.1 at 650 nm. Flasks were left statically for 2 hours to allow the bacteria adapt to the anaerobic growth before supplementation with NOSW every 30 minutes onwards. The optical density of cultures with or without 1 µM NOSW was monitored every hour (Fig 3.2). The growth of both of the strains with the *hcp* mutation under NOSW stress was impaired compared with the unsupplemented control (Fig 3.2 C & D). In contrast, the corresponding *hcp*$^+$ strains grew at the same rates as the control culture (Fig 3.2 A & B). For the two *ytfE* mutants, the *hcp*$^+$ *ytfE* was unaffected by the *ytfE* mutation, whereas the *hcp ytfE* was sensitive to

the nitrosative stress comparing to its unsupplemented control (Fig 3.2 B & D). If YtfE, as being proposed before, is the major player in protection against nitrosative stress, then the *ytfE*$^{+}$ strains should be resistant to NO stress. However, the *hcp ytfE*$^{+}$ strain was sensitive to nitrosative stress despite the presence of the *ytfE* gene (Fig 3.2 C).

3.3. Effect of nitrite on anaerobic growth of the isogenic mutant strains

To induce nitrosative stress that could generate statistically significant differences between different strains, a concentration of 1 mM nitrite was chosen according to the preliminary data in Vine (2011). The four isogenic strains with different combinations of *hcp* or *ytfE* mutations were also grown in aerobic overnight cultures and then transferred to anaerobic culture with or without nitrite. Growth was followed every hour for 4 hours (Fig 3.3). The phenotype of the four strains was similar to that in growth experiment using NOSW as a source of nitrosative stress, but more pronounced. The two *hcp* mutants were unable to grow in the presence of 1 mM nitrite, whereas the *hcp*$^{+}$ strains were not affected. Again, depending on whether *hcp* gene was deleted, the *ytfE* mutants either grew or did not grow in nitrite supplemented cultures (Fig 3.3 B versus D).

3.4. Effect of nitrate on anaerobic growth of the isogenic mutant strains

For growth experiments with nitrate addition, a concentration of 5 mM nitrate was chosen according to the nitrate concentrations used in Vine (2011). Cultures were grown in 1000 mL of MS medium with or without nitrate addition and the optical density was measured every hour (Fig 3.4). Since more energy is conserved during growth with nitrate as an electron acceptor than with fumarate, the average doubling time of the cultures supplemented with nitrate was around 30% less than that of those without

Figure 3.1.

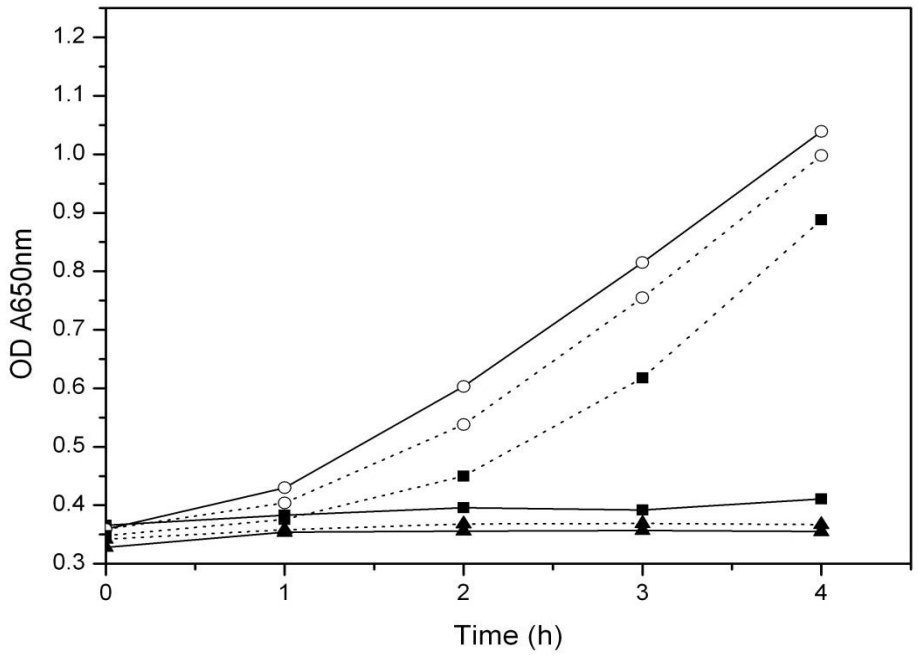

Determination of nitric oxide concentration used for further investigation

The *nirBDC*, *nrfAB*, *norV* and *hmp* strain JCB5210 and the strain JCB5250 with an extra mutation on *hcp* compared to the former, were grown anaerobically in medium that was either unsupplemented (open circles), supplemented with 1 µM (filled squares) or 5 µM nitric oxide (filled triangles). The inoculum was prepared as follows: bacteria was first grown in an overnight culture aerobically until stationary phase, then appropriate amount of the overnight culture was added into steril MS medium, to give a final volume of 100 mL and a starting OD_{650} of 0.2. Cultures were left statically for 2 hours, prior to the addition of NOSW at time 0. As optical density of culture did vary between independent experiments on different days, this graph represents a typical result showing the pattern observed.

Dotted lines, JCB5210; Solid lines, JCB5250.

nitrate. Spot tests indicated that nitrate was gradually converted to nitrite (data not shown). The growth of both of the strains with the *hcp* mutation supplemented with nitrate stopped after approximately 2 to 3 hours while the controls were still growing (Fig 3.4 C & D). On the contrary, strains without the *hcp* mutation were unaffected by the nitrosative stress (Fig 3.4 A & B). The Hcp^+ cultures continued to grow throughout the whole monitored period and those with nitrate addition grew to a higher cell density compared to the control without nitrate supplementation. In contrast, the phenotypes of the *ytfE* mutants were different: growth of the Hcp^- $YtfE^-$ strain, but not the Hcp^+ $YtfE^-$ strain, was inhibited by 5 mM nitrate (Fig 3.4 B & D).

3.5. Complementation of the *hcp* mutants using plasmid-encoded Hcp

For the construction of plasmid pJW11, the *hcp* promoter region together with the *hcp* gene were amplified by PCR from the chromosome of strain RK4353, and digested with HindIII and BamHI. The vector was provided by Dr. Laura Sellar, which was pACYC184 digested with HindIII and BclI. The sticky ends created by digestions with BamHI and BclI are compatible with each other in ligation. As the *hcp* gene on the original position of chromosome in strain JCB5250 had been replaced by a chloramphenicol resistance cassette, strain JCB5250 was already chloramphenicol resistant. In order to proceed with transformation of the Cm^R plasmid pJW11, the chloramphenicol resistance cassette was first removed as described in the Materials and Methods section and JCB5250 was cured of the chloramphenicol resistance (Datsenko and Wanner, 2000). Then the plasmid pJW11 was transformed into the cured JCB5250, while the plasmid pACYC184 was used as the negative control. One transformant for each was purified and grown in minimal salts medium anaerobically, with or without

Figure 3.2.

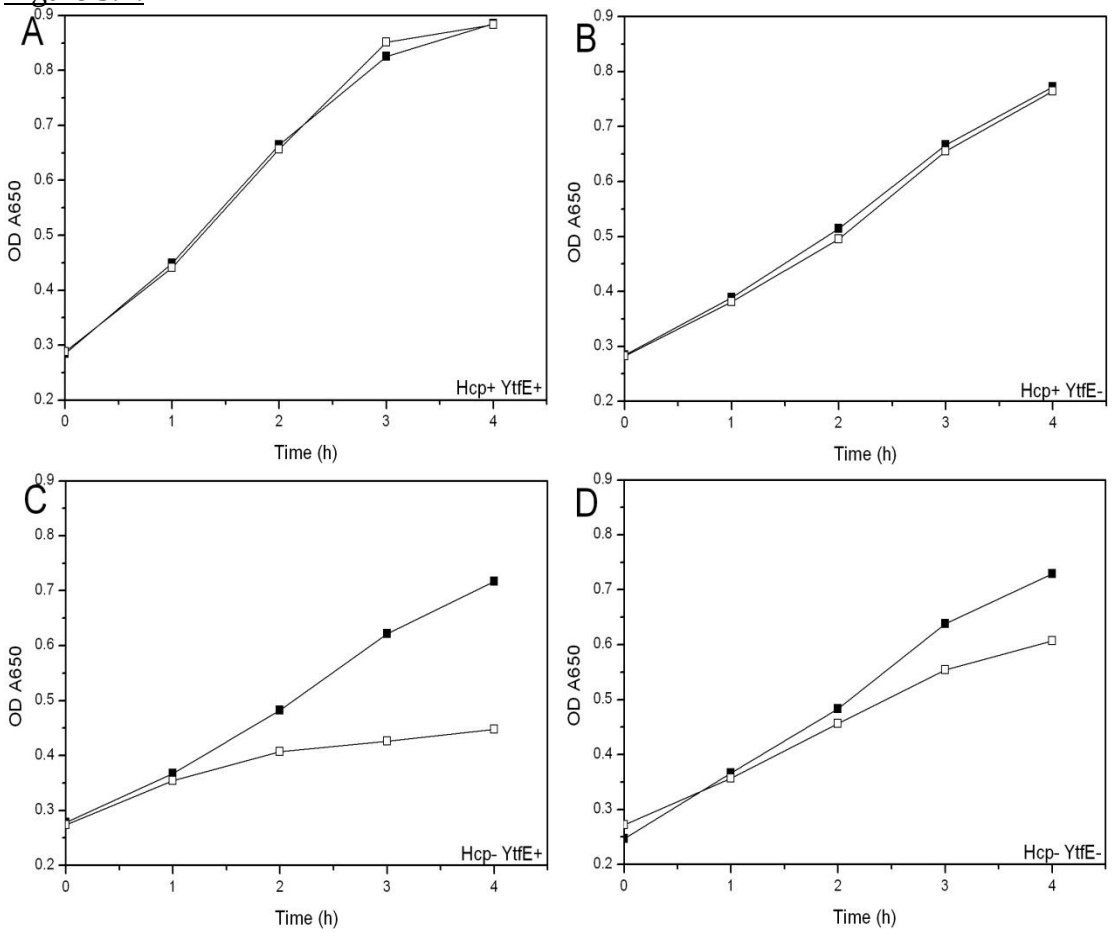

Effect of nitric oxide saturated water on anaerobic growth of strains with different combinations of *ytfE* and *hcp* mutations

A quadruple mutant defective in *nirBD*, *nrfAB*, *norVW* and *hmp* and its derivatives with different combinations of *hcp* and *ytfE* mutations were used. Bacteria were grown anaerobically in minimal salts medium with or without NOSW addition every 30 minutes. The optical density at 650 nm was measured at hourly intervals for 4 hours. Filled squares: control without NOSW addition; Empty squares: 1 µM NOSW addition every 30 min. Growth curves were completed with two independent cultures on different days and this graph represents a typical experiment result. Experiments were not done in triplicate, hence there is no measure of significance.

A, JCB5210; B, JCB5257; C, JCB5250; D, JCB5260.

Figure 3.3.

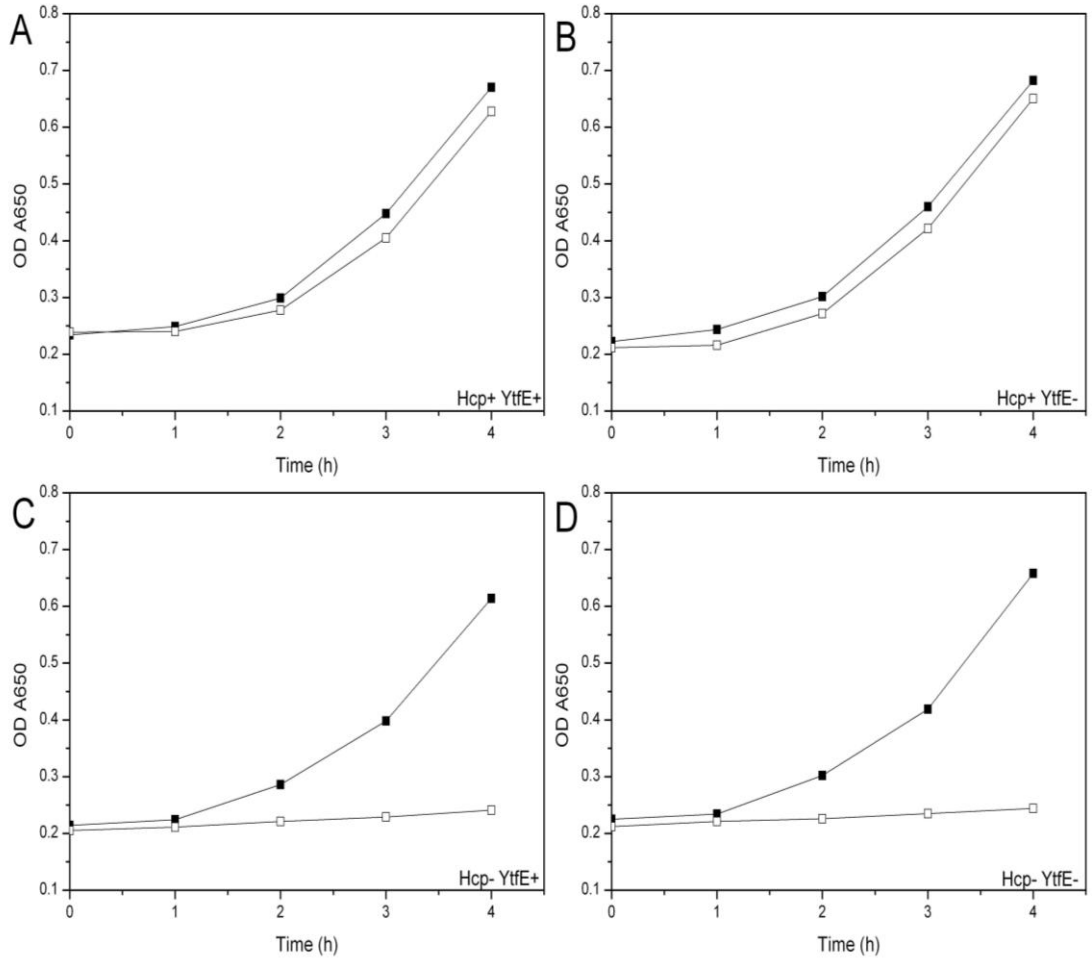

Effect of nitrite on anaerobic growth of strains with different combinations of *ytfE* and *hcp* mutations

Same strains were used as in Fig 3.2. Bacteria were grown anaerobically in minimal salts medium with or without 1 mM nitrite. The optical density at 650 nm was determined at hourly intervals for 4 hours. Filled squares: control without nitrite; empty squares: 1 mM nitrite. Growth curves were completed with two independent cultures on different days and this graph represents a typical experiment result. Experiments were not done in triplicate, hence there is no measure of significance.

A, JCB5210; B, JCB5257; C, JCB5250; D, JCB5260.

Figure 3.4.

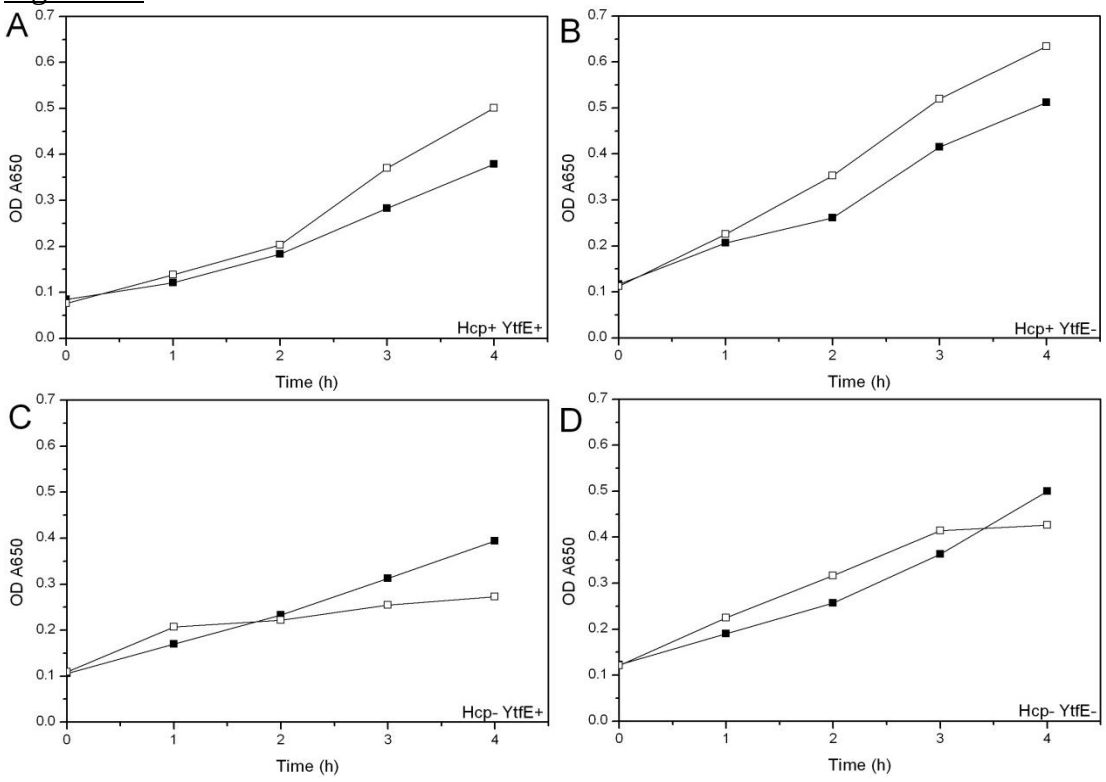

Effect of nitrate on anaerobic growth of strains with different combinations of *ytfE* and *hcp* mutations

The same strains were used as in the previous experiment (Fig. 3. 2). Cultures were grown in 1000 mL MS medium with or without nitrate addition and optical density at 650 nm was determined every hour. Filled squares: control without nitrate addition; Empty squares: 5 mM nitrate addition in the beginning. Growth curves were completed with two independent experiments on different days and this graph represents a typical experiment result. Experiments were not done in triplicate, hence there is no measure of significance.

A, JCB5210; B, JCB5257; C, JCB5250; D, JCB5260.

1 mM nitrite(Fig 3.5 A & B). To check that the sensitivity of nitrosative stress was due to the loss of Hcp instead of YtfE, the $Hcp^{-}YtfE^{-}$ mutant JCB5260 was also included in this complementation (Fig 3.5 C & D). The optical density of cultures with or without nitrite supplemented was determined every two hours to monitor the growth. All four strains grew similarly in anaerobic control cultures without nitrite (Fig 3.5 circles). The *hcp* mutants JCB5250 and JCB5260 transformed with empty plasmid pACYC184 did not grow anaerobically when 1 mM sodium nitrite was added, while the growth of both JCB5250 pJW11 and JCB5260 pJW11 was not affected, compared to the unsupplemented control.

3.6. Study of plasmid-encoded Hcp protein mutants with disrupted hybrid cluster

The plasmid JW11 encoding wild-type *E. coli* Hcp protein was used as the template in mutagenesis reactions to generate derivative plasmids encoding mutated Hcp proteins. The primer pair hcp E492X fwd and hcp E492X rev (Table 2.3) was designed to change the codon encoding the conserved glutamic acid E492 of Hcp from GAA to GNC, which in turn gave four different amino acids: aspartic acid (GAC), valine (GTC), glycine (GGC) and alanine (GCG). The plasmid products from the mutagenesis reactions were isolated and sequenced to confirm each mutation and then transformed into cured JCB5250, the same host strain used in the previous complementation with native Hcp protein. Purified transformants for each mutation were grown anaerobically in the presence or absence of 1 mM nitrite. The transformant with mutated plasmid encoding aspartic acid (D) instead of glutamic acid (E) was referred to as JCB5250 pE492D, the one with valine, glycine, and alanine as JCB5250 pE492V, JCB5250 pE492G, and JCB5250 pE492A, respectively.

Figure 3.5.

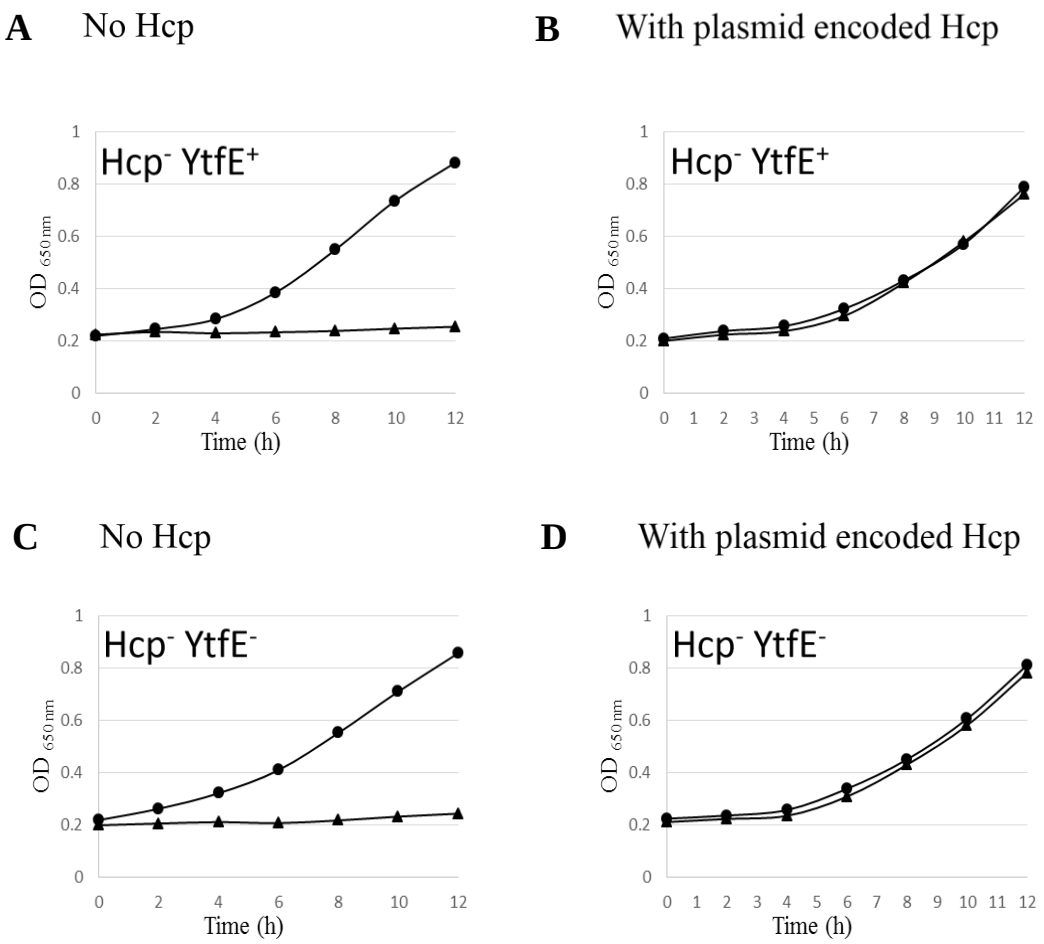

Complementation of *hcp* mutants with plasmid encoding native *E. coli* HCP protein during growth under conditions of nitrosative stress

The *hcp* mutant JCB5250 and JCB5260 were used as host strains for complementation. Bacteria were grown anaerobically at 30°C in minimal salts medium supplemented with chloramphenicol. The optical density at 650 nm of each culture was measured every 2 hours for 12 hours. Growth curves were completed with two independent cultures on different days and this graph represents a typical experiment result.

A, JCB5250 pACYC184; B, JCB5250 pJW11;

C, JCB5260 pACYC184; D, JCB5260 pJW11.

Circles: control without nitrite; Triangles: 1 mM nitrite.

When compared to the cultures without nitrosative stress, two different phenotypes were observed for these four strains grown under nitrosative stress. Growth was restored for strain JCB5250 pE492D (Fig 3.6 C), the same phenotype as the strain JCB5250 pJW11 with plasmid encoding wild-type Hcp protein (Fig 3.5 B). On the other hand, bacterial growth was not observed for the other three strains (Fig 3.6 A, B & D), similar to the growth of the strain JCB5250 pACYC184 used as a negative control without Hcp protein (Fig 3.5 A).

To study the effect of the mutation on Hcp structure, Hcp and its mutants were overexpressed and purified for circular dichroism (CD) spectroscopic analysis. The plasmid pET-HCP overexpressing N-terminal 6xHis-tagged Hcp in pET28a vector was obtained from Almeida *et al* (2006). Following procedures described therein, Hcp protein was overexpressed and purified in this work (Fig 3. 7). The vector pET-Hcp was mutated in the same fashion as previously described for pJW11. The SDS-PAGE analysis showed that the size of the mutant protein was the same as that of the native Hcp, suggesting that mutant proteins were expressed as intact proteins (Fig 3.8). These Hcp mutants were purified in small quantities for the analysis by circular dichroism (CD) spectroscopy.

The CD spectra of the same amount of native Hcp protein and its four mutants were indistinguishable with each other (Fig 3.9 A). Data analysis was completed using CDSSTR method with reference dataset 4, which is explained in the Materials and Methods section (Sreerama and Woody, 2000). According to the analysis, Hcp and its E492X mutants contained about 47% and 12% of α-helical and β-sheet, respectively.

Figure 3.6.

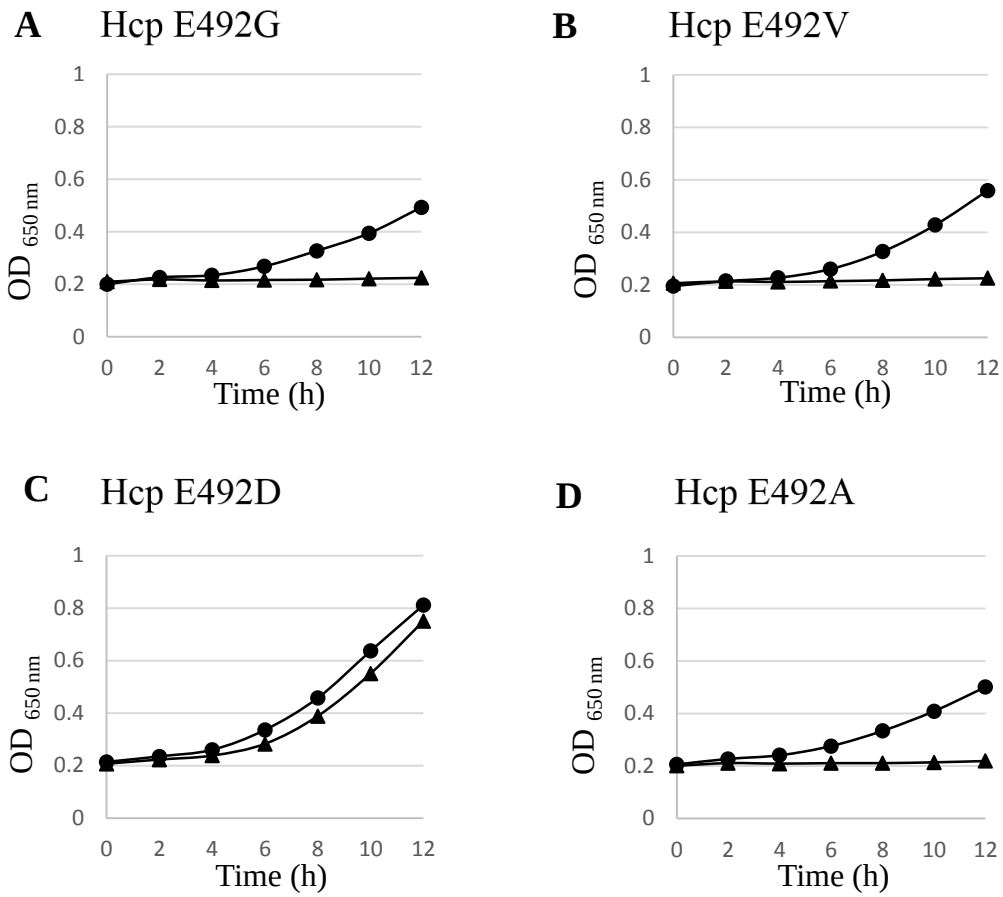

Growth of the *hcp* strain JCB5250 expressing mutated *E. coli* HCP proteins

Bacteria were grown anaerobically in minimal salts medium with or without 1 mM sodium nitrite. The cultures were sampled periodically as indicated. Bacterial growth was monitored *via* measuring optical density at 650 nm. Growth curves were completed with two independent cultures on different days and this graph represents a typical experiment result.

A: JCB5250 pE492G; B: JCB5250 pE492V;

C: JCB5250 pE492D; D: JCB5250 pE492A;

Circles: control without nitrite; Triangles: 1 mM nitrite.

This ratio obtained here using Hcp from *E. coli* matched with that of the predicted secondary structure of Hcp from *D. vulgaris*, which is annotated as containing 50% helical and 11% beta sheet in the Protein Data Bank. The predicted data was calculated from the X-ray crystallography structure (PDB ID: 1W9M), using a well-established algorithm described by Kabsch and Sander in 1983.

3.7. Validation of the method used for the measurement of aconitase activity

In the citric acid cycle, aconitase isomerizes citrate to isocitrate, which is then converted to α-ketoglutarate by the NADP-dependent enzyme isocitrate dehydrogenase (IDH). For one mole of isocitrate oxidized to α-ketoglutarate, one mole of NADP is reduced to NADPH. The generation of NADPH enables continuous spectrophotometric rate determination of the second reaction, which measures the activity of IDH. However, in a coupled reaction where both aconitase and IDH are present and only citrate is added as substrate, the measured activity of IDH is limited by the rate of generation of its substrate isocitrate, which is equal to the aconitase activity, on condition that the activity of IDH is higher than that of aconitase in the same assay. Thus aconitase activity can be determined by measuring the activity of IDH, where the aconitase reaction is the limiting step of the two.

To confirm that IDH of *E. coli* is more active than aconitase in the same cell lysate sample, preliminary experiments compared IDH activity in the coupled reaction with citrate as the substrate and in the single reaction with the same amount of isocitrate. Fig 3.10 indicates that, in strain JCB5210, IDH activity measured using isocitrate as substrate is higher than that using citrate as substrate. The same was also observed for

Figure 3.7.

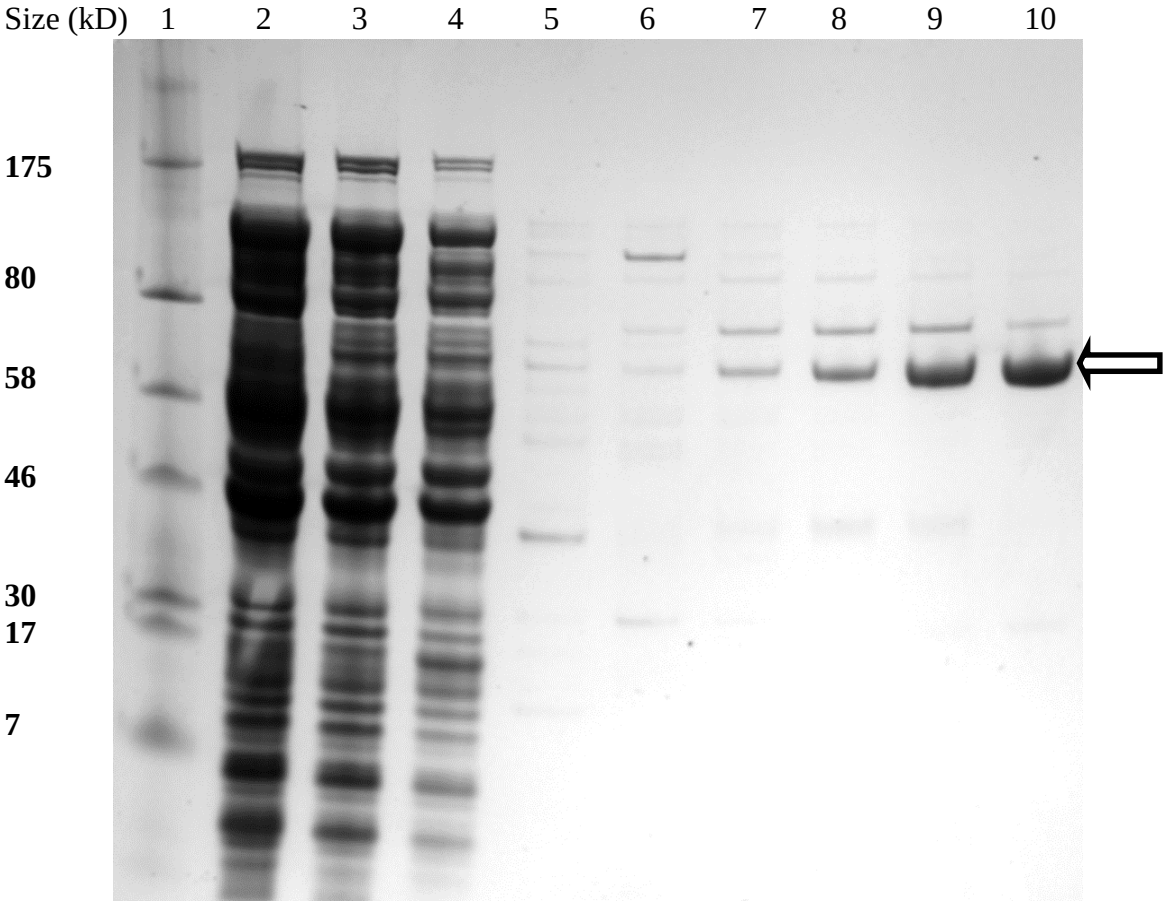

SDS-PAGE gel with samples collected during purification of Hcp

Cell lysate containing Hcp was loaded onto 1 mL His-trap column. Samples were collected during the purification process using gradient elution. Fraction size was set at 2 mL. Arrow indicated band of Hcp protein.

Lane 1: Protein marker;

Lane 2: clear lysate before purification;

Lane 3: flow-through collected while loading column;

Lane 4: fraction collected during wash with 100% (v/v) Buffer A prior to gradient elution;

Lane 5-9: fractions collected from 0 to 30% Buffer B;

Lane 10: fraction collected at around 35% Buffer B;

Figure 3.8.

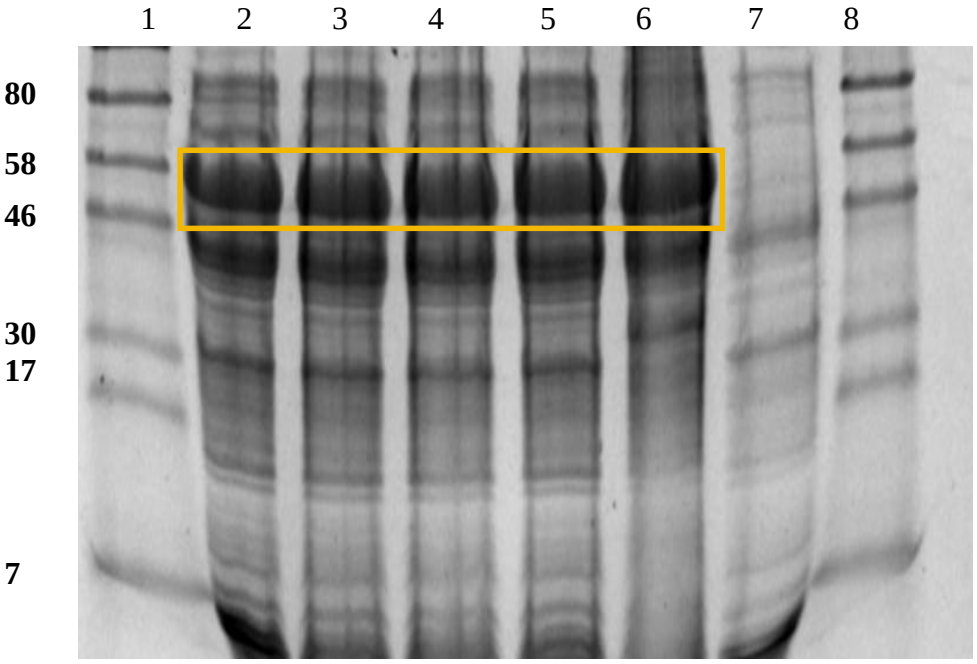

SDS-PAGE analysis of Hcp and the E492X mutants

Plasmid pET-HCP and its E492X derivatives were transformed into BL21(DE3). Cells were harvested after 3 hours of IPTG induction. Protein bands in the yellow square are Hcp and its mutants.

From left to right:

Lane 1: Protein marker;

Lane 2: native Hcp protein;

Lane 3: mutant protein Hcp E492V;

Lane 4: mutant protein Hcp E492G;

Lane 5: mutant protein Hcp E492A;

Lane 6: mutant protein Hcp E492D;

Lane 7: control without IPTG induction;

Lane 8: Protein marker.

Circular dichroism spectra of native Hcp and its E492X mutants

(A) Absorption spectra at the upper half panel showing the overlay of the spectra of the native Hcp and its four mutants with E492X substitutions. All spectra were obtained in 0.01 M phosphate buffer (pH 7.4). The volume of each protein sample used was adjusted so that the final concentration in the cuvette was about 0.02 mg/mL. The bottom half of panel A shows the readings of high tension voltage (HT) at different wavelengths. This is a parameter indicating how difficult the detector is at picking up the signal. If the HT reading exceeds the maximum threshold of 700 mV, the recordings become unreliable. In this experiment, only the data under 600 mV of HT was used in analysis.

Purple: native Hcp protein; Green: Hcp E492V; Blue: Hcp E492G;

Red: Hcp E492A; Black: Hcp E492D.

(B) Graphic output from the Dichroweb comparing spectrum of experimental data and calculated spectrum. The data collected from the native Hcp protein was shown here as an example.

Green line: plot of actual data collected during CD spectrum measurement;

Blue line: calculated spectrum generated by the algorithm of CDSSTR;

Purple vertical lines: difference spectra between experimental and calculated spectra.

Figure 3.9.

A

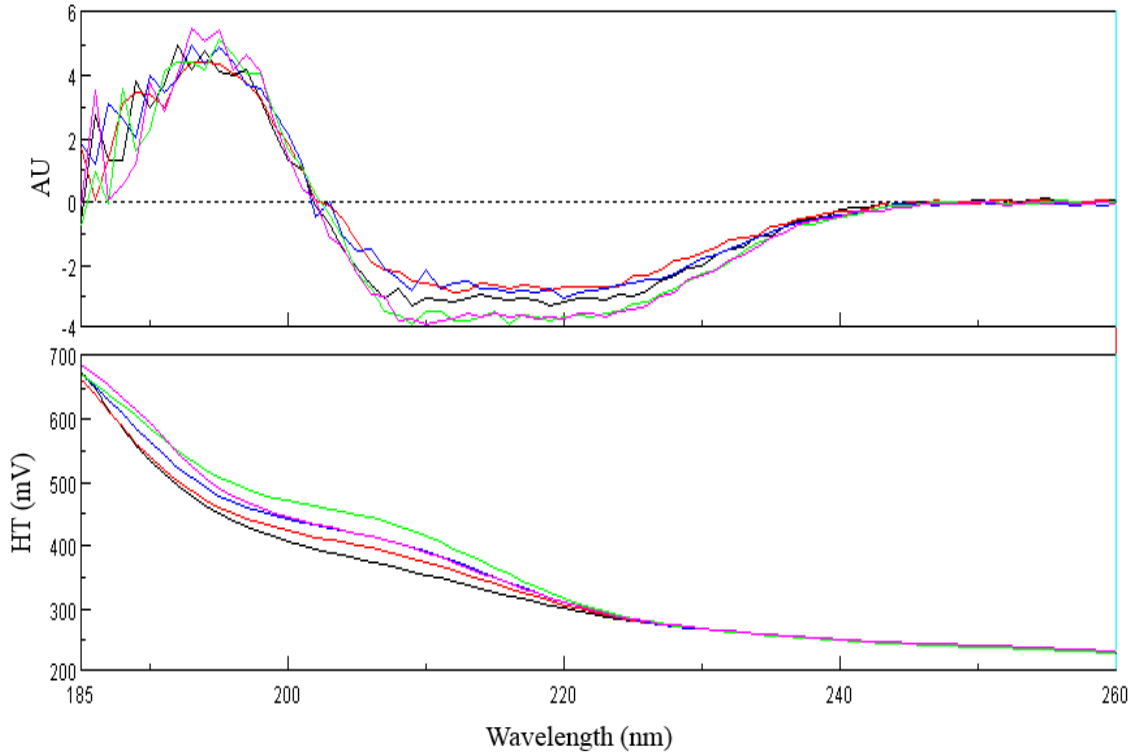
AU
HT (mV)
Wavelength (nm)

B

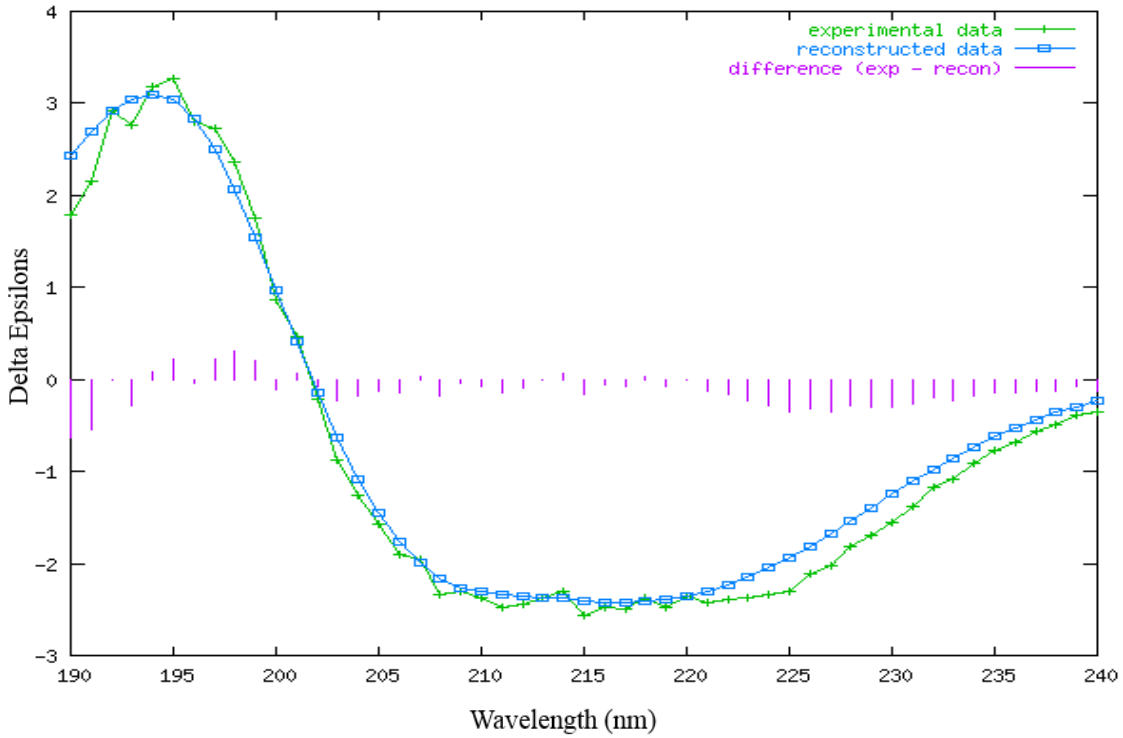
experimental data
reconstructed data
difference (exp - recon)
Delta Epsilons
Wavelength (nm)

the other *E. coli* strains used in this study (data not shown). Thus, the measurable IDH activity determined using citrate as the sole substrate is limited by and equals the aconitase activity.

3.8. Aconitase activities of isogenic mutants under nitrosative stress

Aconitase activities in cell-free extracts of the four isogenic strains that had been grown anaerobically with or without nitrate were determined. Cells from the growth study using nitrate as source of stress were harvested for aconitase activity assay, which was then normalised by protein concentration (Fig 3.11). The aconitase activities of all the control cultures without nitrate could invariably be detected. The aconitase activities of the strain JCB5210, which is *hcp*$^{+}$*ytfE*$^{+}$, were higher than the others. The activity of another enzyme (isocitrate dehydrogenase) was assayed under the same condition and this same phenomenon was also observed (data not shown). For cultures supplemented with nitrate, only two strains had detectable aconitase activity. They were both *hcp*$^{+}$, but either *ytfE*$^{+}$ or *ytfE*. In contrast, aconitase was completely inactivated in *hcp* mutants, again, with or without *ytfE*, under nitrosative stress.

Aconitase activity was also assayed in cultures grown with or without 1 μM NOSW. The same procedure of treating NOSW was followed as in growth experiment in Fig 3.2. However, as the *hcp* mutants were growing poorly under stress, to obtain an adequate amount of cells, the culture volume was scaled up to 2 L each. A similar pattern was observed as that from nitrate supplemented cultures (Fig 3.11 vs. 3.12). However, with *hcp* mutant strains, marginal activity was detected in NOSW supplemented cultures, whereas no activity was detected in nitrate supplemented cultures (Fig 3.12 C & D).

Figure 3.10.

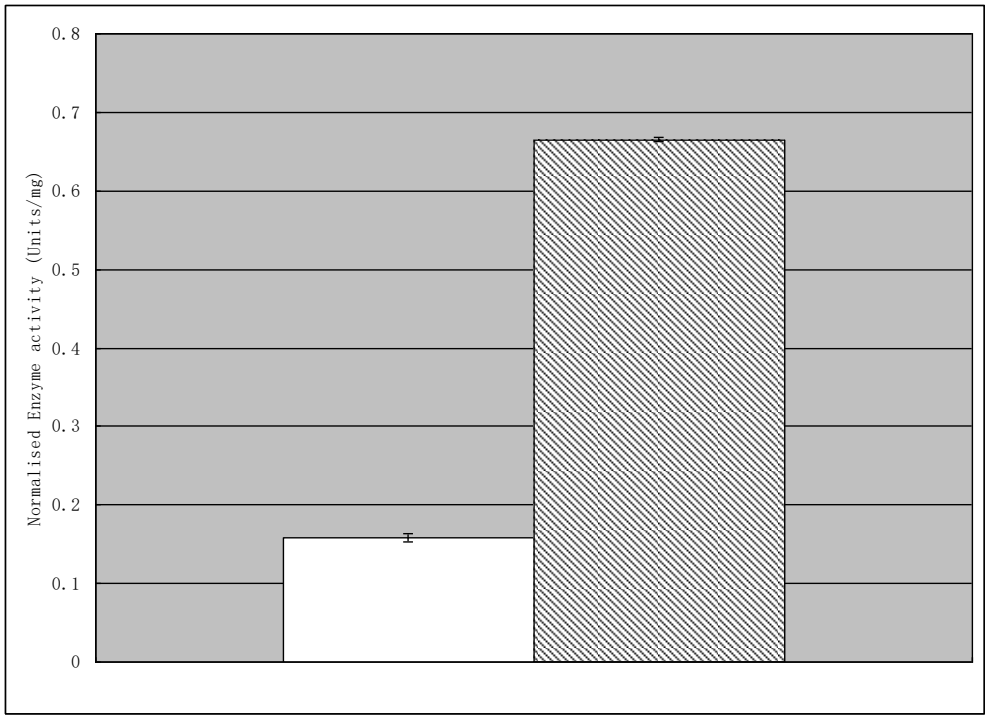

Comparison of measurable isocitrate dehydrogenase activities determined using citrate or isocitrate as substrates

The quadruple mutant, strain JCB5210, defective in *nirBD*, *nrfAB*, *norVW* and *hmp* was used to compare the isocitrate dehydrogenase activities measured using citrate or isocitrate as substrate. Bacteria were grown anaerobically in minimal salts medium. Four hours after inoculation, cells were harvested and sonicated. Then the crude cell extract was centrifuged to obtain clear supernatant. The measurable IDH activities in the supernatant were compared, using either citrate or isocitrate as the sole substrate. Empty bar: IDH activity measured with citrate being added as the only substrate; shaded bar: IDH activity measured with isocitrate being added as the only substrate. Two independent experiments were repeated with each assayed in duplicate and standard deviations of the mean were represented by error bars.

Figure 3.11.

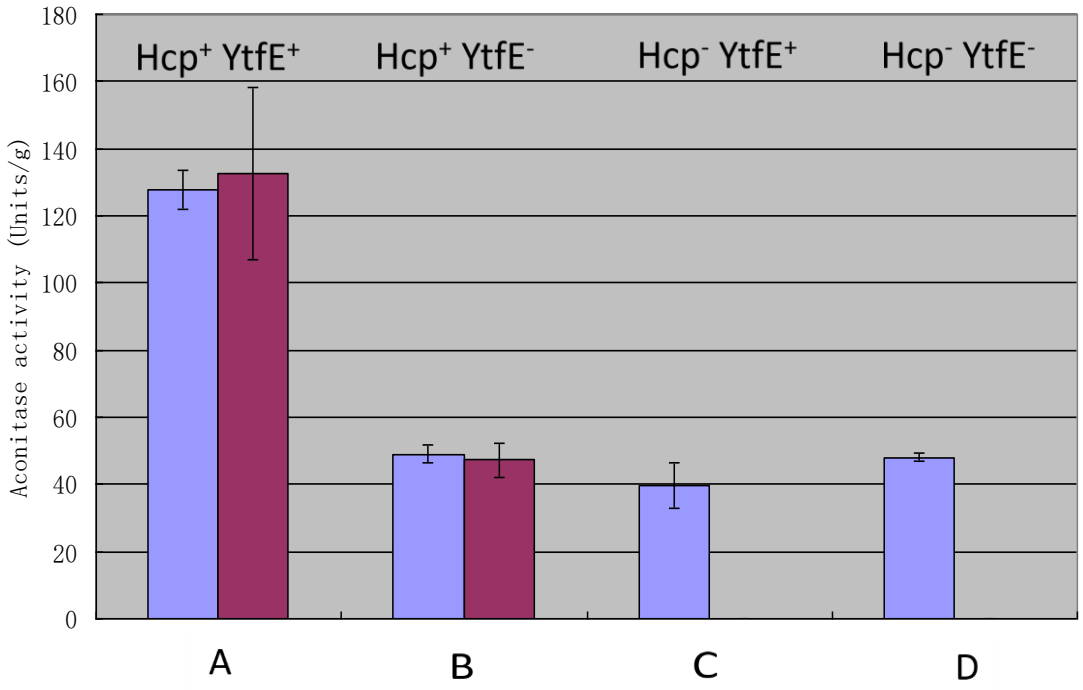

Effect of nitrate on aconitase activity of strains with different combinations of *ytfE* and *hcp* mutations grown anaerobically

Cultures were grown as described in Fig 3. 4. Cells were harvested and sonicated for aconitase assay. Aconitase activities were normalized by protein concentrations. Blue bars: control without nitrate addition; purple bars: 5 mM nitrate addition in the beginning. Two independent experiments were repeated with each assayed in duplicate. Standard deviations of the mean are represented by error bars. Note that aconitase activity was undetectable in nitrate-supplemented cultures of the two Hcp- strains, C and D. Data for this graph was shown in Table 3.1.

From left to right in order: A, JCB5210; B, JCB5257; C, JCB5250; D, JCB5260.

Table 3.1. **Aconitase activity of isogenic mutant strains under nitrosative stress**

Official name	Descriptions	With (+) or without (-) 5 mM nitrate addition	Aconitase activity (Units/g) A§		B§		Average	St Dev
JCB5210	RK4353* *nirBDC nrfAB norV hmp*	+	113.9	115.3	149.7	152.1	132.8	±21.0
		-	129.0	120.0	121.3	125.5	124.0	±4.1
JCB5257	RK4353 *nirBDC nrfAB norV hmp ytfE*	+	45.9	43.8	49.7	51.9	47.8	±3.6
		-	46.0	48.3	51.3	50.6	49.1	±2.4
JCB5250	RK4353 *nirBDC nrfAB norV hmp hcp*	+	<0.1	<0.1	<0.1	<0.1	<0.1	0
		-	47.7	41.5	34.6	35.2	40.0	±6.2
JCB5260	RK4353 *nirBDC nrfAB norV hmp hcp ytfE*	+	<0.1	<0.1	<0.1	<0.1	<0.1	0
		-	47.0	50.7	46.1	47.8	47.9	±1.2

Unit definition: One unit will convert 1.0 µmole of citrate to isocitrate per minute at pH 7.4 at 37℃.

§ Group A and B were independent experiments done on different days. Each cell lysate was assayed twice for aconitase activity.

Figure 3.12.

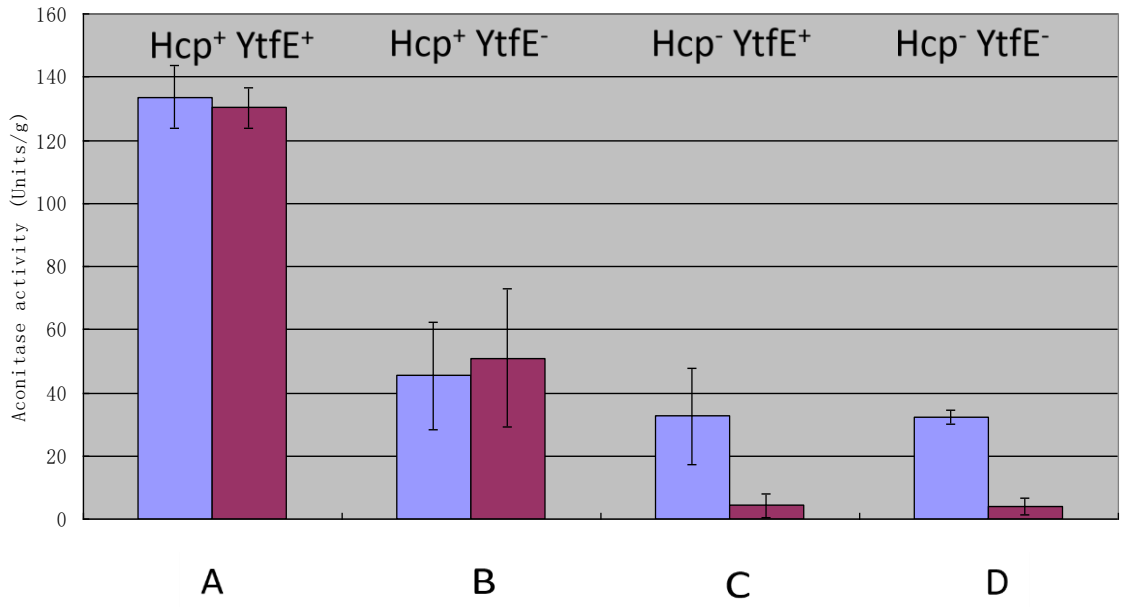

Effect of nitric oxide on aconitase activity of strains with different combinations of *ytfE* and *hcp* mutations grown anaerobically

Cultures were grown as described in Fig 3.2, except that the volume of each culture was scaled up to 2 L. Nitric oxide saturated water (NOSW) was added every 30 minutes for 4 hours. Then cells were harvested and sonicated for aconitase assay. Presented are specific aconitase activities normalized by protein concentrations. Blue bars: control without NOSW; purple bars: 1 μM NOSW addition every 30 minutes. Two independent experiments were repeated with each assayed in duplicate. Standard deviations of the mean are represented by error bars.

From left to right in order: A, JCB5210; B, JCB5257; C, JCB5250; D, JCB5260.

3.9. Construction of strain JCB701 MG1655 *acnB::6xhis*

To purify aconitase B from other proteins in whole cell extract for further study, the *acnB* gene in *E. coli* strain MG1655 was coupled to a 6xHis epitope tag using a chromosomal modification technique termed gene doctoring, which was described in the materials and methods section. First the plasmid *acnB* pDOC-H was constructed in this work, *via* sub-cloning from the plasmids *acnB* pDOC-F and pDOC-H provided by Dr David Lee (Fig 3.13). Plasmid *acnB* pDOC-H was transformed into the competent cells of MG1655. It was the donor plasmid carrying a target DNA sequence containing 475 bp of homology to the 3' end of *acnB* without the stop codon, the coding sequence for the 6 x His tag followed by a stop codon, a kanamycin resistance cassette and 404 bp of homology to the DNA sequence immediately downstream of the chromosomal *acnB* gene. With the aid of a co-transformed recombineering plasmid pACBSCE, this target DNA sequence was excised from the donor plasmid *acnB* pDOC-H *in vivo* and recombined into the chromosome to replace the original 3' end of *acnB* and its immediate downstream sequence. Hence the new recombinant MG1655 *acnB::6* x *His* was generated with the *acnB* gene tagged to a protein marker, and a selectable kanamycin resistance. The target DNA sequence was amplified from the chromosome of the recombinant in PCR reaction (Fig 3.14). The primers used anneal to the upstream and downstream of the recombineered target DNA sequence respectively. The PCR product was sequenced to check that the 3'-end homology of *acnB* is correct and is in frame with the coding sequence of the 6xHis epitope tag. This strain was used by collaborators in the project for a more detailed biochemical study on aconitase.

Figure 3.13.

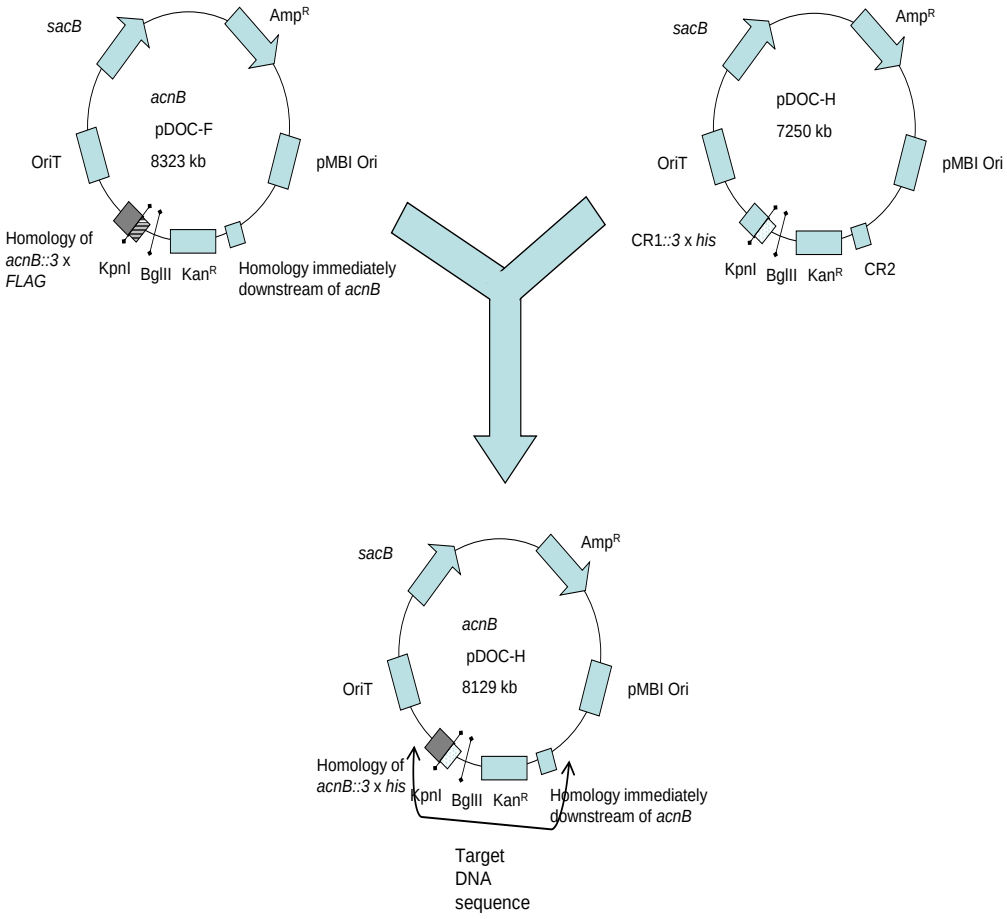

Schematic outline of the construction of *acnB* pDOC-H by sub-cloning

From plasmid *acnB* pDOC-F, a vector was generated by removing the DNA fragment between the two enzyme digestion sites (KpnI and BglII) which contained the undesired FLAG epitope tag. This was replaced by the short DNA fragment containing the 6 x his epitope tag between the two enzyme digestion sites, excised from the pDOC-H plasmid. The vector and insert were ligated to create the donor plasmid *acnB* pDOC-H used in the following gene doctoring procedures. The target DNA sequence to be recombineered to the chromosome was indicated within the bracket.

Figure 3.14.

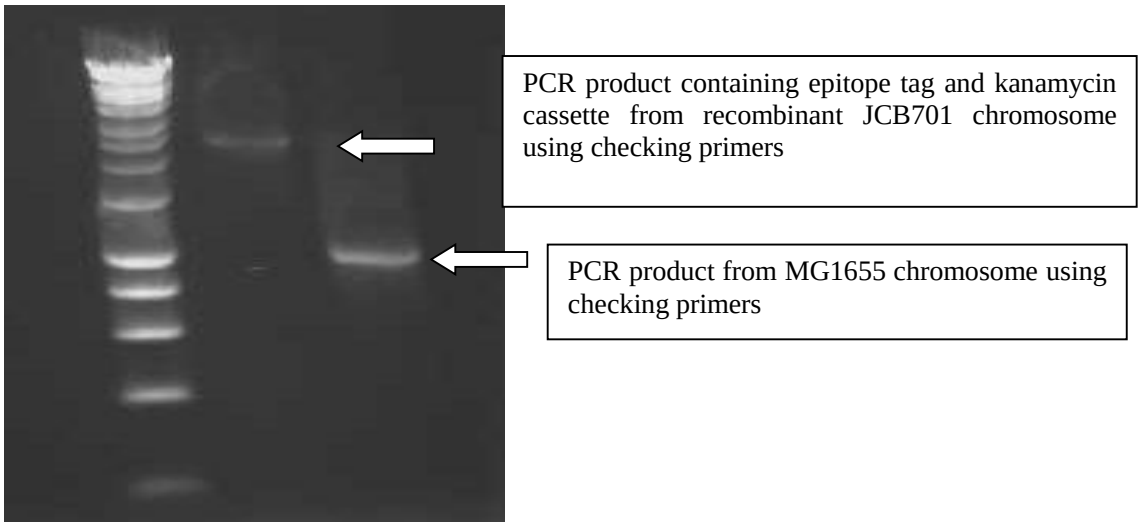

Verification of chromosomal *acnB::His* fusion

Ethidium bromide stained agarose gel showing DNA amplified by PCR from the *acnB* fusion strain JCB701 and parent *E. coli* strain MG1655. Checking primers used in PCR reaction anneal to the upstream and downstream of the modified DNA region on the chromosome. The DNA ladder used was Hyper Ladder I from Bioline.

3.10. Attempts to protect or repair nitrosylated aconitase B using purified Hcp

It was confirmed by Bao (2013) that aconitase B from JCB701 was correctly tagged and can be purified using a nickel affinity column. After purification, aconitase B activity can be reactivated up to 1000 U/g using Fe^{2+}, cysteine and DTT (Bao, 2013). Partially purified aconitase after reactivation was obtained from the MSc student Xiaoyan Bao. The purified Hcp used was purified earlier in this work as shown in lane 10 of Fig 3.7.

The NO concentration used and timing were determined in reference to the *in vitro* experiment reported for the reactivation of aconitase B using YtfE protein (Justino *et al*., 2007). In rubber bung sealed bottles, four reactions were set up in parallel, namely control No.1 with aconitase only, control No.2 with aconitase treated with NO, test No.1 with aconitase being treated with NO and then supplemented with Hcp, and test No.2 with Hcp added prior to aconitase being exposed to NO. Aliquots (2 mL) of aconitase B (54.8 U/g) in 50 mM Tris buffer (pH 7.4) were dispensed into each vial. For test No.2, 100 µM of Hcp was added together with aconitase. Before NO was added, the inner atmosphere of these bottles was made anaerobic by adding the following oxygen scavenging reagents: 30 mM of glucose, 4 U/mL of glucose oxidase, and 20 U/mL of catalase. The vials were left at room temperature for 5 minutes to ensure complete removal of oxygen. At time zero, 50 µM of NO was added into each vial apart from control No.1. Ten minutes after NO addition, Hcp (100 µM) was added into test No.1. Samples were taken every 10 minutes for immediate measurement of aconitase activity (Fig 3. 15). Purified aconitase activity was relatively stable in control No.1 during the time course. Around 63% of the initial activity in control No.2 was detected after 10 minutes of NO treatment, yet the activity did not progressively decrease over the next

20 minutes. In test No.1, 10 minutes after the addition of NO, the supplement of Hcp did not reactivate and increase the aconitase activity. In comparison, in test No.2, the supplement of Hcp before the addition of NO did not protect aconitase from being damaged, as the aconitase activity still decreased down to 60% after 10 minutes. To summarize, the presence of Hcp did not affect aconitase activity treated with NO, regardless of the order of Hcp and NO addition (Fig 3. 15).

Figure 3.15.

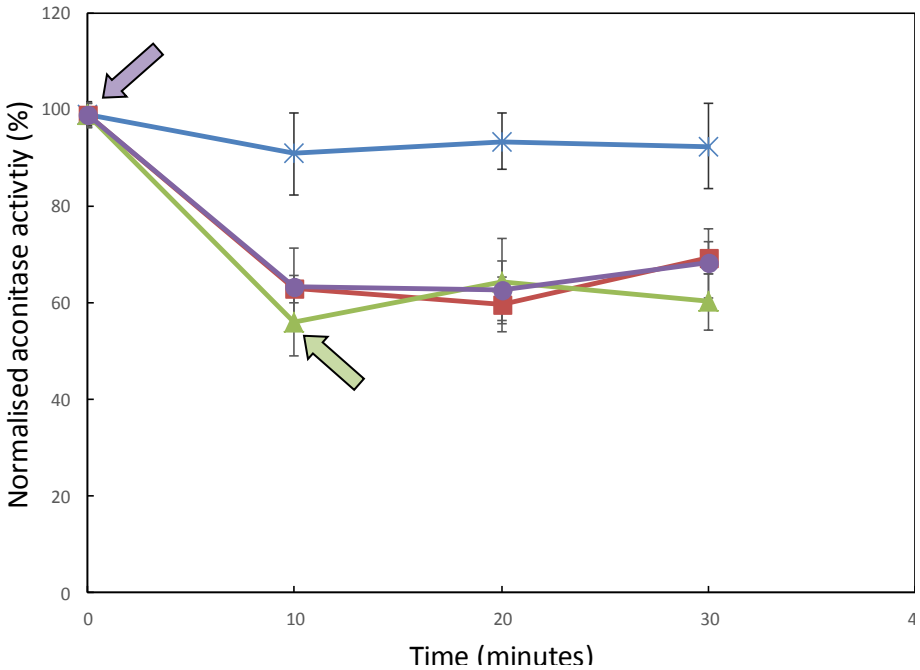

Effect of Hcp addition on aconitase activity in the presence of NO

The experiment was set up in anaerobic vials where oxygen was removed by a mixture of glucose, glucose oxidase and catalase. NOSW was used at time zero to treat aconitase with or without Hcp in the vial. Arrow indicated Hcp addition for each test with corresponding colour. The 100% starting acontiase activity was 54.8 U/g. Aconitase activity was assayed twice for each sample, using two spectrophotometers in parallel. A different batch of protein was used for biological replica. Error bars represented standard deviation of the averaged values.

Asterisks: control No.1 aconitase without NO;

Squares: control No.2 aconitase with 50 µM of NO;

Triangles: test No.1 with aconitase being treated with 50 µM of NO for 10 minutes and then supplemented with 100 µM Hcp;

Circles: test No.2 with 100 µM Hcp added prior to aconitase being exposed to 50 µM NO.

CHAPTER 4

Interaction between Hcp and Hcr

4.1. Introduction

It was demonstrated in Chapter 3 that Hcp has an important role in defending anaerobic cultures of *E. coli* against nitrosative stress. But how does Hcp function to fulfill this role? Several aspects can be considered when searching for an unknown function of a protein, the most obvious one being the protein sequence and structure. For Hcp, the structure has been solved a decade ago when Hcp proteins from *D. vulgaris* and *D. desulfurvibrio* were successfully sequenced and crystallized. However, there have been no reports of the interaction of Hcp with other proteins.

In this chapter, the bacterial two-hybrid system was used to investigate interaction between Hcp and other proteins. It requires the construction of the two-hybrid vectors expressing the prey and bait proteins each fused to functionally reconstitutable enzyme units. At the current stage, a few candidates are shortlisted as possible interactive partners of Hcp. Based on the observation obtained in chapter 3 that aconitase was active in *hcp*$^+$ strains but inactive in *hcp* mutant strains, one possible function of Hcp might be to repair the Fe-S centre of aconitase, a role that has already been proposed for the YtfE protein. Another possible explanation was that Hcp prevents aconitase from being damaged by protecting its Fe-S centre from exposure to NO. In both cases of repair or prevention, direct interaction between Hcp and aconitase was assumed. Another protein candidate is Hcr, the NADH-dependent oxido-reductase of Hcp. The *hcr* gene is immediately downstream of *hcp* in *E. coli*, sharing the same operon. The assessment of the interaction between Hcp and Hcr might provide a positive control among the interactions tested using the plasmid constructs made in this work. Additional proteins of interest were also included. In total the following proteins were

assessed: Hcp, Hcr, YtfE, AcnB and NsrR. Positive interaction was found between Hcp and Hcr. The Hcp E492X mutants were used in the two-hybrid system to test whether the hybrid cluster is required for the interaction between Hcp and Hcr.

The Hcr protein contains FAD and a [2Fe-2S] cluster as cofactors (van der Berg *et al.*, 2000). Judging from the redox potentials of the putative active centres of Hcp and Hcr, it was proposed that the electron was transferred from the redox couple $NADH/NAD^+$ in a step-wise manner, *via* the 2Fe-2S centre of Hcr and the cubane cluster of Hcp, to the hybrid cluster of Hcp (van den Berg *et al.*, 2000, Fig 4.1). Following this electron pathway, Hcp possibly functions as a reductase when the electron is finally passed on to an electron acceptor — the unknown substrate. This was previously suggested to be NO, due to an interesting structure feature of Hcp. The hybrid cluster of Hcp of *D. vulgaris*, especially the Fe8 and its immediate environment, is readily accessible by a hydrophobic cavity (Cooper *et al.*, 2000). Hydrophobic channels in proteins were previously suggested to be involved in gas storage and gaseous substrate access to active sites (Montet *et al.*, 1997).

In this chapter, an attempt was made to reconstitute the theoretical electron transfer chain depicted in Fig 4.1, with NO being the putative terminal electron acceptor. A sensitive NO electrode that is capable of measuring a physiological range of NO concentration was utilized. All the components in this electron transfer chain were prepared, and then added into the NO electrode. The Hcp protein used here was purified previously in the last chapter (Fig 3.7). To obtain Hcr protein, the plasmid pJW21 overexpressing Hcr was constructed in the protein expression vector, pET28a. Then

Figure 4.1.

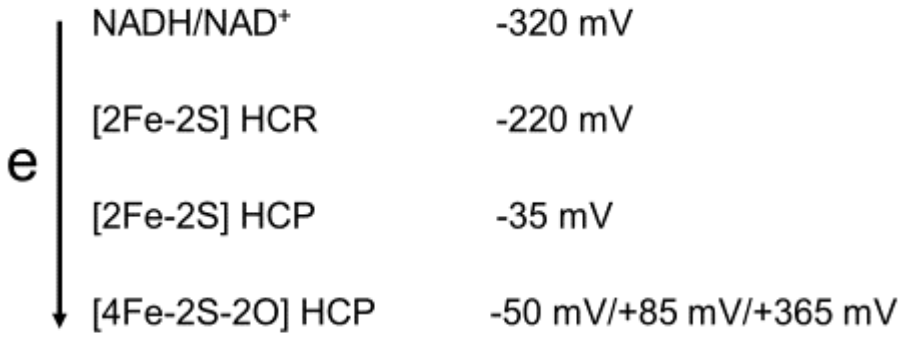

Hypothesized electron transfer pathway for the reduction of Hcp protein

It was proposed by van der Berg *et al* (2000) that electrons flow from NADH with the low reduction potential (Em of the NAD^+:NADH = -320 mV), to the Fe-S centre of Hcr, then to the conventional 4Fe-4S centre of Hcp, and finally to the hybrid cluster of Hcp, which was the putative active centre of Hcp.

Hcr will overexpressed and purified.

Previously Hcp and Hcr have been purified by van der Berg *et al* (2000) under strictly anaerobic conditions throughout. However, stringent anaerobic system is a very demanding condition, which is not plausible for most of the laboratories in the world due to limit of funding and laboratory instruments. The Hcp protein encoded by pET-HCP, purified under ambient conditions, was shown to be biochemically active as a peroxidase (Almeida *et al.*, 2006). It is not clear whether Hcr purified under ambient conditions would remain biochemically active, or can simply be activated after purification like aconitase B. Therefore, purification of these two proteins under ambient conditions was attempted in this work, so that any positive results obtained could be further adapted by others.

The assessment of the ability of Hcp to interact with its oxidoreductase, Hcr, was followed by a question: could Hcp function without Hcr? In an attempt to address this question, an *hcr* derivative of the quadruple mutant JCB5210 was constructed. Its phenotype was compared with the *hcp*$^+$*hcr*$^+$ strain JCB5210 and the *hcp hcr*$^+$ strain JCB5250.

4.2. Construction of two-hybrid plasmids expressing chimeric proteins

The vector plasmids used for the bacterial two-hybrid interaction studies were the pKT25, pUT18 and pUT18C, as described in the Materials and Methods in Chapter 2. Linear vectors were prepared by digesting the aforementioned plasmids with PstI and BamHI (Fig 4. 2 A). Inserts were amplified from the chromosomal DNA (*hcp*, *hcr* and

Preparation of vectors and inserts for subcloning

A, vector plasmids linearised by double digestion with PstI and BamHI.

From left to right: lane 1, Hyper Ladder I; lane 2, pKT25; lane 3, pUT18; lane 4, pUT18C; lane 5, Hypper Ladder I

B, inserts amplified from genomic DNA of *E. coli* strain MG1655. After cleaning-up, inserts were digested by PstI and BamHI. For the inserts of Hcp, the desired upper bands were excised from the gel and purified after digestion. From left to right: Lane 1, Hyper Ladder I; lane 2, digested Hcp insert ready to be ligated into pKT25 (abbreviated as Hcp pKT25, size 1657 bp); 3, Hcp pUT18/C 1656 bp; 4, Hcp pKT25 and pUT18/C primers only control; 5, Hcr pKT25 973 bp; 6, Hcr pUT18/C 972 bp; 7, Hcr pKT25 and pUT18/C primers only control; 8, YtfE pKT25 667 bp; 9, YtfE pUT18/C 666 bp; 10, YtfE pKT25 and pUT18/C primers only control; 11, Hyper Ladder I.

Figure 4.2.

(A) Size (bp) 1 2 3 4 5

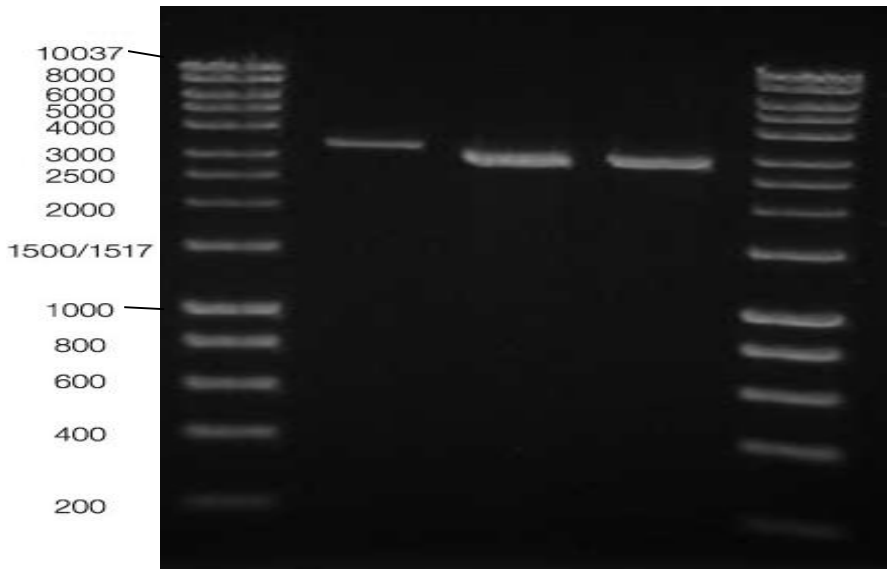

(B) Size (bp) 1 2 3 4 5 6 7 8 9 10 11

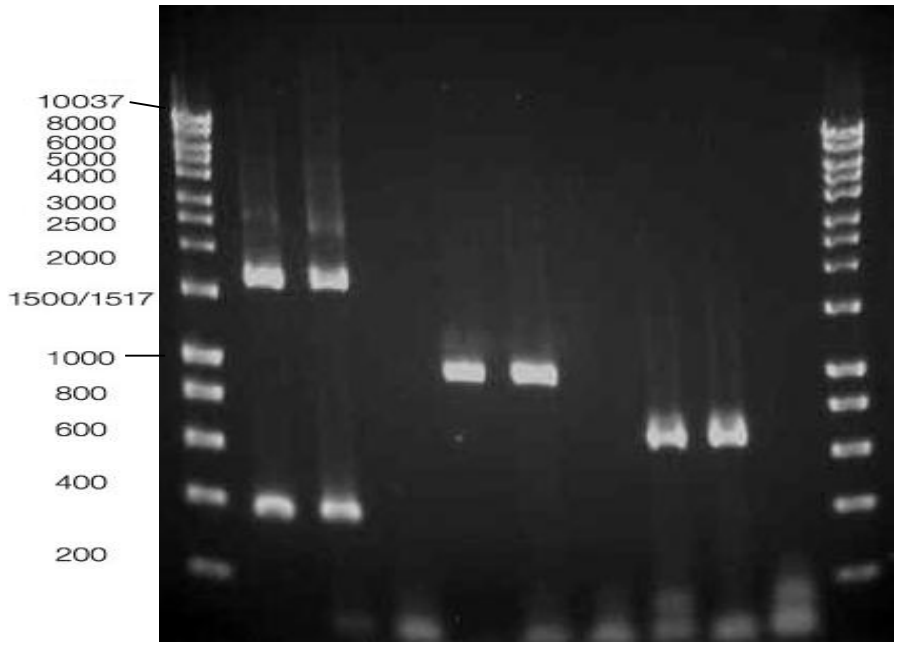

Figure 4.3.

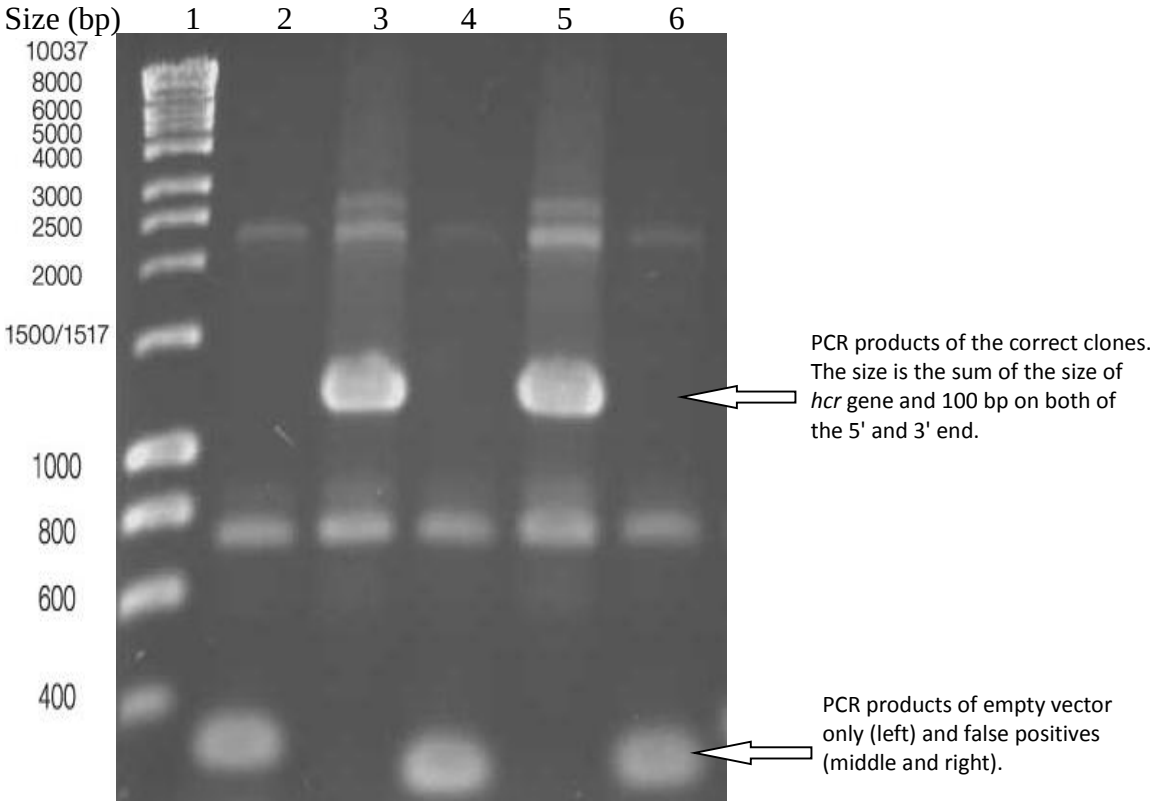

Confirmation by PCR of clones constructed for the bacterial two-hybrid experiment

One representative example for screening the successful pUT18 clones with Hcr protein fusions is given. The primers used were pUT18 fwd/rev checking primers (see primers table), annealing to approximately 100 bp upstream and 100 bp downstream of the cloned *hcr* DNA. Screened candidates with no *hcr* insert would give a PCR product smaller than 400 bp, while successful clones would give a PCR product of approximately 1200 bp due to amplified *hcr* sequence with both 100 bp upstream and downstream small DNA fragments. From left to right: Lane 1, Hyper Ladder I; lane 2, control (*E. coli* strain BTH101 containing empty plasmid pUT18); lane 3, clone candidate No. 1; lane 4, clone candidate No. 2; lane 5, clone candidate No. 3; lane 6, clone candidate No. 4.

ytfE) of *E. coli* strain MG1655 using two-hybrid cloning primers and then also digested with PstI and BamHI (Fig 4.2 B). After ligation, clones were checked by cell PCR using two-hybrid checking primers, which anneal to the vector sequences in the plasmids, approximately 100 bp upstream and downstream of the genes being subcloned. The size of the PCR products of correct clones is larger than that of false positives due to the insertion of the gene (Fig 4.3). The two-hybrid plasmids were subsequently sequenced to ensure that the cloned gene is fused correctly in frame with the coding sequence of the fragment in the vector, using the sequencing service provided by the functional genomics facility in University of Birmingham.

4.3. Quantitative determination of interaction strength using β-galactosidase activity assay

The low-copy number fusion plasmid pKT25-X was transformed into the competent *E. coli* strain BTH101, where X is one of the two proteins to be tested for interaction. The transformant BTH101 pKT25-X was selected on the basis of its kanamycin resistance. TH single tranformant was re-transformed with the high-copy number fusion plasmid pUT18-Y (or pUT18C-Y). The cotransformant was selected using both kanamycin and ampicillin resistance. Cell PCR tests were used to double check that both plasmids with the correct fusion (X or Y) were present in the same clone. For qualitative determination of positive interactions, transformants were first plated onto MacConkey medium plates supplemented with 1% (w/v) maltose and antibiotics. After 48 hours of incubation at 30℃, strains accumulating hybrid proteins that interact gave bright red colonies with a radiating haze in the medium, while negative ones gave colorless colonies, or a red dot in the middle of a colorless colony.

For quantitative measurement of interaction strength, the β-galactosidase activity of the co-transformant was determined after three hours of anaerobic growth in liquid LB medium supplemented with 0.4% (v/v) glycerol. Leucine zip interaction was included as the positive control, which was about 5000 to 6000 β-galactosidase activity units. Putative interaction pairs of interest were tested, including Hcp and Hcr, Hcp and YtfE, Hcp and AcnB, and YtfE and AcnB (Fig 4.4). A plasmid encoding pKT25-AcnB was acquired from Tang *et al* (2005). Proteins Hcp and Hcr interacted with each other. The interaction strength was about 50% of that of the leucine zip positive control. No positive interaction was observed between various combination of Hcp, YtfE and AcnB (Table 4.1). Hcr did not interact with YtfE or AcnB.

The transcriptional regulator NsrR was cloned into the bacterial two hybrid system and tested with other proteins in every combination. It did not interact with Hcp, Hcr, AcnB or YtfE. In addition, each protein was tested with itself to examine the possibility of dimerization, but no positive interactions were found (Table 4.1).

4.4. Positive interactions between Hcr and Hcp proteins with E492X substitutions

The Hcp mutants with the same E492 substitutions were further investigated in their ability to interact with Hcr. Another round of site-directed mutagenesis, using the same primer pair of hcp E492X fwd and hcp E492X rev, was applied to bacterial two-hybrid plasmid pUT18C-Hcp. Four plasmids were obtained: pUT-E492D, pUT-E492V, pUT-E492G, and pUT-E492A. Each was transformed into BTH101 competent cells already harboring the plasmid pKT25 Hcr. Transformants were purified on a MacConkey medium plate supplemented with kanamycin and ampicillin. Colonies of

Figure 4.4.

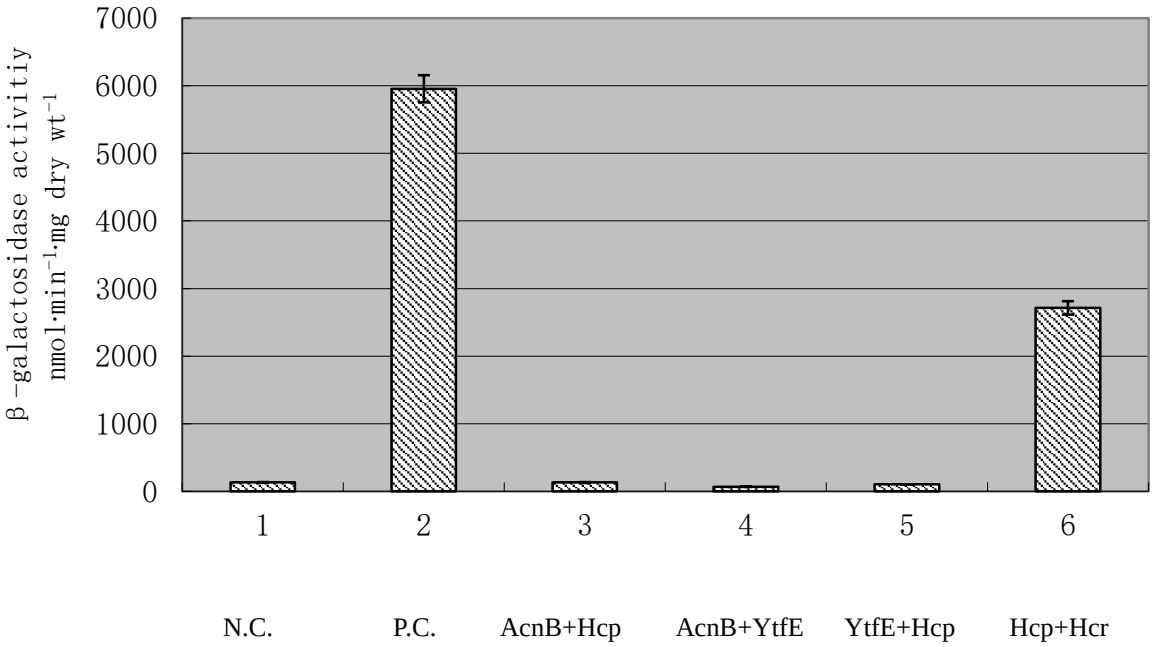

β-galactosidase activities from putative protein pair interactions using the bacterial two-hybrid assay

The β-galactosidase activities were assayed for each indicated protein pairs. Samples were taken 3 hours after inoculation from anaerobic cultures (MS medium supplemented with 0.4 % glycerol) and assayed in duplicate. The data are means ± SD (n=2). The unit of activity is nmol of ONPG hydrolysed·min^{-1}·(mg dry $weight^{-1}$). From left to right as labeled on the horizontal axis:

1, pKT25 and pUT18 (negative control);

2, pKT25-Zip and pUT18-Zip (positive control);

3, pKT25-AcnB and pUT18C-Hcp;

4, pKT25-AcnB and pUT18C-YtfE;

5, pKT25-YtfE and pUT18C-Hcp;

6, pKT25-Hcr and pUT18C-Hcp.

Table 4.1. **galactosidase activity of all clones used in the bacterial two-hybrid system.**

The β-galactosidase activities were assayed for clones with each combination of proteins. This table includes data from Fig 4. 4. The data are means ± SD (n=2). The unit of activity is nmol of ONPG hydrolysed·min^{-1}·(mg dry $weight^{-1}$).

T25 :: protein was expressed by pKT25 vector, Protein :: T18 by pUT 18, and T18 :: protein by pUT18-C.

Protein	**Hcp :: T18**	**T18 :: Hcp**	**Hcr :: T18**	**T18 :: Hcr**	**YtfE :: T18**	**T18 :: YtfE**	**T18 :: AcnB**	**NsrR :: T18**	**NsrR :: T18**
T25 :: Hcp	145 (±8)	136 (±4)	**2989 (±385)**	**2290 (±440)**	93 (±5)	119 (±8)	97 (±11)	125 (±5)	51 (±20)
T25 :: Hcr	**2108 (±315)**	**2715 (±99)**	96 (±4)	172 (±5)	161 (±4)	99 (±18)	122 (±9)	81 (±5)	95 (±14)
T25 :: YtfE	98 (±5)	83 (±7)	177 (±25)	77 (±5)	89 (±3)	51 (±3)	174 (±13)	180 (±15)	130 (±21)
T25 :: AcnB	129 (±40)	84 (±21)	128 (±11)	144 (±16)	129 (±24)	162 (±10)	**1280 (±150)**	91 (±3)	89 (±9)
T25 :: NsrR	117 (±16)	79 (±3)	82 (±6)	79 (±10)	75 (±7)	83 (±5)	91 (±5)	105 (±4)	116 (±12)

Figure 4.5.

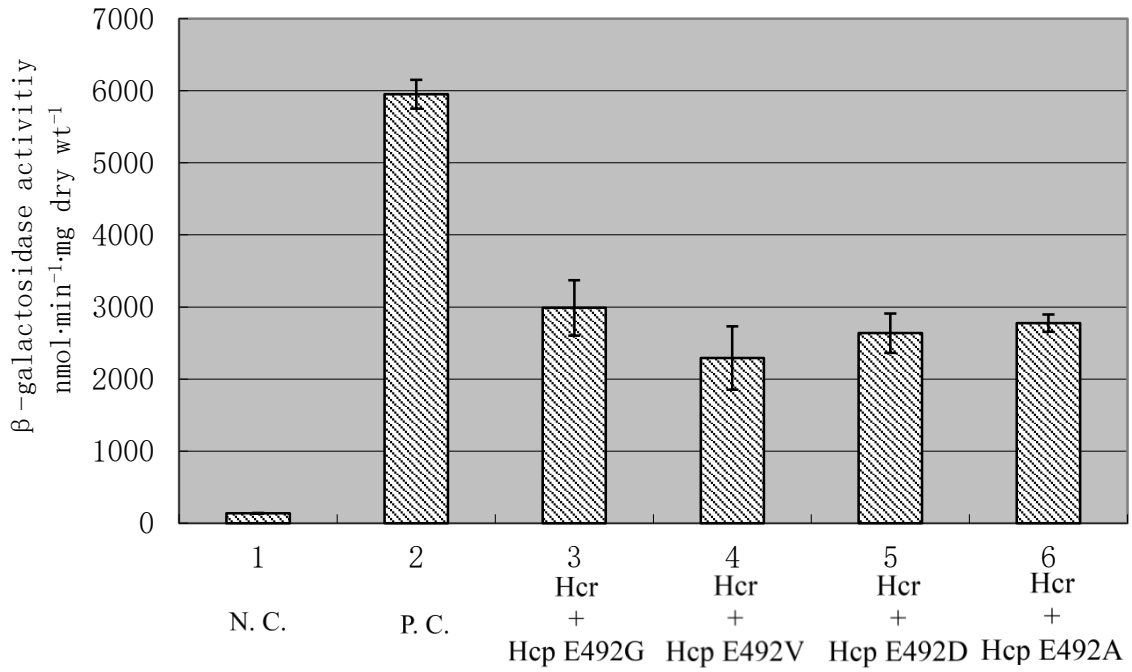

The β-galactosidase activities of transformants with Hcr and the Hcp E492X mutants

The β-galactosidase activities were assayed for the transformants containing pKT25-Hcr and pUT18C-E492X mutants. Samples were taken 3 hours after inoculation and assayed in duplicate. The data are means ± SD (n=2). The unit of activity is nmol of ONPG hydrolysed·min^{-1}·(mg dry $weight^{-1}$). From left to right as labeled on the horizontal axis:

1, pKT25 and pUT18 (negative control);

2, pKT25-Zip and pUT18-Zip (positive control);

3, pKT25-Hcr and pUT18C-E492G;

4, pKT25-Hcr and pUT18C-E492V;

5, pKT25-Hcr and pUT18C-E492D;

6, pKT25-Hcr and pUT18C-E492A.

all four transformants were bright red in appearance, indicative of positive interactions. One single colony was inoculated in LB medium for subsequent β-galactosidase activity assay. The activities detected for the transformants with Hcp mutants were about half of the activity of the leucine zipper positive control, similar to that of the un-mutated Hcp (Fig 4.5).

4.5. Optimization of Hcr protein production with batch cultures and subsequent protein purification

The plasmid pJW21 overexpressing Hcr was constructed in this work. The expression host *E. coli* strain BL21 (DE3) was transformed with pJW21 for the production of Hcr protein. Small scale experiments optimizing the IPTG concentration used for induction were completed in 250 mL shake flasks containing 25 mL of culture. The concentrations of IPTG tested were 0, 10, 50 and 250 μM. Samples were collected 4 hours after induction with IPTG and analysed by SDS-PAGE (Fig 4.6). Optimal induction of Hcr was achieved at 50 μM IPTG. For subsequent protein purification, the culture volume was scaled up to 400 mL in each 2L shake flask (10 flasks for each protein) using 50 μM IPTG for induction. After 4 hours, cells were harvested and sonicated. Clear lysate was obtained by ultracentrifugation and subsequently loaded onto a His-trap column. After extensive washing to remove unbound proteins, bound proteins were eluted with a 0 to 100% linear gradient of Buffer B, which contains 500 mM imidazole. Hcr was eluted when the gradient of Buffer B was increased to above 30%. The fraction containing pure Hcr was concentrated to 3 mg/mL and the purity was estimated to be more than 95% (Fig 4.7 lane 7).

Figure 4.6.

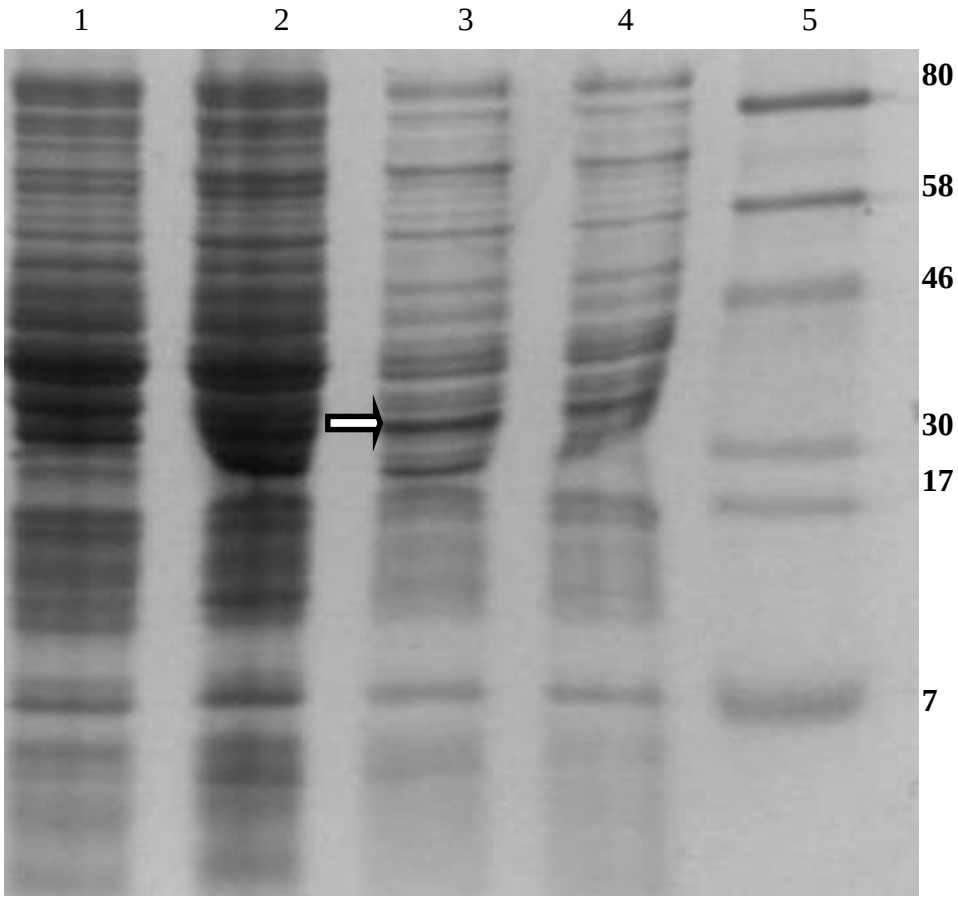

Effect of IPTG concentration on the production of recombinant Hcr protein

Quantity of accumulated Hcr over a range of IPTG was estimated using SDS-PAGE gel. Four parallel cultures of BL21(DE3) pJW21 were induced with different concentrations of IPTG when OD_{650nm} reached 0.5. Samples for SDS-PAGE analysis were collected 4 hours post induction. Arrow indicated the protein band of Hcr. The theoretical protein size of Hcr is 35.74 kDa.

Lane 1: sample without IPTG;

Lane 2: sample with 10 μM IPTG induction;

Lane 3: sample with 50 μM IPTG induction;

Lane 4: sample with 250 μM IPTG induction.

Lane 5: pre-stained protein marker from NEB (kDa).

Figure 4.7.

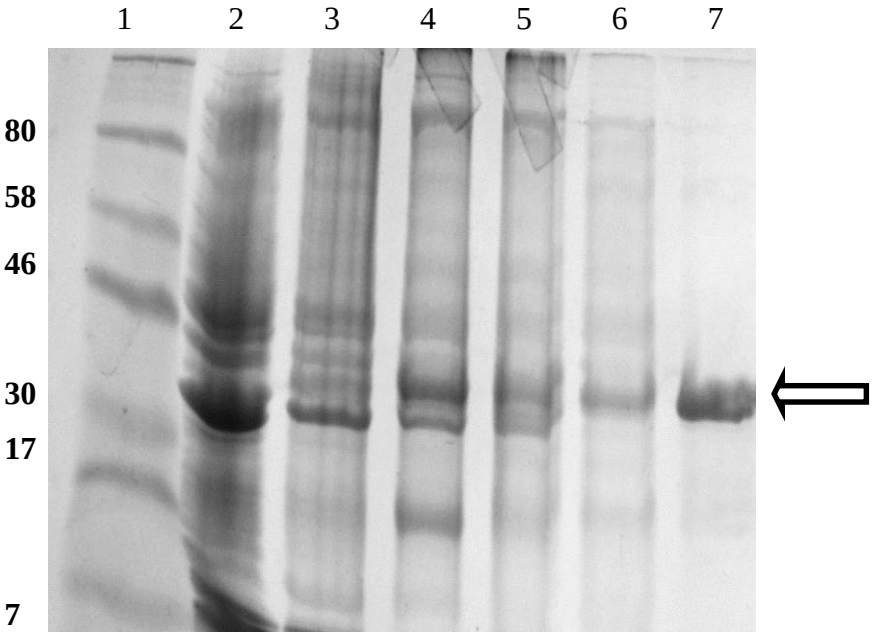

SDS-PAGE gel with samples collected during purification of Hcr

Samples were collected during the purification process using gradient elution. Fraction size was set at 2 mL. Arrow indicated band of Hcr protein.

Lane 1: pre-stained protein marker;

Lane 2: 20 µL of the elution with 100% of Buffer A prior to gradient elution;

Lane 3: 10 µL of the same sample loaded in lane 2;

Lane 4: 20 µL of pool of fractions eluted at 0~20% of Buffer B;

Lane 5: 10 µL of the same sample loaded in lane 4;

Lane 6: pool of adjacent fractions at the shoulders of the peak of UV absorbance curve at around 30% and 40% of Buffer B;

Lane 7: single fraction on the peak of UV absorbance curve at around 35% of Buffer B;

4.6. Detection of aerobically purified Hcr enzyme activity

The purified Hcr was an orange coloured protein, with an apparent molecular mass very close to the theoretical value of 35.74 kDa (Fig 4.7, lane 7). It was reported previously by van den Berg *et al* (2000) that purified Hcr catalyzed the reduction of an artificial electron acceptor 2,6-dichloroindophenol (DCPIP) with NADH as electron donor. This experiment was repeated to check whether the 6xHis-tagged Hcr purified aerobically in this work was active. Following the same protocol described by van den Berg *et al* (2000), it was shown in this study that a low amount of Hcr (40 nM) was capable of reducing 50 µM DCPIP within 5 seconds. No reduction was detected with controls without Hcr or substrate NADH. The activity detected was 20.5 ± 0.024 nmol of DCPIP/(min·µg of Hcr).

4.7. Attempts to reconstitute electron transfer from NADH to NO *in vitro*

An NO electrode was used to measure the NO reduction rate of purified proteins. An enzyme cocktail of catalase, glucose oxidase and glucose was added into the electrode chamber to remove oxygen prior to the addition of NO. After the addition of NO (0.5 µM), purified Hcp (120 µg/mL) or Hcr (140 µg/mL) was added into the electrode chamber with or without 200 µM NADH, and the rate of NO reduction was determined. Purified Hcp alone could not reduce NO, with or without NADH (Fig 4.8 A). Interestingly even without Hcp, in the presence of NADH, purified Hcr reduced NO at a slow rate of 5.9 ± 1.5 nmol/(s · mg protein) (Fig 4.8 B). This rate increased slightly to 6.7 ± 0.9 nmol/(s · mg protein) when Hcp was added into the reaction mixture (Fig 4.8 C). However, this increase was not statistically significant. The protocol used previously to reactivate aconitase after purification was also attempted for reactivating Hcp. An

***In vitro* NO reduction by purified enzymes Hcp and Hcr**

The figure shows the trace recorded by the NO electrode. The unit of electrode response was arbitrary, and the absolute value for a certain NO concentration varied from time to time. However, the change of NO concentration can be calculated and compared between each experiment. The experiment was repeated using proteins prepared on different days, and a similar result was obtained. The final concentration of the components used was: 0.5 μM of NO, 200 μM of NADH, 120 μg/mL of Hcp, and 140 μg/mL of Hcr. Treated Hcp was incubated with 2 mM Fe^{2+} and 2 mM L-cysteine for 30 minutes at room temperature. The addition of each reagent was indicated with an arrow. Red dots indicated addition of NO.

(A) Hcp protein with or without NADH; (B) Hcr protein with or without NADH;

(C) Untreated Hcp with Hcr and NADH present;

(D) Treated Hcp with Hcr and NADH present.

Figure 4.8.

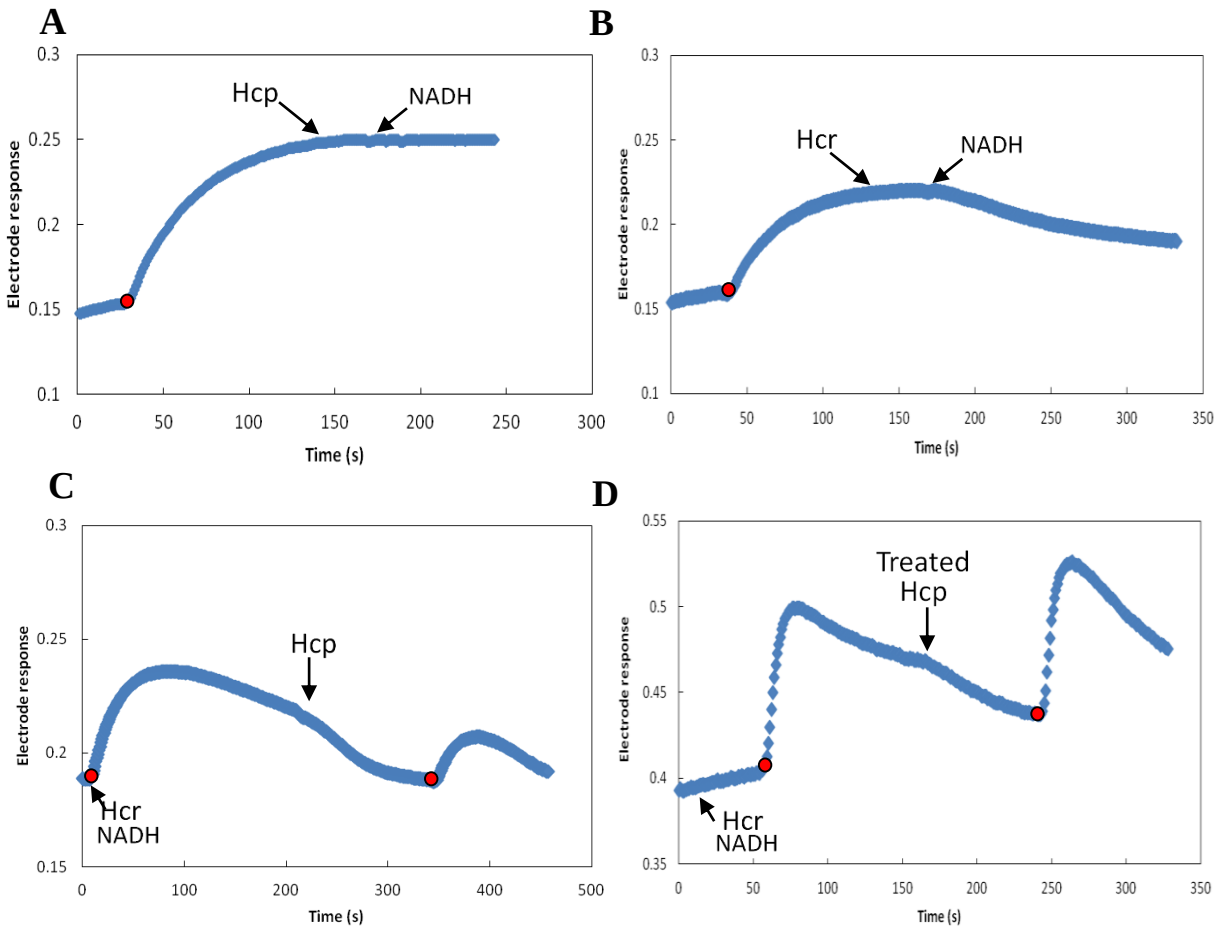
A
Hcp
NADH
Electrode response
Time (s)
B
Hcr
NADH
Electrode response
Time (s)
C
Hcp
Hcr
NADH
Electrode response
Time (s)
D
Treated
Hcp
Hcr
NADH
Electrode response
Time (s)

aliquot (200 µL) of purified Hcp was treated with 2 mM Fe^{2+} and 2 mM L-cysteine for 30 minutes at room temperature. However, this treatment did not increase the rate of NO reduction by Hcp, compared to the untreated Hcp (Fig 4.8 C vs. D).

4.8. Construction of the *hcr* mutant strain JCB5290

To answer the question whether Hcr is required for the function of Hcp, the *hcr* mutant JCB5290 was constructed by transducing JCB5210 with P1 phage propagated on JW5117, in which the gene *hcr* was replaced by a kanamycin resistance cassette. Strain JCB5210 is the quadruple mutant that is defective in four genes known for encoding NO-detoxifying enzymes. JCB5290 is the *Δhcr* derivative of JCB5210 in the same sense as that JCB5250 is the *Δhcp* derivative of JCB5210. The *hcr* mutation in JCB5290 was checked by cell PCR using primers flanking upstream and downstream of the original position of *hcr* gene (Fig 4.9). The PCR product was further purified and sequenced to confirm that the *hcr* gene in JCB5290 had been replaced by a kanamycin resistance cassette.

4.9. Effect of an *hcr* deletion on anaerobic growth under conditions of nitrosative stress

The phenotype of the *hcr* mutant JCB5290 in the presence or absence of nitrosative stress was compared with that of the *hcp* mutant, JCB5250. Three cultures for each strain were grown anaerobically. One of the cultures was unsupplemented; the other two were supplemented with either 0.5 mM or 1 mM sodium nitrite. The hcp^{+}-hcr^{+} strain JCB5210 was used as a positive control. This parent strain was not sensitive to either 0.5 mM or 1 mM nitrite (Fig 4.10 A). Neither strain JCB5290 nor JCB5250 could grow

Figure 4.9.

Verification of the chromosomal *hcr* mutation

Ethidium bromide stained agarose gel showing DNA amplified by PCR from the *hcr* mutants and the parent strain. The primers used in the PCR reaction anneal upstream and downstream of the *hcr* gene on the chromosome.

From left to right:

1, DNA ladder (Hyper Ladder I, Bioline);

2, PCR product from JW5117;

3, PCR product from JCB5290;

4, PCR product from JCB5210;

5, negative control without template;

6, DNA ladder (Hyper Ladder I, Bioline);

Figure 4.10.

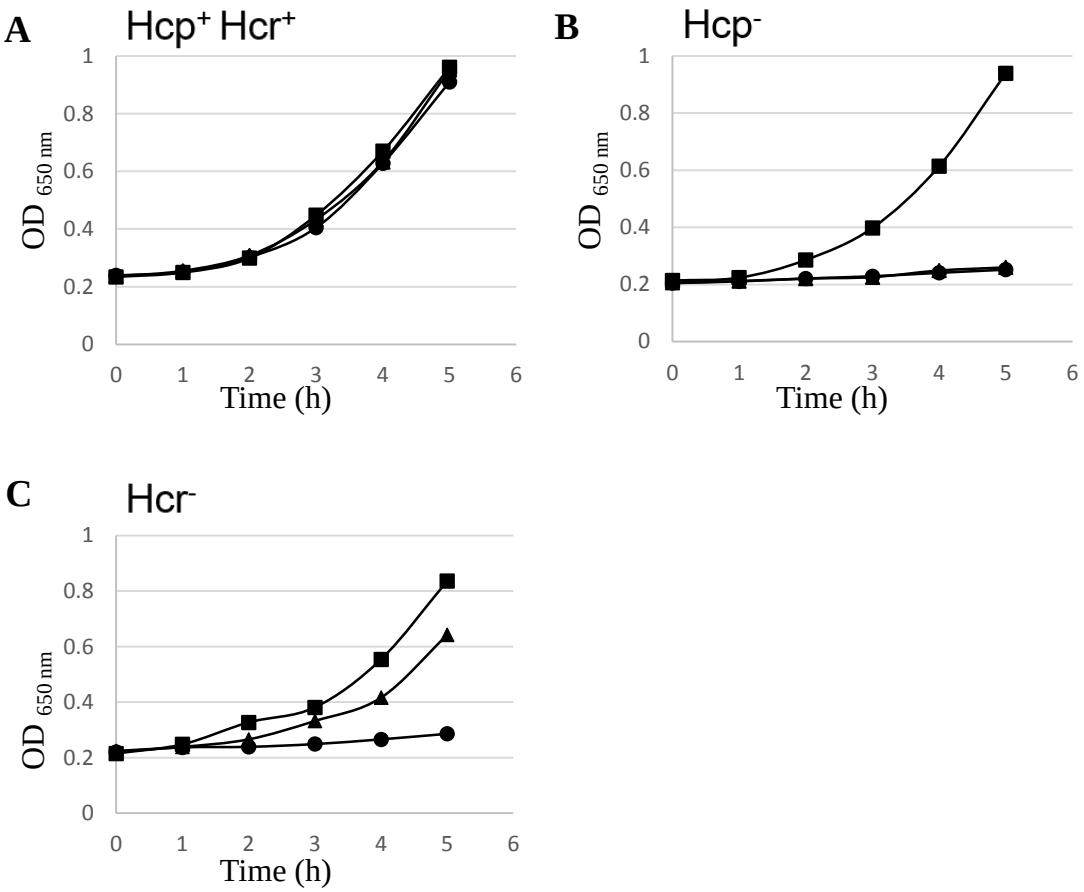

Anaerobic growth of *hcp* or *hcr* mutants

A quadruple mutant defective in *nirBD*, *nrfAB*, *norVW* and *hmp* and its derivatives with *hcp* or *hcr* mutation were used. Bacteria were grown anaerobically in minimal salts medium with or without sodium nitrite. 0.5 mM or 1 mM sodium nitrite was added in the beginning. The optical density at 650 nm of each culture was measured at hourly intervals for 5 hours. Growth curves were completed with two independent cultures on different days and this graph represents a typical experiment result.

A, JCB5210; B, JCB5250; C, JCB5290.

Squares: control without nitrite; Triangles: 0.5 mM nitrite; Circles: 1 mM nitrite.

in cultures supplemented with 1 mM nitrite. However, JCB5290 and JCB5250 exhibited different phenotypes when a lower concentration of nitrite was used. JCB5290 was still able to grow in the presence of 0.5 mM nitrite, albeit not as well as the control culture without nitrite, while JCB5250 was unable to grow at all nitrite concentrations (Fig 4.10 B & C).

CHAPTER 5

In vivo evidence that Hcp is an NO reductase

5.1. Introduction

In this chapter, the hypothesis that Hcp detoxifies NO in *E. coli* will be tested using a gas analysis robotic system. So far the work in previous chapters focused on how Hcp might have directly protected or repaired aconitase that is prone to be damaged by nitrosative stress. It was also possible that the aconitase activity detected in cultures of the Hcp^+ strains was not due to repair after damage, but to aconitase was not damaged because NO was removed efficiently. Two hypotheses were raised thereafter. The first one is that Hcp is a buffer protein that simply binds NO with its unique hybrid cluster at a rate much faster than other usual Fe-S clusters, so that the intracellular concentration of NO will be reduced. This explains why Hcp in the quadruple mutant without other NO reductases could only protect against low amounts of NO. As no catalysis is involved in this hypothesis, it also explains why Hcp alone without Hcr, presumably its co-enzyme, affords protection against nitrosative stress, as observed in Chapter 4. This is not unseen before. Cytochrome *c′* reversibly binds NO due to the haem group, which can be accessed by hydrophobic residues in the proximal environment (reviewed by Watmough *et al.*, 1999). No detectable product, except the NO-Hcp complex is formed if this hypothesis is true. The second hypothesis is that Hcp catalyses the detoxification of NO, either by oxidation or reduction. The interaction observed between Hcp and Hcr can be rationalized as the requirement for electron transfer to occur between these two proteins. Whether it is an oxidization or reduction process can be determined by identifying the product generated. If it is oxidization, the product is possibly nitrate, whereas if it is reduction, the product can be N_2O, N_2, or ammonia. As NO, N_2O and N_2 are all in gaseous form, their concentration can be simultaneously detected by gas chromatography.

To this advantage, a robotic system that integrates a gas chromatography and an automated sampling routine was used. Another advantage of this robotic system is that it is completely sealed so that anaerobic experiments can be conducted *in situ*. Cells can be cultivated without being subjected to isolation in ambient conditions, especially when the protein Hcp under investigation is expressed anaerobically. Living bacteria including JCB5210 and its *hcp* or *hcr* derivatives were used as biochemical catalysts. Their ability to reduce NO will be examined and compared during cell cultivation. The NO concentration will be measured over time, while various gases other than NO will also be analyzed, such as O_2, CO_2, N_2 and N_2O. This could possibly lead to the discovery of the product, if it is in gaseous form, of the NO detoxification catalyzed by Hcp. The wild-type strain RK 4353 was used as a control to test the system in detecting nano-molar gas concentrations. This automatic sampling and gas analysis system was assembled by Molstad *et al* (2007), from the Norwegian University of Life Sciences.

5.2. NO detoxification and N_2O production by the parent strain, RK4353

Preliminary experiments were completed with the parent strain RK4353, in which all previously characterized NO reductases were active. The anaerobic inoculum was raised overnight in N-oxide free minimal salts medium, and then an appropriate amount of inoculum (approx. 10 µL) was transferred to the anaerobic vials installed on the robot so that the initial OD at 650 nm after inoculation was 0.01. Immediately following addition of 1,000 nmol of NO to the gas phase, which generated 620 nM of NO in the liquid phase after equilibration, reduction started and was essentially completed after 4 hours. There was a simultaneous accumulation of N_2O (Fig 5.1). In subsequent experiments,

Robotic analysis of NO reduction and N_2O generation by strain RK4353 in vials injected with 1000 nmol of NO

NO and N_2O concentrations over time in the vial inoculated with RK4353. The initial OD at 650 nm after inoculation was 0.01. An air tight syringe was used to transfer anaerobic inoculum to the vials installed on the robot. All of the anaerobic vials used in this experiment were of a uniform size of 120 mL, containing 50 mL of medium. Gaseous nitric oxide was injected directly into the headspace. The variation in NO and N_2O concentration was followed by continuous sampling of the headspace every 25 minutes until the depletion of nitric oxide. Experiments were repeated twice without noticeable differences.

Dashed line: Amount of NO in the un-inoculated control vial;

Diamonds: Amount of NO in vial inoculated with RK4353;

Squares: Amount of N_2O in vial inoculated with RK4353;

Circles: Amount of CO_2 in vial inoculated with RK4353.

Figure 5.1.

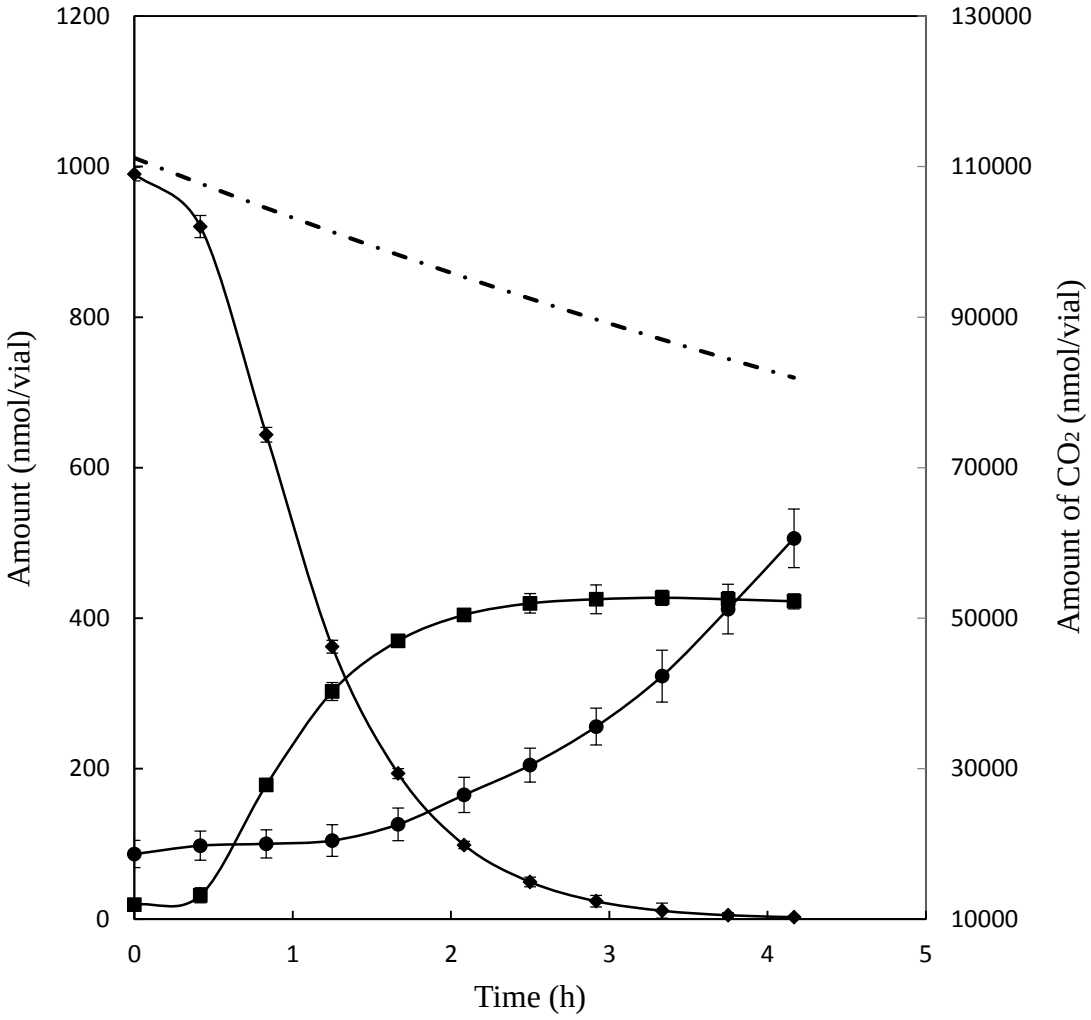
1200
1000
800
600
400
200
0
130000
110000
90000
70000
50000
30000
10000
0
1
2
3
4
5
Amount (nmol/vial)
Amount of CO2 (nmol/vial)
Time (h)

Figure 5.2.

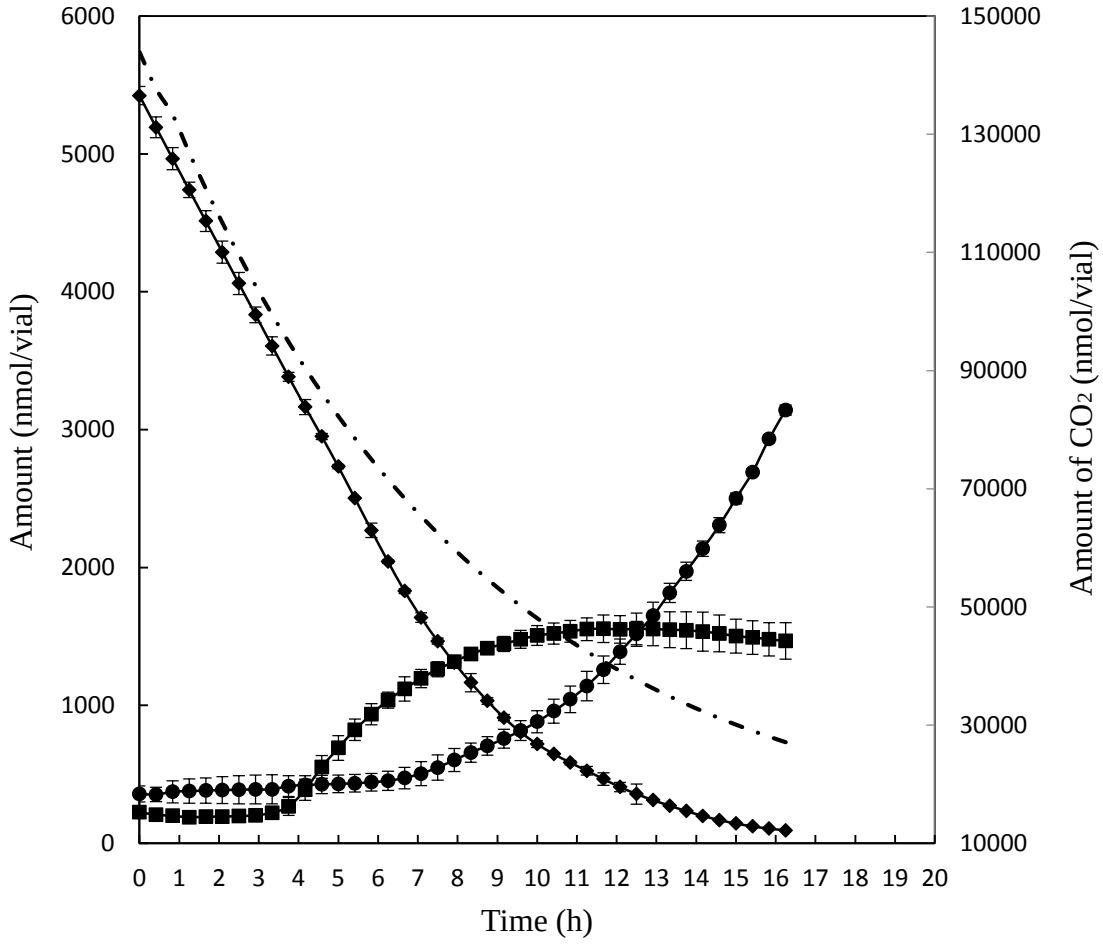

NO reduction and N_2O generation by strain RK4353 in vials injected with 5423 nmol of NO

The same experiment procedure was used as in the Fig 5.1, except that the NO concentration used in here was about 5 fold of that used in Fig 5.1. Experiments were repeated twice without noticeable differences.

Dashed line: Amount of NO in the un-inoculated control vial;

Diamonds: Amount of NO in vial inoculated with RK4353;

Squares: Amount of N_2O in vial inoculated with RK4353.

Circles: Amount of CO_2 in vial inoculated with RK4353.

the initial quantity of NO added to the vials was increased 5-fold to about 5,000 nmol. This resulted in a 2 hour delay before NO reduction and N_2O production commenced (Fig 5.2).

The rates of NO reduction and N_2O accumulation were derived from Fig 5.1 and Fig 5.2, by dividing the change of gas concentration at two adjacent data points with the time between two sampling points. After normalizing these two rates with the biomass at the corresponding sampling point, specific rates of NO reduction and N_2O production were obtained for further detailed analysis. When these two specific rates were plotted against each other, it was shown that the rate of N_2O accumulation was proportional to the rate of NO reduction throughout the time course of experiments (Fig 5.3). A stoichiometric relationship of 2 : 1 between specific rates of NO reduction and N_2O production was shown after linear regression was applied correlating the two rates. This suggested that for every two molecules of NO consumed, one molecule of N_2O was produced. For the *E. coli* strain RK4353, more than one NO detoxifying enzyme is present in the cell. Allowing deviation errors in experimental data, it can be concluded from the data that the collective effect of all of the NO detoxifying enzymes in the wild-type *E. coli* strain resulted in the majority, if not all, of NO being converted to N_2O. This conclusion was drawn based on the logic that if there was another major source of product other than N_2O, such as NH_4^+, being produced at the same rate, the ratio of NO to N_2O after linear regression would become 3:1, or become shifted towards the value 3:1 from 2:1. The ratio obtained from this result was 2:1, therefore, N_2O was the dominant product from NO reduction.

Figure 5.3.

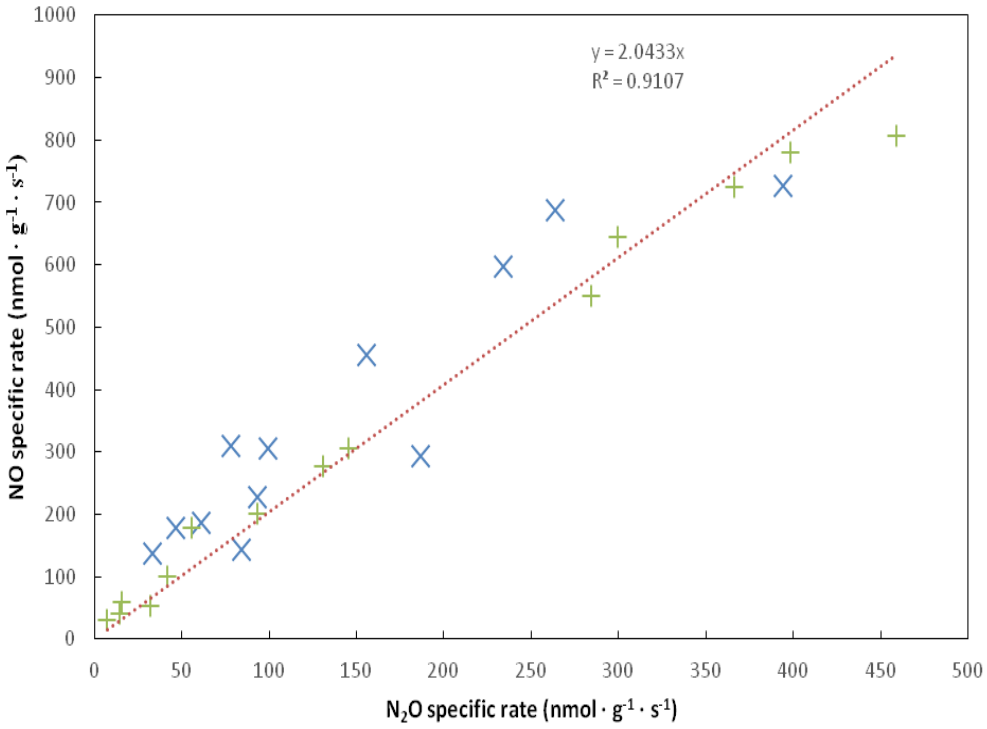

Comparison of specific rate of NO reduction and N_2O formation by RK 4353

Specific rates of NO reduction were plotted on the y-axis versus specific rates of N_2O accumulation on the x-axis. Data were from two independent experiments, and labeled as the cross symbol (x) for one and the plus symbol (+) for the other. Linear regression was applied to analyse the stoichiometric relationship between the specific rates of NO reduction and N_2O production. The best fit was plotted as the red line as the function y=2.0433x. The line was forced to go through the origin.

5.3. NO reduction and N_2O generation by the quadruple mutant JCB5210

The removal of the genes encoding all of the known NO detoxifying enzymes, except the *hcp* gene, rendered strain JCB5210 more sensitive to NO stress when compared to RK4353. Initially 1000 nmol of nitric oxide was injected into each vial inoculated with different strains. This proved to be such a high concentration for strain JCB5210 that the NO reduction did not begin until well after 35 cycles of sampling, which was about 14 hours after NO injection (Fig 5.4). In subsequent experiments, a lower amount of NO was then injected into the vial for further analysis (Fig 5.5). Although much more vulnerable to NO stress when compared to RK4353, the quadruple mutant strain JCB5210 still reduced 300 nmol of NO in total (186 nM in liquid phase), in both of the cases with high and low NO concentrations, which took 250 minutes to complete.

Interestingly N_2O was discovered as the product of NO reduction by strain JCB5210. Compared to RK4353, a similar pattern of simultaneous N_2O generation coupled to NO reduction was shown by this strain (compare Fig 5.2 and Fig 5.4). The deletion of the genes of the known reductases in JCB5210 resulted in a 10-fold decrease in the NO concentration at which NO reduction was initiated and N_2O started to accumulate —around 186 nM for JCB5210 versus 1900 nmol for RK 4353. The correlation between the specific NO and N_2O rates was analysed as previously described for strain RK4353 (Fig 5. 6). The ratio of specific NO reduction rate to N_2O accumulation rate was 1.8, which was also very close to 2. These results suggested that there was still another low-capacity NO reductase present in the quadruple mutant JCB5210, which catalyzed the reduction of two molecules of NO to one molecule of N_2O.

Robotic analysis of NO reduction and N_2O generation by strain JCB5210 in vials injected with 1000 nmol of NO

NO and N_2O concentrations over time in the vial inoculated with JCB5210. The initial OD at 650 nm after inoculation was 0.01. Air tight syringe was used to transfer anaerobic inoculum to the vials installed on the robot. All of the anaerobic vials used in this experiment were of a uniform size of 120 mL, containing 50 mL of medium. Gaseous nitric oxide was injected directly into the headspace. Gaseous nitric oxide was injected directly into the headspace. The variation in NO and N_2O concentration was followed by continuous sampling of the headspace every 25 minutes until the depletion of nitric oxide. Experiments were repeated twice without noticeable differences.

Dashed line: Amount of NO in the un-inoculated control vial;

Diamonds: Amount of NO in vial inoculated with JCB5210;

Squares: Amount of N_2O in vial inoculated with JCB5210;

Circles: Amount of CO_2 in vial inoculated with JCB5210.

Figure 5.4.

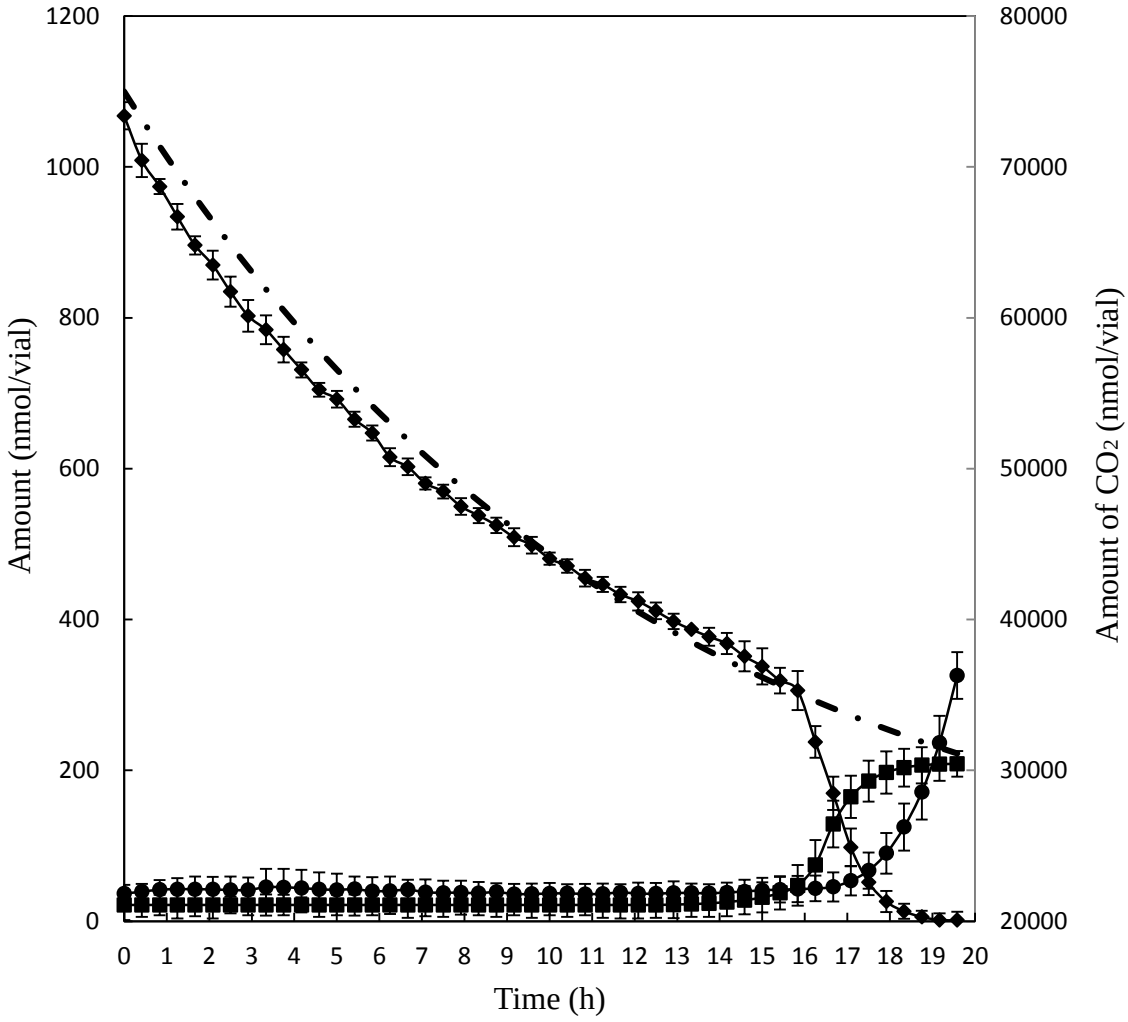
1200
1000
800
600
400
200
0
Amount (nmol/vial)
80000
70000
60000
50000
40000
30000
20000
Amount of CO2 (nmol/vial)
0 1 2 3 4 5 6 7 8 9 10 11 12 13 14 15 16 17 18 19 20
Time (h)

Figure 5.5.

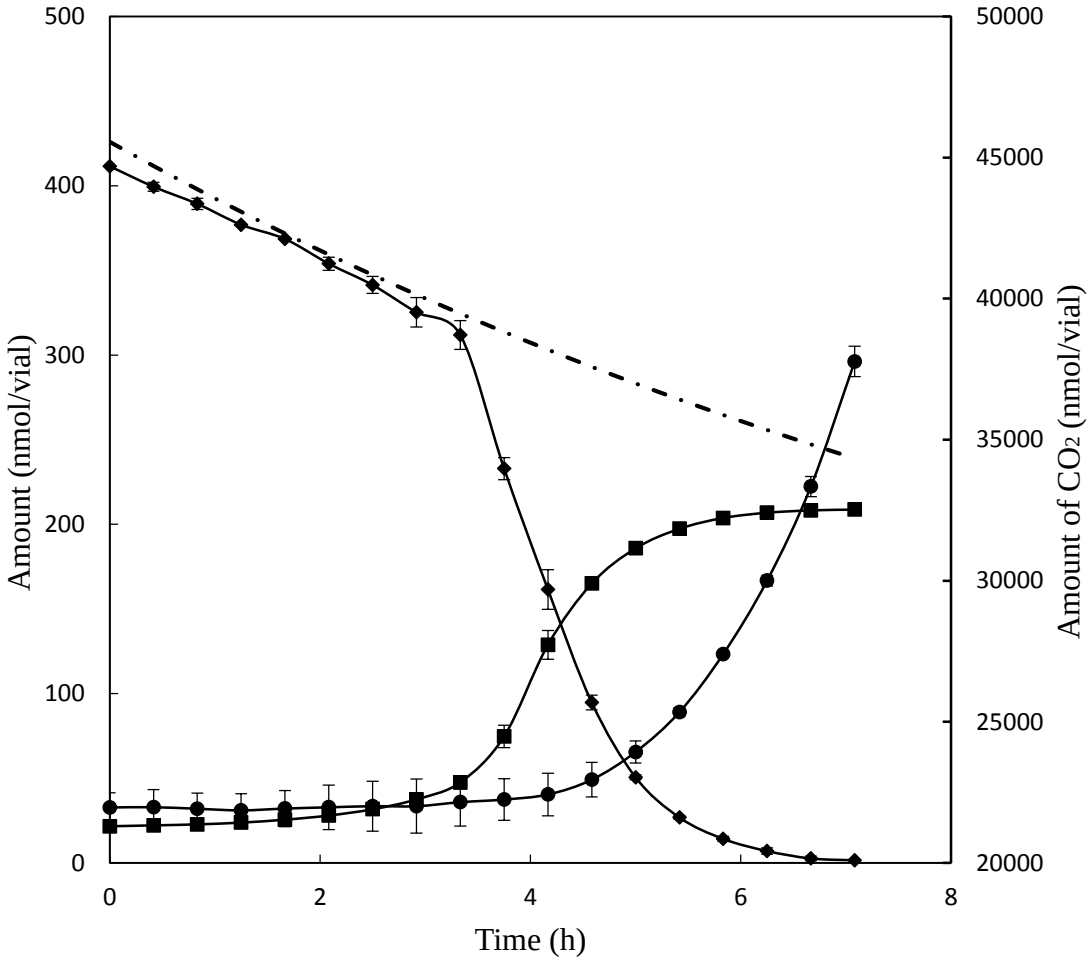

NO reduction and N_2O generation by strain JCB5210 in vials injected with 400 nmol of NO

The same experiment procedure was used as in the Fig 5.4, except that the NO concentration used in here was about half of that used in Fig 5.4. Experiments were repeated twice without noticeable differences.

Dashed line: Amount of NO in the un-inoculated control vial;

Diamonds: Amount of N_2O in vial inoculated with JCB5210;

Squares: Amount of N_2O in vial inoculated with JCB5210;

Circles: Amount of CO_2 in vial inoculated with JCB5210.

Figure 5.6.

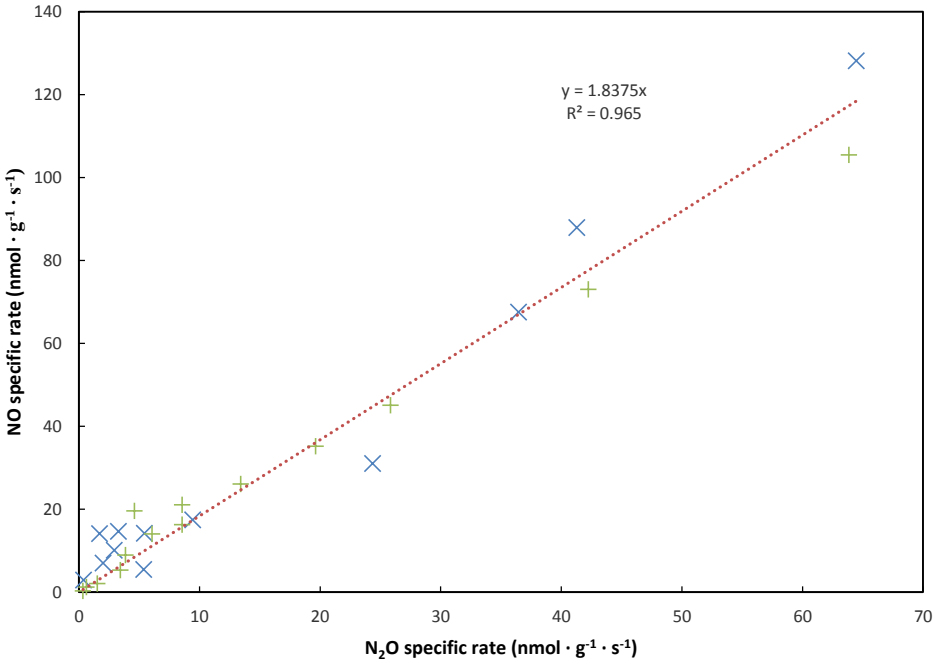

Comparison of specific rate of NO reduction and N_2O formation by strain JCB5210

For the strain JCB5210, specific rates of NO reduction were plotted on the y-axis versus specific rates of N_2O accumulation on the x-axis. Data were from two independent experiments, and labeled as the cross symbol (x) for one and the plus symbol (+) for the other. Linear regression was applied to analyse the stoichiometric relationship between the specific rates of NO reduction and N_2O production at each sampling point. The best fit was plotted as the red line as the function y=1.8375x. The line was forced to go through the origin.

5.4. No NO reduction by the mutant JCB5250 that lacks Hcp

To test whether the observed NO reduction was dependent on Hcp, the rates of NO reduction by the *hcp* derivatives of JCB5210 and JCB5250, were determined. The further deletion of Hcp from the quadruple mutant JCB5210 lacking all known NO reductases resulted in the complete loss of NO reduction observed in Section 5.3. As shown in Fig 5.7, during the entire time course, the NO reduction curve overlapped with the dilution curve due to sampling, and no N_2O was generated. In confirmation with the phenotypic study with or without NOSW in Chapter 3, strain JCB5250 was not able to grow, although only a low concentration of NO was added in the vial. When the NO concentration was further decreased due to dilution towards the end of the experiment, bacterial growth was recovered. However, no NO reduction was detected, and no N_2O was produced.

5.5. NO detoxification and N_2O generation in an Hcr^- mutant

The *hcr* gene was deleted from strain JCB5210 to obtain strain JCB5290, which contained *hcp* gene alone in the originally two-gene operon *hcp-hcr*. In this section, NO reduction by JCB5290 was studied in the same manner as for JCB5210 and JCB5250. It was previously shown in Chapter 4 that JCB5290 was more susceptible to nitrosative stress than JCB5210, but not as sensitive as the *hcp* mutant JCB5250. Hence less NO was used for experiments with strain JCB5290 than that used for strain JCB5210. For an initial amount of 200 nmol NO in the vial, a 2-hour lag was observed as previously for RK4353 and JCB5210 when inhibitory concentrations of NO were used (Fig 5.2 & Fig 5.4). NO reduction and N_2O generation occurred after the amount of NO had decreased to less than 150 nmol in the vial, equilibrated to a concentration of 93 nM of

Figure 5.7.

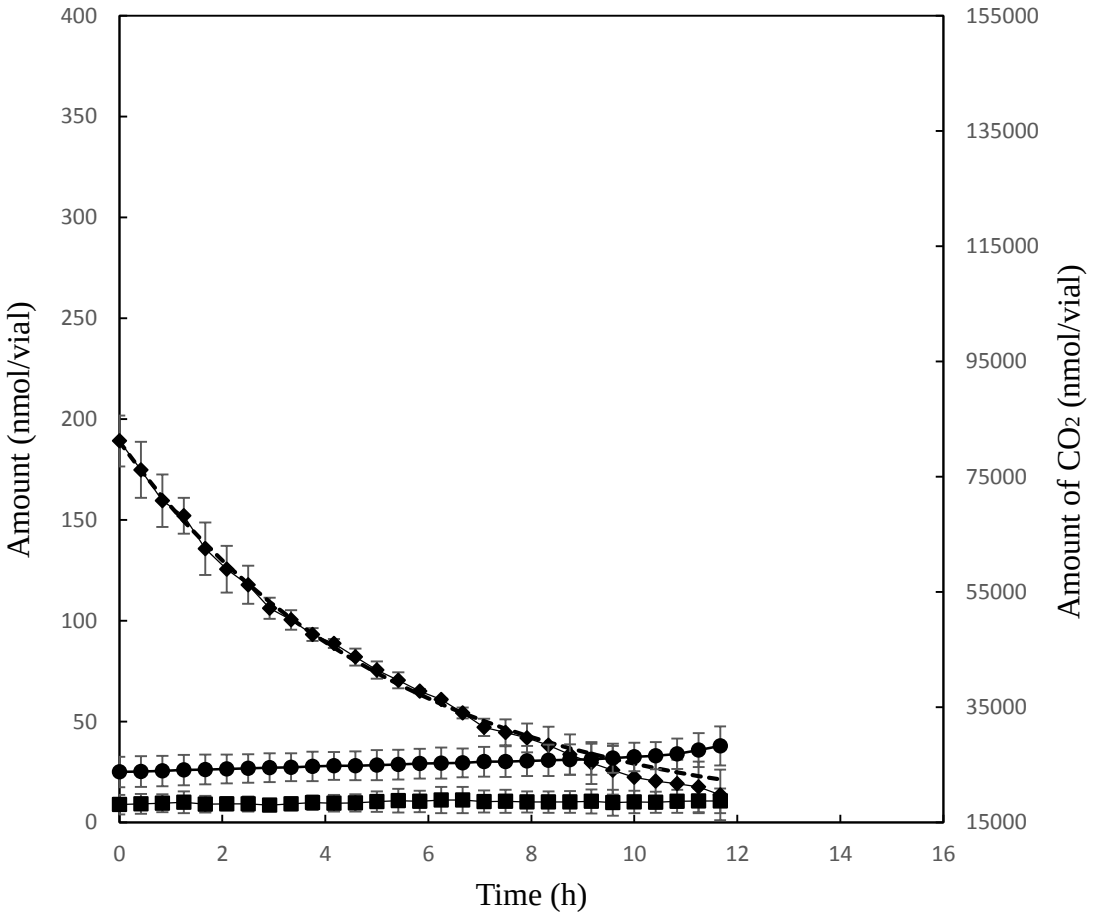

NO and N_2O time course of strain JCB5250 with 250 nmol NO

JCB5250 was the *hcp* derivative of JCB5210. The amount of 250 nmol of gaseous NO was injected into the vial inoculated with JCB5250. NO and N_2O concentration in the vial was measured at each sampling point. Experiments were repeated twice without noticeable differences.

Dashed line: Amount of NO in the un-inoculated control vial;

Diamonds: Amount of NO in vial inoculated with JCB5250;

Squares: Amount of N_2O in vial inoculated with JCB5250;

Circles: Amount of CO_2 in vial inoculated with JCB5250.

Figure 5.8.

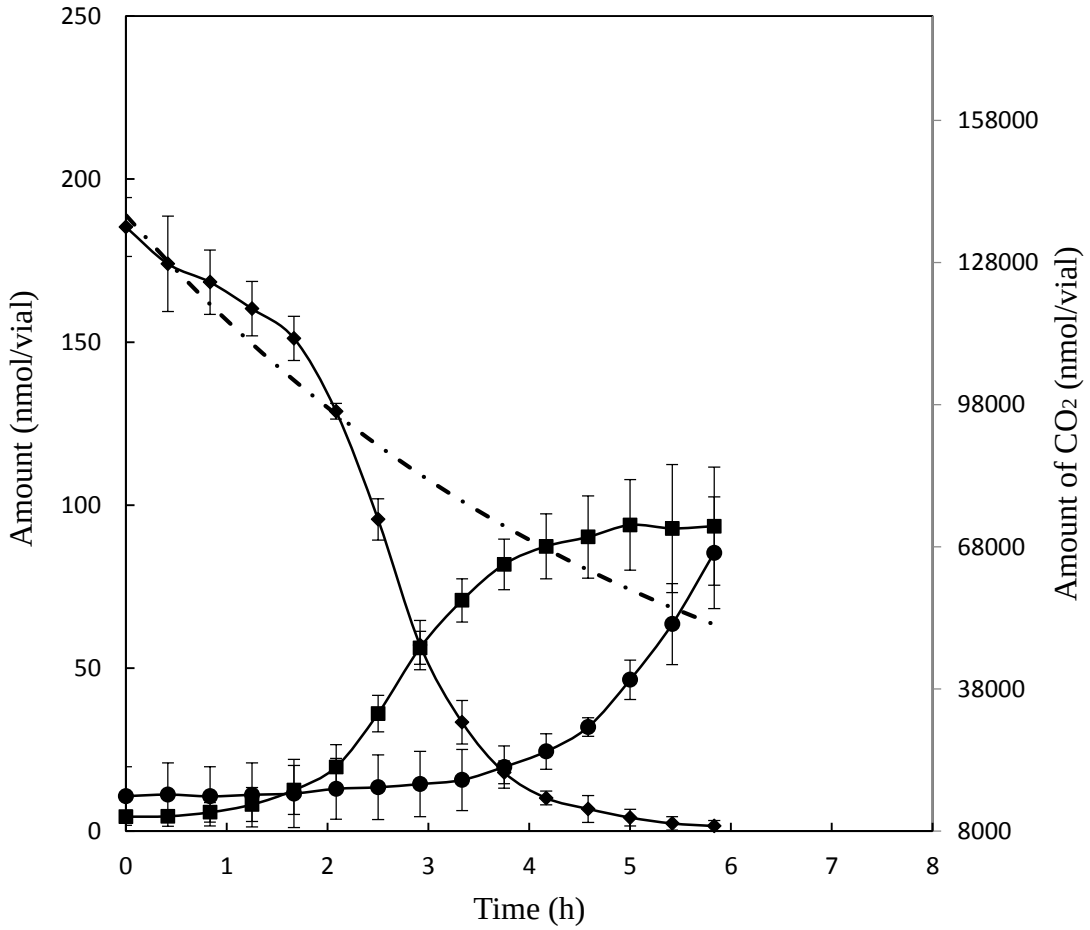

NO reduction and N_2O production by JCB5290 with 200 nmol NO

NO and N_2O concentrations were measured every 25 minutes in the gas phase of the vial inoculated with strain JCB5290 until NO depletion. Less than 200 nmol of NO was injected into the headspace of the vial in the beginning. Experiments were repeated twice without noticeable differences. The experiment in this figure was completed in this work once, with the replica completed by Dr. Linda Bergaust independently.

Dashed line: Amount of NO in the un-inoculated control vial;

Diamonds: Amount of NO in vial inoculated with JCB5290;

Squares: Amount of N_2O in vial inoculated with JCB5290;

Circles: Amount of CO_2 in vial inoculated with JCB5290.

NO in the liquid phase (Fig 5.8). The stoichiometric relationship between the specific rates of NO reduction and N_2O generation at each sampling point was also about 2:1.

5.6. Kinetic analysis of the NO reduction process

During NO reduction, the time course of bacterial growth and the specific rate of NO reduction were first investigated. For bacterial growth, a positive linear correlation was observed between CO_2 emission and bacterial growth in this experiment, which was described in details in Material and Methods, hence the change of biomass was represented by the change of CO_2 concentration at each time increment. The absolute values of CO_2 were not used for calculation, as the initial OD and final OD were determined by taking samples immediately before and after the experiment. The change of CO_2 concentration and the time course of the specific rate of NO reduction are shown in detail, using the *hcp*$^+$-*hcr*$^+$ strain JCB5210 as an example (Fig 5.9 Panel A). The growth of bacteria was affected by the NO concentration present inside the vial. As already observed in the phenotypic study in Chapter 3, the growth of strain JCB5210 was affected by how much nitrosative stress was present — it grew normally when 1 μM NOSW was supplemented, but growth was inhibited by 5 μM NOSW. However, the tolerance of the quadruple mutant JCB5210 was much lower in this experiment. The strain JCB5210 could not grow until the amount of NO was diluted to 300 nmol in the vial, when the NO concentration was 186 nM in the liquid phase. When more than 300 nmol of NO was injected into the vial, bacterial growth commenced after the amount of NO had decreased down to about 300 nmol/vial. This was at the same time when the NO reduction began, which was described in detail for each strain in its own section.

As no reduction occurred at high NO concentrations, the specific rate of NO reduction was almost zero during early sampling points (Fig 5.9 B). The maximum rate of NO reduction occurred much later than the start of NO reduction. All strains tested showed similar patterns of variation in the NO specific reduction rate over time, hence for simplicity, a detailed example of JCB5210 was illustrated in Fig 5. 9. This specific rate of NO reduction was further analysed against substrate (NO) concentration in the liquid medium in Fig 5.10. As the NO concentration decreased, the concentrations of NO on the left of the peak shown in Fig 5.9 B are higher than those on the right, whereas the concentrations of NO on the left of the peak shown in Fig 5.10 are lower than those from the right. Therefore, the peak shown in Fig 5.10 is the direct reverse of that shown in Fig 5.9 B.

Fig. 5.10 A shows a comparison between the parent RK4353 and JCB5210. Apart from the data generated from Fig 5.1- Fig 5.5, also included in Fig 5.10 were data from experiments in which various lower NO concentrations were used for the parent strains RK4353 and JCB5210. In the previous *in vivo* study regarding NO metabolism of the NorV enzyme in *E. coli*, cells were exposed to NO for at least 30 minutes for the induction of enzymes before being used in measuring NO reduction rate (Gardner *et al.*, 2002). In this experiment it was assumed that during the initial period after NO injection, enzymes were still being induced in the cells, while traces of oxygen added with the reagents were being reduced. Hence specific rates of NO reduction for the first five sampling points (appr. 2 hours) were not included in Fig 5.10.

The same kinetic pattern was found for both RK4353 and JCB5210. A peak

The time course of bacterial growth and NO specific reduction rate

The example of strain JCB5210 was illustrated for detailed demonstration of the time profile of bacterial growth and NO specific reduction rate. NO reduction curve was included in each panel as a connection between panel A and B, and between current figure and previous figures in this Chapter.

Panel A showed the correlation between NO and growth. The growth was represented by CO_2 emission as explained in material and methods.

Panel B showed the correlation between NO concentration and NO specific reduction rate over time.

Diamonds: Amount of NO in the vial;

Circles: Amount of CO_2 in the vial;

Triangles: NO specific reduction rate.

Figure 5.9.

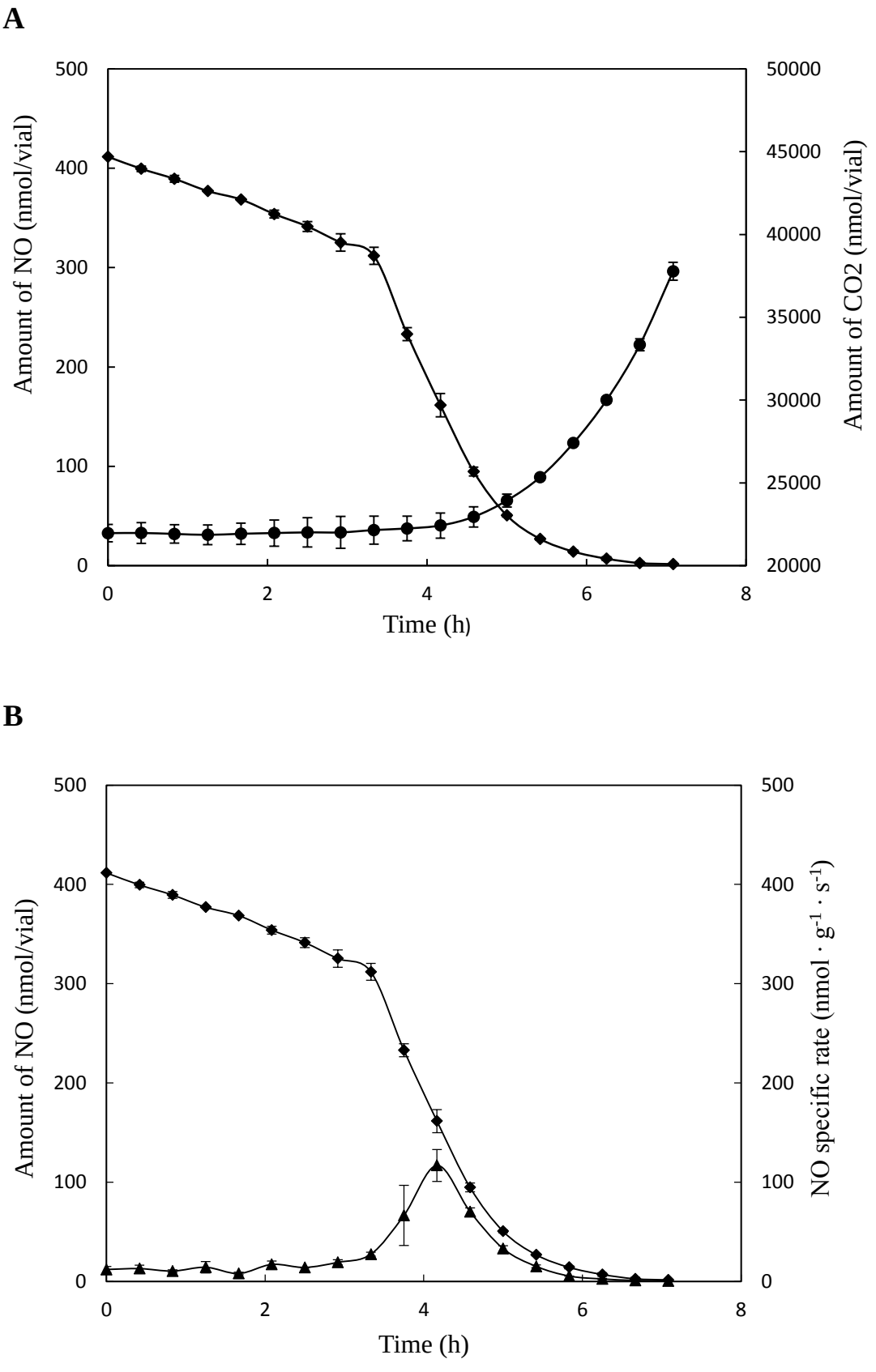
A
Amount of NO (nmol/vial)
Amount of CO2 (nmol/vial)
Time (h)
B
Amount of NO (nmol/vial)
NO specific rate (nmol · g-1 · s-1)
Time (h)

representing a maximum NO reduction rate occurred at a critical NO concentration (for strain RK4353 ~2000 nM; this was for JCB5210 ~150 nM). Here this NO reduction process was tentatively analysed using a model put forward by Girsch and de Vries (1997):

$$V = V_{max}/(1 + K_2(\frac{1}{[NO]} + \frac{k_1}{[NO]^2}) + [NO]/K_i)$$

where: V_{max} = the maximum rate;

K_1=half saturation constants (6 μM);

K_2=half saturation constants (0.55 μM);

K_i=half saturation constant for inhibition (13 μM);

[NO]=concentration of NO in the liquid phase.

This equation describes the NO reduction kinetics by NO reductase *in vitro*. It is adopted here as an approximation for this study, as such kinetic analysis on *in vivo* experiments using bacteria has not been documented before. In this study, the NO concentrations used were less than 3 μM, which is well below the K_i (13 μM), hence the inhibition term was ignored. Also, due to only low concentrations of NO were used in this study, the square of the NO concentration in the equation ($K_1/[NO]^2$) makes no contribution to the rate. Without these two terms involving K_i and K_1, the final equation equals to a standard Michaelis Menten equation.

However, it should be noted that there are substantial differences between the experiments for the standard Michaelis Menten kinetic analysis and experiments in this study. For a standard Michaelis Menten analysis, independent measurements were made frequently by following replicate initial reaction rate, immediately after mixing isolated enzyme and substrate (both of known concentrations) in a vial and in the absence of all

other cellular components. In this study, the data used in Fig 5.10 were derived from a single continuous measurement of NO concentrations *in vivo*, with unkown concentration of enzyme at any of the time points. As detailed in Materials and Methods, NO concentrations in liquid phase were determined from gas phase pressure.

Based on visual estimation and assuming that the velocity at the top of the curves in Fig 5.10 is the maximum velocity, the apparent Km and apparent Vmax from the lower concentration range of NO were 900 nM and 800 nmol· g^{-1}· s^{-1} for the parent strain RK4353, and 75 nM and 85 nmol· g^{-1}· s^{-1} for strain JCB5210 (Fig 5.10 A). The same also applied to the JCB5290 strain that has a lower NO tolerance compared to strain JCB5210. The apparent Km and apparent Vmax for JCB5290 were 20 nM and 40 nmol· g^{-1}· s^{-1} (Fig 5.10 B).

Kinetic analysis of NO reduction rate versus substrate concentration

For strains, RK4353, JCB5210 and JCB5290 capable of reducing NO, the specific NO reduction rate was derived from NO reduction experiments, by first dividing the amount of NO decreased between two neighbouing sampling points with the sampling interval, then normaling the rate with the biomass estimated from CO_2 readings. Therefore, this is not a standard kinetic plot with initial velocity points, but with data points collected throughout the entire course of the experiments. The blue time course arrow shows that the data were collected in the order of from right to left in the graph. NO concentration in liquid phase was estimated from measured NO concentration in gas phase. The gray shading represents the confidence interval area where 95% of the unknown population parameters are likely to fall within.

Panel A: Comparison between RK4353 and JCB5210. The inset is the enlarged region showing NO metabolism of JCB5210.

Red line: specific rate of NO reduction of the quadruple mutant JCB5210;

Blue line: wild-type strain RK4353.

Panel B: Comparison between JCB5210 and JCB5290.

Red line: specific rate of NO reduction of the quadruple mutant JCB5210;

Blue line: the *hcr* derivative strain JCB5290.

Figure 5.10.

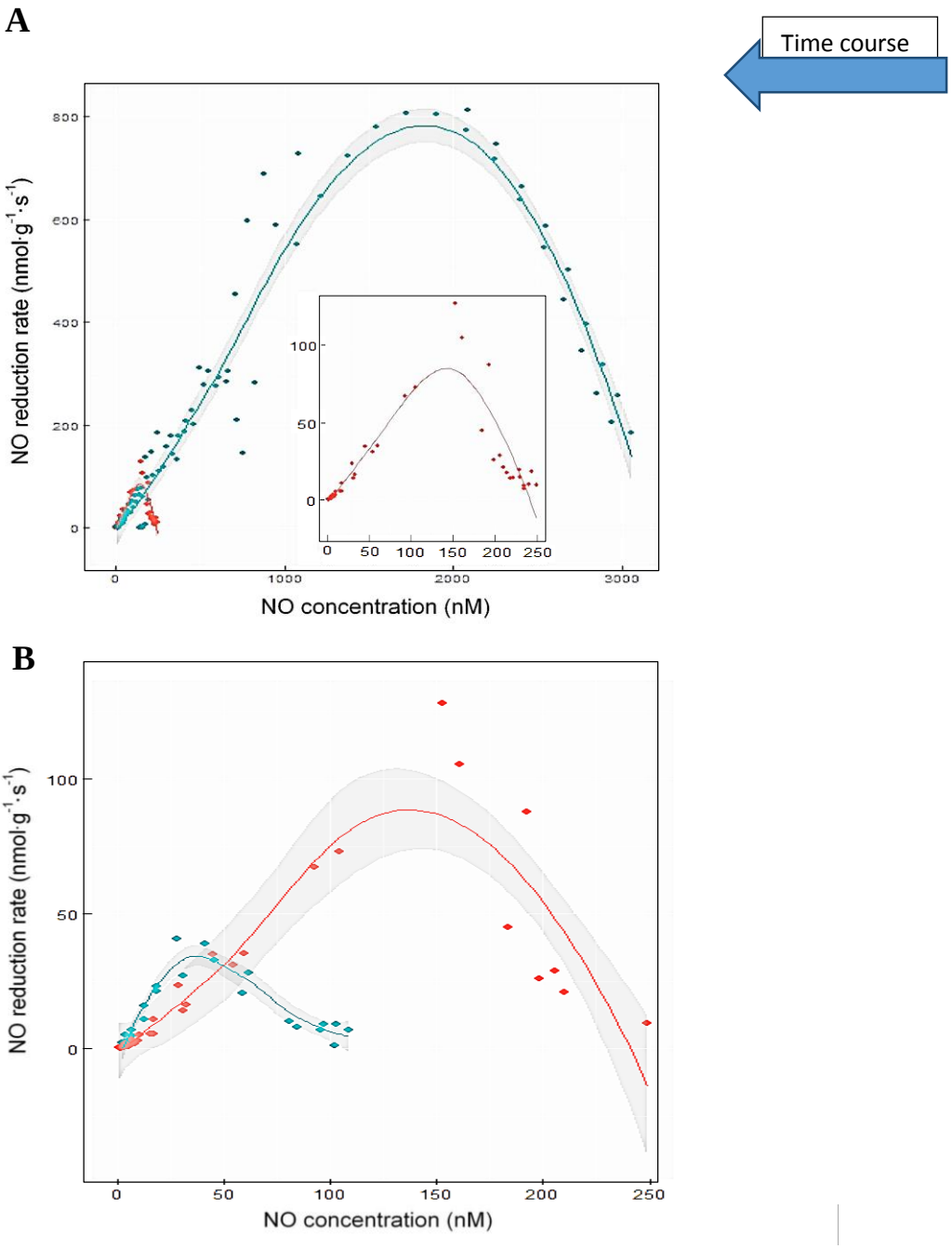
A
Time course
NO reduction rate (nmol·g⁻¹·s⁻¹)
NO concentration (nM)
B
NO reduction rate (nmol·g⁻¹·s⁻¹)
NO concentration (nM)

CHAPTER 6

DISCUSSION

6.1 Overview

This work first evaluated the phenotype of *hcp* mutation in a genetic background without all known NO detoxifiers. The *hcp* mutant is more sensitive to nitrosative stress, and its aconitase is found inactive. To further investigate the function of Hcp, the following work assessed four hypotheses, as introduced previously in the aims of this work. In the first and second hypotheses, Hcp was postulated to repair nitrosylated aconitase or protect aconitase from being damaged. Two experiments were completed in Chapter 3 and Chapter 4 to test these two hypotheses. In Chapter 3, the activity of purified aconitase was determined in the presence or absence of purified Hcp protein when treated with NO. Purified Hcp neither reactivated the nitrosylated aconitase to restore its activity, nor protected aconitase from being inactivated by NO. In Chapter 4, the bacterial two-hybrid system was used to study direct interaction between Hcp and aconitase B, but no positive interaction was found between these two proteins. The results obtained from these two experiments did not support the first two hypotheses. Then this work proceeded to test the other two hypotheses, in which the role of Hcp in detoxification of NO was assumed, either by chemically binding NO or biochemically reacting with NO. In Chapter 4, an attempt was made to reconstitute a putative electron transfer chain from NADH to NO, through purified Hcp and its oxidoreductase Hcr, so as to determine the NO reduction ability of Hcp. However, this approach did not yield evidence to support any hypothesis raised. Finally in Chapter 5, *in vivo* work was completed to compare the NO reduction ability between Hcp^+ and Hcp^- strains lacking all other NO detoxifiers. It was found that the Hcp^+ strain was able to reduce NO to N_2O, and the further deletion of the *hcp* gene abolished the NO reduction ability of this strain. As N_2O was formed as the end product, the third hypothesis was therefore rejected. This

result provides an important evidence to support the fourth hypothesis that Hcp is an NO reductase.

During the course of investigation, two additional findings were made in this work that contributes to a better understanding of the function of Hcp. In Chapter 3, using site-directed mutagenesis, the hybrid cluster of Hcp was shown to be important for the function of Hcp. In Chapter 4, Hcp was shown to interact with its oxidoreductase, Hcr, using the bacterial two-hybrid system. However, both phenotypic study in Chapter 4 and robotic gas analysis in Chapter 5 of the Δ*hcr* derivative mutant strain showed that this interaction is not essential for Hcp to function. The following sections will discuss in details the conclusions drawn based on the experiment results obtained in this thesis.

6.2. Hcp protects *E. coli* from nitrosative stress and the hybrid cluster centre is essential for Hcp to function

Phenotype study of *hcp* and *ytfE* mutations on a background of no other NO reductases was first completed in Chapter 3. In the growth experiments, along with the building up of nitrosative stress in the cytoplasm using different sources of nitric oxide, including nitrate, nitrite and nitric oxide saturated water (NOSW), two major phenotypes could be observed altogether in each growth study of isogenic mutants of *hcp* and *ytfE* – mutants that were unaffected with the others being impaired by nitrosative stress. One thing in common about the latter was that *hcp* was missing regardless of the presence or absence of *ytfE* (Fig 3.2-4 A & B versus C & D). YtfE, on the other hand, could not be correlated to the same conclusion. The results here indicate that Hcp, instead of YtfE, confers protection against nitrosative stress in *E. coli*, under the conditions tested in this study.

Incidentally, in earlier literature, it was reported that the disruption of the *hcp* gene alone in *E. coli* did not affect normal growth when 5 mM or 10 mM of nitrate or nitrite was supplemented (van den Berg *et al*., 2000). In another study, a subtle phenotype was observed. The growth rate of RK4353 *hcp* was inhibited by ~45% while that of RK4353 was ~25% in the presence of 10 µM NOSW, while same extent of inhibition between two strains was found in the presence of 40 µM NOSW possibly due to full inhibition to both strains (Squire, 2009). In this work, it was clearly shown that the *hcp* null mutant with the quadruple mutation background was more sensitive than its isogenic parent strain. The toxicity of NO was much more pronounced when no other enzymes were detoxifying NO at the same time. Therefore, the lack of clean phenotype in previous studies was due to the presence of several other differently expressed systems that masked the function of Hcp in *E. coli*. Such techniques to create isogenic mutants for the study of individual NO detoxifying enzymes was previously used in *Salmonella enterica*, in which several NO detoxification systems were also found (Mills *et al.*, 2008). Recent studies using another microorganism *Porphyromonas gingivalis* also demonstrated the important role of Hcp in protecting against nitrosative stress. A microarray study of this strict anaerobe under nitrosative stress also revealed the highly up-regulated level of *hcp*, as in *E. coli* (Lewis *et al.,* 2012). It showed the inhibited growth of an *hcp* deficient *P. gingivalis* under nitric oxide stress (Boutrin *et al.,* 2012). In this organism *P. gingivalis*, the deletion of the *hcp* gene alone caused significant growth inhibition under nitrosative stress conditions (Boutrin *et al.,* 2012).

The complementation using plasmid-encoded Hcp of the *hcp* mutants JCB5250 (*hcp*

ytfE^{+}) and JCB5260 (*hcp ytfE*) confirmed that the sensitivity of these two strains was indeed caused by the loss of Hcp (Fig 3.5). The site-directed mutagenesis was designed to disrupt the unique hybrid cluster of Hcp, by substituting the highly conserved glutamic acid E492 with other amino acids, including very different amino acids, such as valine, alanine and glycine, or with a similar aspartic acid. It was shown that apart from the E492D substitution, other mutations led to the loss of function of the plasmid-encoded Hcp, which no longer complemented the *hcp* mutant strain (Fig 3.6). Further CD analysis of the Hcp protein mutants showed that the secondary structure of the Hcp proteins was not affected by the substitution of E492 (Fig 3.9). This suggests that apart from the similar substitution of E492D, the Hcp E492X mutants lose their ability to complement the *hcp* mutation due to the disruption of the hybrid cluster, rather than the mis-folding of the entire protein. Therefore, the hybrid cluster is essential for the function of Hcp to afford protection against nitrosative stress.

Damage to labile Fe-S centres in Fe-S proteins, such as aconitase, may account for the NO toxicity *in vivo* (Gardner *et al.*, 1997). To further assess the role of protection of Hcp in *E. coli*, aconitase activity from the cultures of the four isogenic mutant strains under nitrosative stress were determined. Aconitase was inactive in the *hcp* mutants harvested from cultures supplemented with 5 mM nitrate (Fig 3.11 C and D). To confirm that the loss of aconitase activity was due to NO mediated damage in nitrate supplemented cultures, aconitase activity from NOSW treated cultures was also determined. In cultures supplemented with 1 μM of NOSW, the aconitase activity of the *hcp* mutant was inactive, whereas the aconitase activity of the *hcp*$^{+}$ strains was not affected (Fig 3.12). Therefore, it can be concluded that aconitase was damaged without

Hcp under nitrosative stress. The results of the aconitase assays coincided with the results obtained from the phenotypic study. The presence of Hcp corresponded to the survival of cells and enduring aconitase activities under nitrosative stress. For the repair function of YtfE, the aconitase was still inactive in *hcp ytfE*$^{+}$ mutant strain, suggesting that even if YtfE repairs Fe-S proteins *in vitro* as previously reported by Justino *et al* (2006), the rate of the repair reaction is too slow to be effective.

There are two types of aconitase (aconitase A and aconitase B) in *E. coli*. The expression of aconitase A is induced under oxidative stress but surpressed under anaerobic conditions (Lu *et al.*, 2004, Gruer and Guest, 1994). On the contrary, aconitase B is expressed under anaerobic conditions and serves as the major catalytic enzyme during exponential growth (Cunningham *et al.*, 1997, Gruer *et al.*, 1997). Based on these previous reported observations, the activity assayed in this study could be largely attributed to aconitase B, as the cells used in this study were harvested from anaerobic cultures during the mid-exponential phase of growth. Aconitase was inactivated in *hcp* strains under nitrosative stress conditions, but remained active in *hcp*$^{+}$ strains. Hcp might interact with aconitase to prevent its fragile [4Fe-4S] centre from NO exposure, or function to directly repair damaged aconitase. However, it was shown that the activity of the purified aconitase B did not vary when treated with NO in the presence or absence of purified Hcp protein (Fig 3.15). Hcp protein did not reactivate the inactivated aconitase either (Fig 3.15).

6.3. No interaction between Hcp and AcnB, YtfE or NsrR

Hcp was shown to be important in protecting the quadruple mutant strain against

nitrosative stress, but the question remains as how it fulfilled its role. The bacterial two-hybrid system was used in this work for studying protein-protein interactions, as the unknown function of Hcp might be extrapolated if its binding partners can be identified. Several candidates, including AcnB, YtfE, NsrR and Hcr, were tested for their ability to interact with Hcp or each other. Aconitase was active in the Hcp^+ strains and inactive in the Hcp^- strains under nitrosative stress conditions (Fig 3.11). It was postulated that Hcp might be able to repair inactivated aconitase, or simply bind to aconitase so as to prevent its fragile [4Fe-4S] from being damaged. However, no interaction was detected between aconitase B and Hcp. Therefore, this hypothesis was neither supported by the result from the experiment in Chapter 3 studying aconitase activity using purified Hcp in the presence of NO, nor by the negative result obtained here between Hcp and AcnB (Fig 3.15 and Fig 4.4). Unexpectedly, the YtfE protein did not interact with AcnB either, although YtfE was previously proposed to repair the Fe-S centre of the Fe-S proteins (Justino *et al*., 2006). Both of *ytfE* and *hcp* were highly up-regulated when the repressor NsrR was inactivated under nitrosative stress. The lack of interaction between YtfE and Hcp indicates that these two proteins do not form any enzyme complex.

Coworkers in our group working on the function of YtfE proposed that the different extent of growth defect observed between *hcp ytfE* and *hcp* $ytfE^+$ mutants under the same nitrosative stress level, as shown in Fig 3.2 and Fig 3.4, was due to the function of YtfE in accumulating free NO in the cytoplasm, presumably *via* releasing the NO molecule from nitrosated Fe-S proteins in the process of repairing the Fe-S centre. Evidence supporting this hypothesis was collected from experiments measuring the

β-galactosidase activities induced by intracellular NO concentration from a reporter plasmid, with or without *ytfE* in a genetic background where other genes of proteins capable of generating NO have been deleted (unpublished data from PhD student Basema Balasiny). Recently, it was reported by Nobre *et al* (2014) from the same research group as Justino *et al* (2006) that YtfE can donate iron to Fe-S clusters, with the aid of the components from the Isc system that functions to assemble Fe-S clusters *in vivo*. This agrees with the negative interaction observed between YtfE and AcnB in this study. If YtfE simply donates iron and exerts its effect through a sophisticated Fe-S cluster synthesis system, rather than directly repairs the nitrosylated Fe-S core on its own, YtfE will not be required to contact with the many Fe-S proteins such as aconitase, but only need to interact with some of the Isc proteins. Therefore, it will be interesting to further test in the two-hybrid system whether YtfE interacts with any of the Isc proteins.

The NO sensor, NsrR, contains an NO-sensitive Fe-S cluster (Tucker *et al.*, 2008). To further examine the hypothesis that Hcp repairs Fe-S proteins, the interaction between Hcp and NsrR was also tested. However, no interaction was found between Hcp and NsrR (Table 4.1). This result does not support the first two hypotheses raised on the function of Hcp protein. It also does not support the possibility that Hcp might play an indirect role by affecting the activity of the NsrR regulator. NsrR did not interact with itself when tested in the bacterial two-hybrid system (Table 4.1). NsrR belongs to the Rrf2 family transcription factors featuring a helix-turn-helix motif in the DNA-binding domain. Its binding site has been shown to be an inverted repeat (GATG N_{11} CATC) (Bodenmiller and Spiro, 2006). It is very likely that two NsrR monomers are required to

occupy this type of binding site. After incubation of NsrR monomers and a DNA probe containing an *nsrR* binding site, the weight of the DNA-protein complex indicated that NsrR bound to DNA as a homodimer after ultracentrifugation (Tucker *et al.,* 2008). Therefore, possibly the negative result of NsrR self-dimerization obtained in this study is a false negative. As in the bacterial two-hybrid system used in this study, proteins are fused to T25 or T18 polypeptides. These tags might inhibit certain interactions, or affect the proper folding of the tested protein.

6.4. Hcr interacts with Hcp, but Hcr is not essential for Hcp to function

Positive protein interaction was observed between Hcp and Hcr in this study. The interaction strength was around half of that of the positive control of the system (Fig 4.4). This interaction was later corroborated by the *in vitro* result from another MSc student John Rizk. Proteins Hcp with an N-terminal His-tag and Hcr without any tag were overexpressed together using the plasmid pJW22 constructed in this work. In John Rizk's experiment, during protein purification using Ni^{++} affinity chromatography, the overexpressed Hcp protein was bound to the column by the 6xHis tag at the N-terminal end. The Hcr protein, albeit untagged, was not washed out during the column-wash under low imidazole concentrations prior to elution. It remained bound to Hcp until these two proteins were eluted together during batch elution at a higher imidazole concentration (Fig 6.1).

In *E. coli*, the *hcr* gene is co-regulated on the same operon with *hcp*, and Hcr was suggested to be the NADH-dependent oxidoreductase of Hcp (van den Berg *et al.*, 2000). In this work, the 6xHis tagged Hcr protein overexpressed from pJW21 could be

purified in a single step using immobilized metal affinity chromatography (Fig 4.7). Using the DCPIP assay, it was shown that the Hcr protein was still highly active as an oxidoreductase when purified aerobically. Therefore, the expression and purification of Hcr protein do not necessarily require strictly anaerobic conditions. Hcr even exhibited a marginal NADH-dependent ability of NO reduction on its own, which was not observed for the purified Hcp protein (Fig 4.8 B vs A). However, when Hcp and Hcr were combined together with NADH and NO to reconstitute the theoretical electron transfer pathway as depicted in Fig 4.1, no significant increase of NO reduction rate was observed when compared to that of the control of Hcr only (Fig 4.8 C vs. B). Is this a genuine negative result that suggests this theoretical electron transfer chain is faulty, such as in the electron transfer between Hcp and Hcr, or the choice of the terminal electron acceptor as NO? During the drafting of this thesis, new positive *in vitro* evidence was acquired by the project student John Rizk, using the anaerobically co-purified Hcp and Hcr protein as shown in Fig 6.1. This Hcp-Hcr protein mixture could reduce NO at a rate of 2390 nmol of NO reduced$\cdot s^{-1}\cdot$(mg of protein)$^{-1}$. This is significantly higher than the NO reduction rate of Hcr protein alone obtained in this study, which is 5.9 ± 1.5 nmol/(s · mg protein) (Fig 4.8). Therefore, possibly the Hcp protein purified under ambient conditions lost its activity to react with NO. Fe-S cluster is known for its sensitivity towards oxidative stress (Gardner *et al.*, 1997b). O_2 can damage the Fe-S core in different mechanisms, as two cases were already encountered in this study: the [4Fe-4S] core of aconitase loses one Fe while the 4Fe-4S core of FNR dissociate into [2Fe-2S], as introduced previously. It is possible that the hybrid cluster of the aerobically isolated Hcp shown in Fig 1.9 B is not in a reversible oxidation state that can be reduced by its oxidoreductase Hcr, and therefore catalytically inactive.

Figure 6.1.

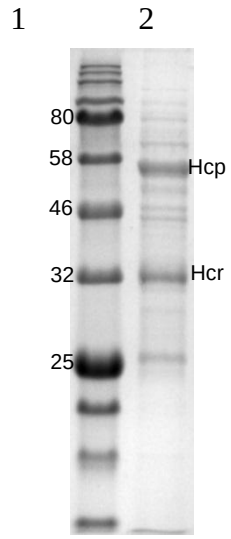

Co-purification of Hcp and Hcr during batch elution

This is an experiment result from project student John Rizk. Plasmid pJW22 overexpressing Hcp (N-terminal 6xHis tagged) and Hcr (not tagged) was transformed into an *E. coli* K-12 strain HMS184. Culture was grown anaerobically and the expression was induced with 50 μg/ml of IPTG. Cells were harvested and broken *via* sonication, then clear lysate was loaded onto a 1 mL His-trap column. The column was first washed with 6 column volumes of buffer A. Then the column was eluted in a single batch with a mixture of buffer A and B (1:1).

Lane1: protein Marker;

Lane2: sample collected during batch elution.

The finding of the interaction between Hcp and Hcr suggests that these two proteins work closely with each other *in vivo*. In order to find out whether this interaction is essential for the function of Hcp in defending the quadruple mutant JCB5210 against nitrosative stress, the *hcr* derivative strain JCB5290 was constructed and compared with its parent strain as well as the *hcp* derivative strain JCB5250. The deletion of the *hcr* gene increased the sensitivity to nitrosative stress when compared to the parent strain, as JCB5290 was not able to grow when 1 mM nitrite was supplemented, whereas the parent strain JCB5210 grew normally. When the concentration of nitrite was reduced to 0.5 mM, the *hcr* mutant strain was able to grow moderately, whereas the *hcp* mutant strain was unable to grow at all (Fig 4.10). This result confirmed the critical role of Hcp, rather than Hcr, in conferring protection against nitrosative stress, although no activity of Hcp purified under ambient conditions was observed earlier. The sensitivity to nitrosative stress of the *hcr* mutant strain falls in between those of the parent strain and the *hcp* mutant strain. As the *hcr* mutant strain JCB5290 is more resistant to nitrosative stress than the *hcp* mutant, this suggests that the Hcp protein in the *hcr* mutant strain is still functional even in the absence of Hcr. The *hcr* gene is only found in facultative anaerobes, not in obligate by anaerobic bacteria and archaea, in which Hcp has to function without Hcr. In *E. coli*, Hcp could possibly be reduced by alternative oxido-reductases, which are likely to have orthologues in strict anaerobes.

6.5. An *in vivo* evidence that Hcp is an NO reductase that reduces NO to N_2O

In Chapter 5, an *in vivo* experiment was completed, subjecting the cultures of the hcp^+ and *hcp* strains in sealed anaerobic vials to NO gas. The headspace gas sample of the cultures was continuously analysed by gas chromatography. The wildtype strain

RK4353 was included as a control to show that nano-molar concentrations of NO and the N_2O generated could indeed be detected accurately (Fig 5.1 and Fig 5.2). The generation of N_2O is expected, as NorV in the wildtype strain RK4353 is known to reduce NO to N_2O (Gomes *et al.*, 2002). Interestingly, it was found that for the strain JCB5210, which was an *hcp*$^+$ strain, but lacked all other known NO reductases including NorV, NO was still reduced to N_2O, although its tolerance to NO was much lower than the strain RK4353, which is a wild-type in all the known NO reductases (Fig 5.4 and Fig 5.5). For the *hcp* derivative strain JCB5250, neither NO reduction nor N_2O generation was detected. For JCB5210, at non-inhibiting concentrations of NO, every molecule of N_2O was generated stoichiometrically from two molecules of NO. This showed that N_2O was the product of NO reduction. If Hcp is a buffer protein, no product formation would be observed from NO reduction. The third hypothesis raised on the function of Hcp was therefore rejected. To the best of our knowledge, the result obtained here is the first evidence reported so far to support the fourth hypothesis that Hcp acts as an NO reductase, reducing NO to N_2O. In another organism *S. typhimurium*, recently it was reported by Runkel (2014) that the deletion of *hcp* gene resulted in less N_2O production in nitrate supplemented cultures, when compared to the wildtype strain. This can be explained by the result obtained here. Hcp is reducing the NO generated during nitrate metabolism to N_2O. The deletion of Hcp resulted in less NO being reduced to N_2O, hence the total amount of N_2O detected in *hcp* mutant is lower than that in the wildtype strain.

The *hcp*$^+$*hcr* strain JCB5290 was also found to be able to reduce NO to N_2O, but with a lower NO tolerance than the *hcp*$^+$*hcr*$^+$ parent strain JCB5210 (Fig 5.8 vs Fig 5.5). This

observation is in concert with the phenotype of the Δ*hcr* strain JCB5290 being partially resistant to nitrosative stress (Fig 4.10). In comparison, NorW is the NADH-dependent oxidoreductase of NorV, the well characterized NO reductase. Interestingly, a partial phenotype of Δ*norW* strain was also observed previously, and the existence of another reductase of NorV was suggested (Gardner *et al*. 2002). Here three hypotheses are raised to explain the partial phenotype of the Δ*hcr* strain JCB5290. First, it was shown in Fig 4.8 that Hcr was able to reduce NO on its own. Possibly the removal of the ancillary reduction of NO by Hcr increased the sensitivity of nitrosative stress. On the other hand, the rate of NO removal by Hcr is much lower than the Hcp-Hcr mixture co-purified together as shown in Fig 6.1. It is more likely that the NO reduction by Hcr is too slow to cause an effect, but it is the loss of electron transfer from Hcr to Hcp that causes the partial sensitivity of the Δ*hcr* strain JCB5290. Hence the second hypothesis is that Hcp might receive electrons from an alternative electron transfer partner that is less efficient than Hcr, as suggested by Gardner *et al* (2002) for the NorV-NorW system, hence the NO reduction by Hcp is hindered by this electron transfer step. Further experiments to compare the NO reduction rate between anaerobically purified Hcr and Hcp-Hcr, and to characterize the electron transfer rate between Hcp and Hcr, can be completed to examine the first two hypotheses. Finally, it was shown in Fig 4.4 that Hcr interacted with Hcp. Possibly this interaction has a positive effect on the activity of Hcp, such as protecting Hcp under higher NO concentrations. The protective role of Hcr for Hcp is not in contradiction with the second hypothesis. The binding of Hcr to Hcp is highly likely to be a necessity for electrons to be transferred between these two proteins. Meanwhile, upon protein interaction, Hcr might partially block substrate accessibility to the active centre of Hcp, or conformational changes might occur in the Hcp structure, so

as to increase the stability of Hcp under high NO concentrations. The nature of this interaction can be studied in more detail to examine the second and third hypotheses.

For the wild-type strain RK4353, Hmp detoxifies NO in aerobic, but not anaerobic conditions (Gardner and Gardner, 2002). NrfA and NorV are mainly responsible for anaerobic NO reduction, and the products are ammonia and N_2O respectively (van Wonderen et al., 2008; Gomes *et al.*, 2002). It was shown that NorV made the majority of the contribution under the conditions tested in this study (Fig 5.3). When the anaerobic culture of RK4353 was subjected to NO, the reduction of NO was about twice as fast as the formation of N_2O. If the production of ammonia was also significant, more than two molecules of NO would be used during the time one molecule of N_2O is generated, then the stoichiometric relationship between NO reduction rate and N_2O production rate would be significantly higher than 2:1. This result shows that Nrf is not reducing NO in the range of NO concentration (<3 μM) used in this study for the wildtype strain RK4353, which agrees with the kinetic data on Km values reported for Nrf (300 μM) and NorV (0.4 μM) by Wonderen *et al*. (2008). It was confirmed that the substrate affinity of Nrf is much lower than that of NorV in anaerobic NO reduction.

For all the strains used in this study, a different threshold NO concentration at which NO reduction began was observed for each strain, determined by the tolerance of nitrosative stress of each individual strain (Fig 5.2, 5.4, and 5.8). No rate of NO reduction can be observed at high concentrations of NO. As only data from 2 hours after injection of NO was included for data analysis in Fig 5.10, the low NO reduction rate at the right proportion of the peak is therefore not due to lack of induction for the NO

detoxifying enzymes. This is confirmed by the identical results of repeated robotic experiments obtained by Dr. Linda Bergaust, using a bacterial inoculum already exposed to NO. Therefore, it was not due to poor expression of enzymes, but possibly the enzymes were inhibited by NO at the threshold concentrations of NO, or maybe due to lag growth phase with reduced cell vitality under high NO concentrations, thus affecting the supply of precursors needed for NO reduction. For RK4353, several enzymes including Hmp, NrfA, NorV, and the Hcp protein under investigation, coexist to detoxify NO. The combined capacity of NO reduction by these enzymes is 10 times higher than that of Hcp and Hcr together, whereas a further deletion of Hcr reduced the capacity down to about one third (Fig 5.10). As these kinetic data were obtained from living bacteria that are sensitive to NO possibly due to other cellular components, this entire curve cannot be fitted with a standard Michaelis-Menten equation of substrate inhibition. Upon visual estimation, the apparent Km and Vmax from the lower concentration range of NO were 900 nM and 800 nmol· g^{-1}· s^{-1} for the parent strain RK4353, and 75 nM and 85 nmol· g^{-1}· s^{-1} for strain JCB5210 (Fig 5.10 A). As explained earlier most of the NO reduction can be attributed to NorV judging from product formation. The capacity of NO reduction by Hcp is lower than the NO reductase NorV, however, the low apparent Km suggests a high affinity of Hcp to the substrate NO. Therefore, it is proposed that Hcp is a low capacity, high affinity NO reductase.

6.6. Suggested experiments

6.6.1. Comparative study between NorV-NorW and Hcp-Hcr

The NorV-NorW and Hcp-Hcr systems share several similarities. Both of them couple NADH oxidation to NO reduction, with the same terminal product N_2O. In both systems,

electrons are passed through the oxidoreductase NorW or Hcr to the reductase NorV or Hcp, although the latter is so far hypothetical, not proved by this work using the aerobically purified Hcp and Hcr (Vicente *et al.*, 2007). For future work, efforts can be made to purify Hcp anaerobically and to establish a protocol to reactivate Hcp after purification. The interaction of Hcp and Hcr was demonstrated in this work. After searching in all the completely sequenced genomes, the *norW* gene, like *hcr*, is also found in facultative anaerobes. It would be interesting to clone NorV and NorW into the bacterial two-hybrid system, and find out whether NorV and NorW interact and whether the interaction strength equals to that detected between Hcp and Hcr. This result will show whether the interaction between Hcp and Hcr is unique for its own purpose, or whether it is possibly a universal trait of electron transfer between a cytoplasmic reductase and its oxidoreductase.

NorV and Hcp have been previously found involved in pathogenicity of enteric bacteria (Gardner *et al.*, 2002; Kim *et al.*, 2002). This is hardly surprising as NorV and Hcp are capable of reducing NO, an antimicrobial reagent produced by macrophages to kill the invading bacteria. But the results turned out to be counter-intuitive, for both of them in different microorganisms. In theory, the mutation or deletion of the NO detoxifying enzymes should lead to a decreased ability of the pathogen to deal with the NO produced by macrophages, and therefore reduce their pathogenicity. On the contrary, in the strain *E. coli* strain O157:H7 that previously caused two major outbreaks, the NorV in the isolated strain was found to be a mutant without the critical FMN binding domain and possibly dysfunctional (Gardner *et al.*, 2002). Likewise, when compared to the wildtype strain, the *hcp-hcr* mutant of *Salmonella enterica* serovar Typhimurium was

more lethal during infection to mice (Kim *et al.*, 2002). Possibly this is the advantage of having more than one NO detoxifiers, so that increased NO concentration caused by the inactivation of one system will be circumvented by the performance of the other. It might be interesting to check the pathogenicity of these pathogenic strains lacking both Hcp and NorV, or in combination with other known NO detoxifiers including Nrf and Hmp.

Both Hcp and NorV are found in anaerobes. However, they are subjected to regulation by Fnr, the master regulator for anaerobiosis, in the opposite directions (Fig 1.5 vs Fig 1.7). The *hcp* promoter is activated by Fnr, whereas the norV promoter is repressed by Fnr. The transcription of *hcp* can simply be initiated by the activation of Fnr alone in spite of the repression by NsrR (Chismon, 2011). As a matter of fact, Hcp was first purified from a *D. vulgaris* strain under normal anaerobic growth conditions. In the presence of nitrate or nitrite, the transcription of *hcp* will be maximized due to activation by NarL/NarP in response to nitrate or nitrite, possibly as well as the de-repression of NsrR in response to the NO generated as a by-product. By contrast, the expression of NorV is repressed by the pleiotropic regulator Fnr and NarL/NarP under anaerobiosis, but activated by the exclusive NO sensor NorR (Fig 1.5). This suggests that under normal anaerobic growth conditions, Hcp is constitutively produced whereas NorV is not normally expressed unless required, such as when cells are exposed to NO. As a signaling molecule, NO is known to play a critical role in cellular physiology, but the accumulation of NO should be avoided due to its toxicity. It is important for bacteria to keep a balanced NO concentration within a narrow physiological range at all times during anaerobic growth. The constitutive expression of Hcp and its high affinity of NO

will enable Hcp to fulfill a role as the housekeeping modulator, especially when the most favored electron acceptor nitrate is available, so that the NO generated during anaerobic nitrate respiration will not accumulate to a toxic level. NorV, on the other hand, is a more specialized NO detoxifier to deal with accidental bursts of high NO concentrations, such as the NO produced by macrophage during host-pathogen interaction. To test this hypothesis, further work can be completed using *lacZ* fusion reporters to compare the induction of these two promoters at physiological NO and N-oxide concentrations. Also, the robotic gas analysis system can be further utilized to compare the NO reduction ability of NorVW and Hcp-Hcr within physiological NO concentrations without other NO detoxifiers. For *in vitro* work using anaerobically purified proteins, this system needs to be modified to operate with smaller vials, as the current compatible size is 120 mL. For further *in vivo* work, two isogenic strains are required with the following phenotypes: *ΔnrfABΔhmpΔhcp* and *ΔnrfABΔhmpΔnorV*. The anaerobic cultures of these two strains can be treated with a range of physiological NO concentrations such as 10 nM, 100 nM and 1 μM, and the time course of NO reduction and N_2O generation can be analysed.

6.6.2. Interaction between Hcp and Hcr

An intriguing question is why Hcr is only found in facultative anaerobes, but not any other types of microorganisms, considering the wide-spread distribution of Hcp in all three kingdoms of life? So far the data from chapter 4 of this thesis suggest that Hcr still functions after being purified aerobically, whereas Hcp is not. If the reason for the inactivation of Hcp is due to oxygen inactivation, the *hcr* gene is possibly acquired by facultative anaerobes so as to adapt better to the frequent exposure to oxygen. On the

other hand, to go back to where it was before this project began, it is also highly likely that the interaction between Hcp and Hcr is required for electron transfer, especially if these two proteins can move around freely in the cytosol. Electron transfer will occur only when these two proteins are within electron transfer range.

In order to gain more understanding of the nature of the interaction between Hcp and Hcr, X-ray crystallography data will be needed to model the interaction interface between Hcp and Hcr. At present, there is no data available for Hcp or Hcr from *E. coli*, or any other facultative anaerobes, although Hcp proteins from the strict anaerobes such as *D. vulgaris* and *D. desulfuricans* have been characterized more than once. It will be optimal if Hcp and Hcr from *E. coli* can be purified and then crystallized to obtain the accurate structural data, which can be used in protein modelling data bases for prediction of the possible sites of interaction. Co-crystallization of these two proteins can even be attempted, as no modeling would be required if it turns out to be successful.

A search for other proteins with crystal structure available that share a moderate sequence similarity with Hcr might help modeling the interaction at the present. The protein sequence of Hcr from *E. coli* was compared with those deposited in the Protein Data Bank. The top hit is the phthalate dioxygenase reductase from *Pseudomonas cepacia* (PDB code: 2PIA) with 28% of identity and 58.7% of similarity. Like Hcr, it is also an NADH-dependent oxidoreductase containing a 2Fe-2S centre and a flavin (Correll *et al.*, 1992). The difference is that this protein uses FMN as cofactor rather than FAD in Hcr. To simulate docking between the two proteins Hcp and Hcr, the Hcp from *D. vulgaris* (PDB code: 1W9M) was used as a substitute as Hcp from *E. coli*,

while the structure data of PDR was tentatively used as a substitute as Hcr (2PIA). The docking was achieved using the Hex server for protein docking, and the result is demonstrated in Fig 6.2. The residues of interface from Hcp during this interaction mainly come from domain 1 and 3. From this simulation, the Fe-S centres between the two proteins are not within direct electron transfer range. The closest edge-to-edge distance is approximately 30 Angstrom, whereas the normal accepted maximum distance of non-rate limiting electron transfer is about 14 Angstrom. PDR can be cloned into the two-hybrid system and tested whether it interacts with Hcp. If they do interact, it would be interesting to study the residues on the interaction interface *via* a systematic site-directed mutagenesis approach, and to better understand the nature of interaction between Hcp and Hcr.

Figure 6.2

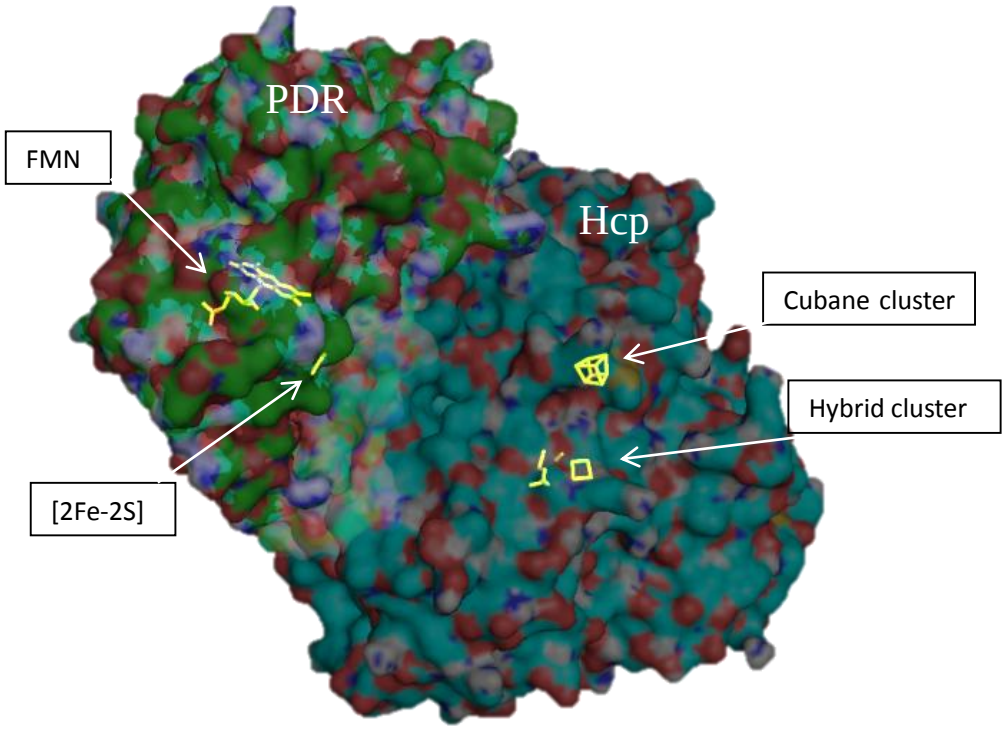

Predicted interaction between Hcp and PDR

The domain arrangement of Hcp is the same with that shown in Fig 1.7. The protein on the left is PDR coloured in green. The blue-coloured protein on the right is Hcp, oriented in the same way as depicted in Fig 1.7. This docking was achieved using the Hex server for protein interaction. Image is generated using Pymol.

References

Alberty, R.A. (2004) Standard apparent reduction potentials of biochemical half reactions and thermodynamic data on the species involved. Biophys. Chem. **111**:115-122

Almeida, C.C., Romão, C.V., Lindley, P.F., Teixeira, M. and Saraiva, L.M. (2006) The role of the hybrid cluster protein in oxidative stress defence. J. Biol. Chem. **281**: 32445-32450

Aragão, D., Macedo, S., Mitchell, E.P., Romão, C.V., Liu, M.Y., Frazão, C., Saraiva, L.M., Xavier, A.V., LeGall, J., van Dogen, W.M.A.M., Hagen, W.R., Teixeira, M., Carrondo, M.A. and Lindley, P.F. (2003) Reduced hybrid cluster proteins (HCP) from *Desulfovibrio desulfuricans* ATCC 27774 and *Desulfovibrio vulgaris* (Hildenborough): X-ray structures at high resolution using synchrotron radiation. J. Biol. Inorg. Chem. **8**: 540–548

Aragão, D., Mitchell, E.P., Frazão, C.F., Carrondo, M.A. and Lindley, P.F. (2008) Structural and functional relationships in the hybrid cluster protein family: structure of the anaerobically purified hybrid cluster protein from *Desulfovibrio vulgaris* at 1.35 Å resolution. Acta. Cryst. **D64**: 665-674

Aravind, L., Anantharaman, V., Balaji, S., Babu, M.M. and Iyer, L.M. (2005) The many faces of the helix-turn-helix domain: transcription regulation and beyond. FEMS Microbiol. Rev. **29**: 231–262

Arendsen, A.F. Hadden, J., Card, G. *et al.*, (1998) The "prismane" protein resolved: X-ray structure at 1.7 Å and multiple spectroscopy of two novel 4Fe clusters. J. Biol. Inorg. Chem. **3**: 81-95

Averill, B.A. (1996) Dissimilatory nitrite and nitric oxide reductases. Chem. Rev. **96**: 2951-2964

Ayala-Castro, C., Saini, A. and Outten, F.W. (2008) Fe-S cluster assembly pathways in bacteria. Microbiol. Mol. Biol. Rev. **72**: 110-125

Baba, T., Ara, T., Hasegawa, M., Takai, Y., Okumura, Y., Baba, M., Datsenko, K., Tomita, M., Wanner, B.L. and Mori, H. (2006) Construction of *Escherichia coli* K-12 in-frame, single-gene knockout mutants: the Keio collection. Mol. Syst. Biol. **2**: 2006.0008

Bamford, V.A., Angove, H.C., Seward, H.E., Thomson, A.J., Cole, J.A., Butt, J.N., Hemmings, A.M. and Richardson, D.J. (2002) Biochemistry. **41**: 2921-2931

Bao, X. (2013) Biochemical characterization of citric acid cycle enzyme, aconitase B, in *Escherichia coli*. MSc disseration, University of Birmingham

Barras, F., Loiseau, L. and Py, B. (2005) How *Escherichia coli* and *Saccharomyces*

cerevisiae build Fe/S proteins. Adv. Microb. Physiol. **50**:41-101

Beinert, H., Holm, R.H. and Münck, E. (1997) Iron-sulfur clusters: nature's modular, multipurpose structures. Science. **277**: 653–659

Blasco, F., Iobbi, C., Ratouchniak, J., Bonnefoy, V. and Chippeaux, M. (1990) Nitrate reductases of *Escherichia coli*: sequence of the second nitrate reductase and comparison with that encoded by the *narGHJI* operon. Mol. Gen. Genet. **222**: 104-111

Bodenmiller, D.M. and Spiro, S. (2006) The *yjeB* (*nsrR*) Gene of *Escherichia coli* encodes a nitric oxide-sensitive transcriptional regulator. J. Bacteriol. **188**: 874-881

Boutrin, M.C., Wang, C., Aruni, W., Li, X. and Fletcher, H.M. (2012) Nitric oxide stress Resistance in *Porphyromonas gingivalis* is mediated by a putative hydroxylamine reductase. J. Bacteriol. **194**: 1582-1592

Brock, M., Maerker, C., Schutz, A., Volker, U. and Buckel, W. (2002) Oxidation of propionate to pyruvate in *Escherichia coli*. Involvement of methylcitrate dehydratase and aconitase. Eur. J. Biochem. **269**: 6184-6194

Browning, D.F., Grainger, D.C., Beatty, C.M., Wolfe, A.J., Cole, J.A. and Busby, S.J. (2005) Integration of three signals at the *Escherichia coli nrf* promoter: a role for Fis protein in catabolite repression. Mol. Microbiol. **57**: 496-510

Browning, D.F., Lee, D.J., Spiro, S. and Busby, S.J.W. (2010) Down-regulation of the *Escherichia coli* K-12 *nrf* promoter by binding of the NsrR nitric oxide-sensing transcription repressor to an upstream site. J. Bacteriol. **192**: 3824-3828

Cadby, I. T. (2014) The regulation of gene expression in sulphate reducing bacteria. PhD thesis, University of Birmingham

Chang A.C. and Cohen S.N. (1978) Construction and characterization of amplifiable multicopy DNA cloning vehicles derived from the P15A cryptic miniplasmid. J. Bacteriol. **134**: 1141-1156

Chaudhry, G.R. and MacGregor, C.H. (1983) Cytochrome *b* from *Escherichia coli* nitrate reductase: its properties and association with enzyme complex. J. Biol. Chem. **258**: 5819-5827

Chismon, D.L. (2011) Architecture of *Escherichia coli* promoters that respond to reactive nitrogen species. PhD thesis, University of Birmingham

Chismon, D.L., Browning, D.F., Farrant, G.K. and Busby, S.J. (2010) Unusual organisation, complexity and redundancy at the *Escherichia coli hcp-hcr* operon promoter. Biochem. J. **430:** 61-68

Clegg, S., Yu, F., Griffiths, L. and Cole, J.A. (2002) The roles of the polytopic membrane proteins NarK, NarU and NirC in *Escherichia coli* K-12: two nitrate and three nitrite transporters. Mol. Microbiol. **44**: 143-155

Cole, J. (1996) Nitrate reduction to ammonia by enteric bacteria: redundancy, or a strategy for survival during oxygen starvation? FEMS Microbiol. Lett. **136**: 1-11

Cole, J.A. and Brown, C.M. (1980) Nitrite reduction to ammonia by fermentative bacteria: a short circuit in the biological nitrogen cycle. FEMS Microbiol. Lett. **7**: 65-72

Collins, M.D. and Jones, D. (1981) Distribution of isoprenoid quinone structural type in bacterian and their taxonomic implication. Microbiol. Rev. **45**: 316-354

Compton, L.A. and Johnson, W.C.Jr. (1986) Analysis of protein circular dichroism spectra for secondary structure using a simple matrix multiplication. Anal. Biochem. **155**: 155–167

Constantinidou, C., Hobman, J.L., Griffiths, L., Patel, M.D., Penn, C.W., Cole, J.A. and Overton, T.W. (2006). A reassessment of the FNR regulon and transcriptomic analysis of the effects of nitrate, nitrite, NarXL, and NarQP as *Escherichia coli* K12 adapts from aerobic to anaerobic growth. J. Biol. Chem. **281:** 4802-4815

Cooper, S.J., Garner, C.D., Hagen, W.R., Lindley, P.F. and Bailey, S. (2000) Hybrid-cluster protein (HCP) from *Desulfovibrio vulgaris* (Hildenborough) at 1.6 Å resolution. Biochemistry. **39**: 15044-15054

Corker, H. and Poole, R.K. (2003) Nitric oxide formation by *Escherichia coli*. J. Biol. Chem. **278**: 31584-31592

Correll, C.C., Batie, C.J., Ballou, D.P. and Ludwig, M.L. (1992) Phthalate dioxygenase reductase: A modular structure for electron transfer from pyridine nucleotides to [2FE-2S]. Science. **258**: 1604-1610

Crack, J.C., Gaskell, A.A., Cheesman, M.R., Le Brun, N.E. and Thomson, A.J. (2008) Influence of the environment on the $[4Fe\text{-}4S]^{2+}$ to $[2Fe\text{-}2S]^{2+}$ cluster switch in the transcriptional regulator FNR. J. Am. Chem. Soc. **130**: 1749-1758

Cruz-Ramos, H., Crack, J., Wu, G., Hughes, M.N., Scott, C., Thomson, A.J., Green, J. and Poole, R.K. (2002) NO sensing by FNR: regulation of the *Escherichia coli* NO-detoxifying flavohaemoglobin, Hmp. EMBO J. **21**: 3235-3244

Cunningham, L., Gruer, M.J. and Guest, J.R. (1997) Transcriptional regulation of the aconitase genes (*acnA* and *acnB*) of *Escherichia coli*. Microbiology. **143**: 3795-3805

Datsenko, K.A. and Wanner, B.L. (2000) One step inactivation of chromosomal genes in *Escherichia* K-12 using PCR products. Proc. Natl. Acad. Sci. USA **97:** 6640-6645

D'Autréaux, B., Tucker, N.P., Dixon, R. and Spiro, S. (2005) A non-haem iron centre in the transcription factor NorR senses nitric oxide. Nature. **437**: 769-772

Ding, H. and Demple, B. (1997) *In vivo* kinetics of a redox-regulated transcriptional switch. Proc. Natl. Acad. Sci. USA **94**: 8445-8449

Dobbek, H., Svetlitchnyi, V., Gremer, L., Huber, R. and Meyer, O. (2001) Crystal structure of a carbon monoxide dehydrogenase reveals a [Ni-4Fe-5S] cluster. Science. **293**: 1281-1285

Enoch, H.G. and Lester, R.L. (1975) The purification and properties of formate dehydrogenase and nitrate reductase from *Escherichia coli*. J. Biol. Chem. **250**: 6693-6705

Einsle, O., Messerschmidt, A., Huber, R., Kroneck, P.M.H. and Neese, F. (2002) Mechanism of the six-electron reduction of nitrite to ammonia by cytochrome *c* nitrite reductase. J. Am. Chem. Soc. **124**: 11737-11745

Fang, F. C. (2004) Antimicrobial reactive oxygen and nitrogen species: concepts and controversies. Nat. Rev. Microbiol. **2**: 820-832

Figueiredo, M.C.O., Lobo, S.A.L., Sousa, S.H., Pereira, F.P., Wall, J.D., Nobre, L.S. and Saraiva, L.M. (2013) Hybrid cluster protein and flavodiiron proteins afford protection to *Desulfovibrio vulgaris* upon macrophage infection. J. Bactriol. **196**: 2684-2690

Filenko, N.A. (2005) Roles and regulation of the iron-sulphur proteins, HCP, NapG and NapH, induced during anaerobic growth of *E. coli*. PhD thesis, University of Birmingham

Filenko, N.A., Browning, D.F. and Cole, J.A. (2005) Transcriptional regulation of a hybrid cluster (prismane) protein. Biochem. Soc. Trans. **33**: 195-197

Filenko, N., Spiro, S., Browning, D.F., Squire, D., Overton, T.W., Cole, J. and Constantinidou, C. (2007) The NsrR regulon of *Escherichia coli* K-12 includes genes encoding the hybrid cluster protein and the periplasmic, respiratory nitrite reductase. J. Bacteriol. **189**: 4410-4417

Forget, P. (1974) The bacterial nitrate reductases. Solubilization, purification and properties of the enzyme A of *Escherichia coli* K12. Eur. J. Biochem. **42**: 325-332

Gardner, P.R. (1997) Superoxide-driven aconitase Fe-S center cycling. Biosci. Rep. **17**: 33-42

Gardner, P.R., Costantino, G., Szabo, C and Salzman, A.L. (1997) Nitric oxide sensitivity of aconitases. J. Biol. Chem. **272**: 25071-25076

Gardner, P.R. and Fridovich, I. (1991) superoxide sensitivity of the *Escherichia coli*

aconitase. J. Biol. Chem. **266**: 19328-19333

Gardner, P.R. and Fridovich, I. (1993) Effect of glutathione on aconitase in Escherichia coli. Arch. Biochem. Biophys. **301**: 98-102

Gardner, A.M. and Gardner, P.R. (2002) Flavohemoglobin detoxifies nitric oxide in aerobic, but not anaerobic, *Escherichia coli*. J. Biol. Chem. **277**: 8166-8171

Gardner, A.M., Helmick, R.A. and Gardner, P.R. (2002) Flavorubredoxin, an inducible catalyst for nitric oxide reduction and detoxification in *Escherichia coli*. J. Biol. Chem. **277**: 8172-8177

Gennis, R.B., Stewart, V. (1996) Respiration. In: *Escherichia coli* and *Salmonella*. Neidhardt, F.C. (ed). 217-261

Gilberthorpe, N.J. and Poole, R.K. (2008) Nitric oxide homeostasis in Salmonella typhimurium: roles of respiratory nitrate reductase and flavohemoglobin. J. Biol. Chem. **283**: 11146-11154

Girsch, P. and de Vries, S. (1997) Purification and initial kinetic and spectroscopic characterization of NO reductase from *Paracoccus denitrificans*. Biochim. Biophys. Acta. **1318**: 202-216

Gomes, C.M., Giuffrè, A., Forte, E., Vicente, J.B., Saraiva, L.M., Brunori, M. and Teixeira, M. (2002) A novel type of nitric-oxide reductase. J. Biol. Chem. **277**: 25273-25276

Grainger, D.C., Aiba, H., Hurd, D., Browning, D.F. and Busby, S.J. (2007) Transcription factor distribution in *Escherichia coli*. Studies with FNR protein. Nucleic. Acids. Res. **35**: 269-278

Gruer, M.J. and Guest, J.R. (1994) Two genetically-distinct and differentially-regulated aconitases (AcnA and AcnB) in *Escherichia coli*. Microbiology. **140**: 2531-2541

Gruer, M.J., Bradbury, A.J. and Guest, J.R. (1997) Construction and properties of aconitase mutants of Escherichia coli. Microbiology. **143**: 1837-1846

Guest, J.R., Green, J., Irvine, A.S. and Spiro, S. (1996) Regulation of Gene Expression in *Escherichia coli*. Springer US. pp:317-342

Hagen, W.R., Pierik, A.J. and Veeger, C. (1989) Novel electron paramagnetic resonance signals from an Fe/S protein containing six iron atoms. J. Chem. Soc. Faraday Trans. 1. **85**: 4083-4090

Halla, C. and Garthwaiteb, J. (2009) What is the real physiological NO concentration *in vivo*? Nitric Oxide. **21**: 92-103

Hentze, M.W. and Kuhn, L.C. (1996) Molecular control of vertebrate iron metabolism:

mRNA-based regulatory circuits operated by iron, nitric oxide, and oxidative stress. Proc. Natl. Acad. Sci. USA **93**: 8175-8182

Heo, J., Wolfe, M.T., Staples, C.R. and Ludden, P.W. (2002) Converting the NiFeS carbon monoxide dehydrogenase to a hydrogenase and a hydroxylamine reductase. J. Bacteriol. **184**:5894-5897

Hussain, H., Grove, J., Griffiths, L., Busby, S. and Cole, J. (1994) A seven-gene operon essential for formate-dependent nitrite reduction to ammonia by enteric bacteria. Mol. Microbiol. **12**: 153-163

Hutchings, M.I., Mandhana, N. and Spiro, S. (2002) The NorR protein of *Escherichia coli* activates expression of the flavorubredoxin gene *norV* in response to reactive nitrogen species. J. Bacteriol. **184**: 4640-4643

Hutchings, M.I., Shearer, N., Wastell, S., van Spanning, R.J. and Spiro, S. (2000) Heterologous NNR-mediated nitric oxide signaling in *Escherichia coli*. J. Bacteriol. **182**: 6434–6439

Iobbi, C., Santini, C.L., Bonnefoy, V. and Giordano, G. (1987) Biochemical and immunological evidence for a second nitrate reductase in *Escherichia coli* K12. Eur. J. Biochem. **168**: 451-459

Iobbi-Nivol, C., Santini, C.L., Blasco, F. And Giordano, G. (1990) Purification and further characterization of the second nitrate reductase of *Escherichia coli* K12. Eur. J. Biochem. **188**: 679-687

Isabella, V.M., Lapek, J.D., Jr., Kennedy, E.M. and Clark, V.L. (2009) Functional analysis of NsrR, a nitric oxide-sensing Rrf2 repressor in *Neisseira gonorrhoeae*. Mol. Microbiol. **71**: 227-239

Jayaraman, P.S., Gaston, K.L., Cole, J.A. and Busby, S.J.W. (1988) The *nirB* promoter of *Escherichia coli*: location of nucleotide sequences essential for regulation by oxygen, the FNR protein and nitrite. Mol. Microbiol. **2**: 527-530

Ji, X.B. and Hollocher, T.C. (1988) Reduction of nitrite to nitric oxide by enteric bacteria. Biochem. Biophys. Res. Commun. **157**: 106-108

Jia, W., Tovell, N., Clegg, S., Trimmer, M. and Cole, J. (2009) A single channel for nitrate uptake, nitrite export and nitrite uptake by *Escherichia coli* NarU and a role for NirC in nitrite export and uptake. Biochem. J. **417**: 297-304

Johnson, D., Dean, D.R., Smith, A.D. and Johnson, M.K. (2005) Structure, function and formation of biological iron–sulfur clusters. Annual. Rev. Biochem. **74**: 247–281

Justino, M.C., Almeida, C.C., Goncalves, V.L., Teixeira, M. and Saraiva, L.M. **(**2006) *Escherichia coli* YtfE is a di-iron protein with an important function in assembly of iron-sulphur clusters. FEMS Microbiol. Lett. **257:** 278-84

Justino, M.C., Almeida, C.C., Teixeira, M. and Saraiva, L.M. (2007) *Escherichia coli* di-iron YtfE protein is necessary for the repair of stress-damaged iron-sulphur clusters. J. Biol. Chem. **282**: 10352-10359

Justino, M.C., Baptista, J.M. and Saraiva, L.M. (2009) Di-iron proteins of the Ric family are involved in iron-sulphur cluster repair. Biometals. **22**: 99-108

Justino, M.C., Vicente J.B., Texiera, M. and Saraiva, L.M. (2005) New genes implicated in the protection of anaerobically grown *Escherichia coli* against nitric oxide. J. Biol. Chem. **280:** 2636-2643

Kabsch, W. and Sander, C. (1983) Dictionary of protein secondary structure: Pattern recognition of hydrogen-bonded and geometrical features. **22**: 2577-2637

Karimova, G., Pidoux, J., Ullmann, A. and Ladant, D. (1998) A bacterial two-hybrid system based on a reconstituted signal transduction. Proc. Natl. Acad. Sci. USA **95**: 5752-5756

Keseler, I.M., Bonavides-Martinez, C., Collado-Vides, J., Gama-Castro, S., Gunsalus, R.P., Johnson, D.A., Krummenacker, M., Nolan, L.M., Paley, S., Paulsen, I.T., Peralta-Gil, M., Santos-Zavaleta, A., Shearer, A.G. and Karp, P.D. (2009) EcoCyc: a comprehensive view of *Escherichia coli* biology. Nucleic. Acids. Res. **37**:D464-D470

Khoroshilova, N., Popescu, C., Münck, E., Beinert, H. and Kiley, P.J. (1997) Iron-sulfur cluster disassembly in the FNR protein of Escherichia coli by O2: [4Fe-4S] to [2Fe-2S] conversion with loss of biological activity. Proc. Natl. Acad. Sci. USA **94**: 6087-6092

Kiley, P. and Beinert, H. (2003) The role of Fe-S proteins in sensing and regulation in bacteria. Curr. Opin. Microbiol. **6**: 181–185

Kiley, P.J. and Reznikoff, W.S. (1991) Fnr mutants that activate gene expression in the presence of oxygen. J. Bacteriol. 173**: 16-22**

Kim, S.O., Orii, Y., Lloyd, D., Hughes, M.N. and Poole, R.K. (1999) Anoxic function for the *Escherichia coli* flavohaemoglobin (Hmp): reversible binding of nitric oxide and reduction to nitrous oxide. FEBS. Lett. **445**: 389-394

Lee, D.J., Bingle, L.E.H., Heurlier, K., Pallen, M.J., Penn, C.W., Busby, S.J.W. and Hobman J.L. (2009) Gene doctoring: a method for recombineering in laboratory and pathogenic *Escherichia coli* strains. BMC Microbiol. **9**: 252

Lewis, J.P., Yanamandra, S.S. and Anaya-Bergman, C. (2012) HcpR of *Porphyromonas gingivalis* is required for growth under nitrosative stress and survival within host cells. Infect. Immun. **80**: 3319-3331

Lill, R. (2009) Function and biogenesis of iron–sulphur proteins. Nature. **460**: 831–838

Lin, H-Y., Bledsoe, P.J. and Stewart, V. (2007) Activation of *yeaR-yoaG* operon transcription by the nitrate-responsive regulator NarL is independent of oxygen-responsive regulator Fnr in *Escherichia coli* K-12. J. Bacteriol. **189**: 7539-7548

Lowry, O.H., Rosebrough, N.J., Farr, A.L. and Randall, R.J. (1951) Protein measurement with the Folin phenol reagent. J. Biol. Chem. **193**: 265-275

Lu, C., Bentley, W.E. and Rao, G. (2004) A high-throughput approach to promoter study using green fluorescent protein. Biotechnol. Prog. **20**: 1634-1640

Macedo, S., Aragão, D., Mitchell, E.P. and Lindley, P. (2003) Structure of the hybrid cluster protein (HCP) from *Desulfovibrio desulphuricans* ATCC 27774 containing molecules in the oxidised and reduced states. Acta. Cryst. **D59**: 2065-2071

Macedo, S., Mitchell, E.P., Romão, C.V., Cooper, S.J., Coelho, R., Liu, M.Y., Xavier, A.V., LeGall, J., Bailey, S., Garner, C.D., Hagen,W.R., Teixeira, M., Carrondo, M.A. and Lindley, P. (2002) Hybrid cluster proteins (HCPs) from *Desulfovibrio desulfuricans* ATCC 27774 and *Desulfovibrio vulgaris* (Hildenborough): X-ray structures at 1.25 Å resolution using synchrotron radiation. J. Biol. Inorg. Chem. **7**: 514–525

Macindoe, G., Mavridis, L., Venkatraman, V., Devignes, M. and Ritchie, D.W. (2010) HexServer: an FFT-based protein docking server powered by graphics processors. Nucleic. Acids. Res. **38**: W445-W449

Malkin, R. and Rabinowitz, J.C. (1966) The reconstitution of clostridial ferredoxin. Biochem. Biophys. Res. Commun. **23:** 822–827

Metheringham, R. and Cole, J.A. (1997) A reassessment of the genetic determinants, the effect of growth conditions and the availability of an electron donor on the nitrosating activity of *Escherichia coli* K-12. Microbiology. **143**: 2647–2656

Meyer, J. (2008) Iron-sulfur protein folds, iron-sulfur chemistry, and evolution. J. Biol. Inorg. Chem. **13**: 157-170

Mills. P.C., Rowley, G., Spiro, S., Hinton, J.C.D. and Richardson, D.J. (2008) A combination of cytochrome *c* nitrite reductase (NrfA) and flavorubredoxin (NorV) protects *Salmonella enterica* serovar Typhimurium against killing by NO in anoxic environments. Microbiology. **154**: 1218-1228

Molstad, L., Dörsch, P. and Bakken, L.R. (2007) Robotized incubation system for monitoring gases (O_2, NO, N_2O N_2) in denitrifying cultures. J. Microbiol. Meth. **71**:202-211

Moncada, S., Palmer, R.M. and Higgs, E.A. (1991) Nitric oxide: physiology, pathophysiology, and pharmacology. Pharmacol. Rev. **43**: 109-142

Montet, Y., Amara, P., Volbeda, A., Vernede, E., Hatchikian, C., Field, M., Frey, M. and Fontecilla-Camps, J.C. (1997) Gas access to the active site of Ni-Fe hydrogenases probed by X-ray crystallography and molecular dynamics. Nat. Struct. Biol. **4**: 523-526

Morrison, J.F. (1954) The purification of aconitase. Biochem. J. **56**: 99-105

Moura, I., Tavares, P., Moura, J.J., Ravi, N., Huynh, B.H., Liu, M.Y. and LeGall, J. (1992) Direct spectroscopic evidence for the presence of a 6Fe cluster in an iron-sulfur protein isolated from *Desulfovibrio desulfuricans* (ATCC 27774). J. Biol. Chem. **267**: 4489-4496

Murphy, M.J., Siegel, L.M., Tove, S.R. and Kamin, H. (1974) Siroheme: a new prosthetic group participating in six-electron reduction reactions catalyzed by both sulfite and nitrite reductases. Proc. Natl. Acad. Sci. USA **71:** 612-616

Nilavongse, A., Brondijk, T.H.C., Overton, T.W., Richardson, D.J., Leach, E.R. and Cole, J.A. (2006) The NapF protein of the *Escherichia coli* periplasmic nitrate reductase system: demonstration of a cytoplasmic location and interaction with the catalytic subunit, NapA. Microbiology. **152**: 3227–3237
Nobre, L.S., Ricardo, G-S., Todorovic, S., Hidebrandt, P., Teixeira, M., Latour,J-M. and Saraiva, L.M. (2014) *Escherichia coli* RIC is able to donate iron to iron-sulfur clusters. PLoS ONE. **9**: e95222

Noriega, C.E., Lin, H.Y., Chen, L.L., Williams, S.B. and Stewart, V. (2010) Asymmetric cross-regulation between the nitrate-responsive NarX-NarL and NarQ-NarP two-component regulatory systems from *Escherichia coli* K-12. Mol. Microbiol. **75**: 394-412

Novagen (1998) pET-28a-c(+) vectors [Online] Available from:
http://www.staff.ncl.ac.uk/p.dean/pET.pdf

Overton, T.W., Justino, M.C., Li, Y., Baptista, J.M., Melo, A.M.P., Cole, J.A. and Saraiva, L.M. (2008) Widespread distribution in pathogenic bacteria of di-iron proteins that repair oxidative and nitrosative damage to iron-sulphur centers. J. Bacteriol. **190**: 2004-2013

Page, L., Griffiths, L. and Cole, J.A. (1990) Different physiological roles of two independent pathways for nitrite reduction to ammonia by enteric bacteria. Arch. Microbiol. **154**: 349-354

Peakman, T., Crouzet, J., Mayaux, J.F., Busby, S., Mohan, S., Harborne, N., Wootton, J., Nicolson, R. and Cole, J. (1990) Nucleotide sequence, organisation and structural analysis of the products of genes in the *nirB-cysG* region of the *Escherichia coli* K-12 chromosome. Eur. J. Biochem. **191**: 315-323

Pereira, A.S., Tavares, P., Krebs, C., Huynh, B.H., Rusnak, F., Moura, I. And Moura, J.J.G. (1999) Biochemical and spectroscopic characterisation of overexpressed fuscoredoxin from *Escherichia coli*. Biochem. Biophys. Res. Commun. **260**: 209-215

Pierik, A.J., Wolbert, R.B.G., Mutsaers, P.H.A., Hagen, W.R., and Veeger, C. (1992) Purification and biochemical characterization of a putative [6Fe-6S] prismane-cluster-containing protein from *Desulfovibrio vulgaris* (Hildenborough). Eur. J. Biochem. **206**: 697-704

Poock, S.R., Leach, E.R., Moir, J.W.B., Cole, J.A. and Richardson, D.J. (2002) Respiratory denitrification of nitric oxide by the cytochrome *c* nitrite reductase of *Escherichia coli*. J. Biol. Chem. **277**: 23664-23669

Poole, R.K. and Hughes, M.N. (2000) New functions for the ancient globin family: bacterial responses to nitric oxide and nitrosative stress. Mol. Microbiol. **36**: 775-783

Potter, L.C., Millington, P., Griffiths, L., Thomas, G.H. and Cole, J.A. (1999) Competition between *Escherichia coli* strains expressing either a periplasmic or a membrane-bound nitrate reductase: does Nap confer a selective advantage during nitrate-limited growth? Biochem. J. **344**: 77-84

Pullan, S.T., Gidley, M.D., Jones, R.A., Barrett, J., Stevanin, T.M., Read, R.C., Green, J. and Poole, R.K. (2007) Nitric oxide in chemostat-cultured *Escherichia coli* is sensed by Fnr and other global regulators: unaltered methionine biosynthesis indicates lack of S-Nitrosation. J. Bacteriol. **63**: 1845-1855

Py, B. and Barras, F. (2010) Building Fe-S proteins: bacterial strategies. Nat. Rev. Microbiol. **8**: 436–446

Py, B., Moreau, P.L. and Barras, F. (2011) Fe-S clusters, fragile sentinels of the cell. Curr. Opin. Microbiol. **14**: 218–223

Rabin, R.S. and Stewart, V. (1993) Dual response regulators (Nar L and Nar P) interact with dual sensors (Nar X and Nar Q) to control nitrate- and nitrite-regulated gene expression in *Escherichia coli* K-12. J. Bacteriol. **175**: 3259-3268

Richardson, D.J., Wehrfritz, J.M., Keech, A., Crossman, L.C., Roldan, M.D., Sears, H.J., Butler, C.S., Reilly, A., Moir, J.W., Berks, B.C., Ferguson, S.J., Thomson, A.J. and Spiro, S. (1998) The diversity of redox proteins involved in bacterial heterotrophic nitrification and aerobic denitrification. Biochem. Soc. Trans. **26**: 401-408

Richardson, D.J. (2000) Bacterial respiration: a flexible process for a changing environment. Microbiology. **146**: 551-571

Richardson, D.J. (2001) Introduction: nitrate reduction and the nitrogen cycle. Cell. Mol. Life. Sci. **58**: 163-164

Richardson, D. and Sawers, G. (2002) PMF through the redox loop. Science. **295**: 1842-1843

Roche, B., Aussel, L., Ezraty, B., Mandin, P., Py, B. and Barras, F. (2013) Iron/sulphur

proteins biogenesis in prokaryotes: Formation, regulation and diversity. Biochim. Biophys. Acta. **1827**:455-469

Rodionov, D.A., Dubchak, I.L. Arkin, A.P., Alm, E.J. and Gelfand, M.S. (2005) Dissimilatroy metabolism of nitrogen oxides in bacteria: comparative reconstruction of transcriptional networks. PLoS Computational Biol. **1**: 415-431

Rouault, T.A., Haile, D.J., Downey, W.E., Philpott, C.C., Tang, C., Samaniego, F., Chin, J., Paul, I., Orloff, D., Harford, J.B. and Klausner, R.D. (1992) An iron-sulfur cluster plays a novel regulatory role in the iron-responsive element binding protein. Biometals. **5**: 131-140

Runkel, S. (2014) Endogenous production and detoxification of a potent cytotoxin, nitric oxide, in *Salmonella enterica* serovar Typhimurium and *Escherichia coli*. PhD thesis, University of East Anglia

Seth, D., Hausladen, A., Wang, Y-J. and Stamler, J.S. (2012) Endogenous protein S-nitrosylation in *E. coli*: Regulation by OxyR. Science. **336**: 470-473

Simon, J. (2002) Enzymology and biogenetics of respiratory nitrite ammonification. FEMS Microbiol. Rev. **26**: 285-309

Simon, J., Gross, R., Einsle, O., Kroneck, P.M.H., Kroeger, A. and Klimmek, O. (2000) A NapC/NirT-type cytochrome c (NrfH) is the mediator between the quinone pool and the cytochrome c nitrite reductase of *Wolinella succinogenes*. Mol. Microbiol. **35**:686-696

Spector, M.P., Garcia del Portillo, G., Bearson, S.M.D., Mahmud, A., Magut, M., Finlay, B.B., Dougan, G., Foster, J.W. and Pallen, M.J. (1999) The *rpoS*-dependent starvation-stress response locus *stiA* encodes a nitrate reductase (*narZYWV*) required for carbon-starvation-inducible thermotolerance and acid tolerance in *Salmonella typhimurium*. Microbiology. **145**: 3035-3045

Spiro, S. and Guest, J.R. (1990) FNR and its role in oxygen–regulated gene expression in *Escherichia coli*. FEMS Microbiol. Rev. **6**:399-428

Spek, E.J., Wright, T.L., Stitt, M.S., Taghizadeh, N.R., Tannenbaum, S.R., Marinus, M.G. and Engelward, B.P. (2001) Recombinatorial repair is critical for survival of *Escherichia coli* exposed to nitric oxide. J. Bacteriol. **183**: 131-138

Squire, D. (2009) The regulation of genes of unknown function implicated in nitrosative stress tolerance in *Escherichia coli* K-12. PhD thesis, University of Birmingham

Stewart, V. (1993) Nitrate regulation of anaerobic respiratory gene expression in *Escherichia coli*. Mol. Microbiol. **9**: 425-434

Stewart, V. (1998) Bacterial two-component regulatory systems. In: Busby, S.J, Thomas, C.M., Brown, N.L. (eds.) Mol. Microbiol. NATO ASI series, series H: cell

biology. **103**: 141-158.

Stewart, V. and Bledsoe, P.J. (2003) Synthetic *lac* oerator substitutions for studying the nitrate- and nitrite-responsive NarX-NarL and NarQ-NarP two-component regulatory systems of *Escherichia coli* K-12. J. Bacteriol. **185**: 2104-2111

Stewart, V. and Bledsoe, P.J. (2005) Fnr-, NarP- and NarL-Dependent Regulation of Transcription Initiation from the *Haemophilus influenzae* Rd *napF* (Periplasmic Nitrate Reductase) Promoter in *Escherichia coli* K-12. J. Bacteriol. **187**: 6928-6935

Stewart, V., Lu, Y. and Darwin, A.J. (2002) Periplasmic Nitrate Reductase (NapABC Enzyme) Supports Anaerobic Respiration by *Escherichia coli* K-12. J. Bacteriol. **184**: 1314-1323

Strube, K., deVires, S. and Cramm, R. (2007) Formation of a dinitrosyl iron complex by NorA, a nitric oxide-binding diiron protein from *Ralstonia eutropha* H16. J. Biol. Chem. **282**: 20292-20300

Sreerama, N., Venyaminov, S.Y. and Woody, R.W. (2000) Estimation of protein secondary structure from circular dichroism spectra: inclusion of denatured proteins with native protein in the analysis. Anal. Biochem., **287**: 243–251

Sreerama, N. and Woody, R.W. (2000) Estimation of protein secondary structure from circular dichroism spectra: comparison of CONTIN, SELCON, and CDSSTR methods with an expanded reference set. Anal. Biochem. **287**: 252–260

Tang, Y., Guest, J.R., Artymiuk, P.J. and Green, J. (2005) Switching aconitase between catalytic and regulatory modes involves iron-dependent dimer formation. Mol. Microbiol. **56**: 1149-1158

Todorovic, S., Justino, M.C., Wellenreuther, G., Hildebrandt, P., Murgida, D.H., Meyer-Klaucke, W. and Saraiva, L.M. (2008) Iron-Sulphur repair YtfE protein from *Escherichia coli*: structural characterisation of the di-iron center. J. Biol. Inorg. Chem. **13**: 765-770

Tucker, N.P., Autreaux, B.D., Spiro, S. and Dixon, R. (2005) Mechanism of transcriptional regulation by the *Escherichia coli* nitric oxide sensor NorR. Biochem. Soc. Trans. **34**: 191-194

Tucker, N.P., Hicks, M.G., Clarke, T.A., Crack, J.C., Chandra, G., Le Brun, N.E., Dixon, R. and Hutchings, M.I. (2008) The transcriptional repressor protein NsrR senses nitric oxide directly *via* a [2Fe-2S] cluster. PLoS ONE. **3**: e3623

Tyson, K., Metheringham, R., Griffiths, L. and Cole, J. (1997) Characterisation of Escherichia coli K-12 mutants defective in formate-dependent nitrite reduction: essential roles for hemN and the menFDBCE opeon. Arch. Microbiol. **168**: 403-411

Unden, G., Becker, S., Bongaerts, J., Holighaus, G., Schirawski, J. and Six, S. (1995) O_2

sensing and O_2 dependent gene regulation in facultatively anaerobic bacteria. Arch. Microbiol. **164**: 81-90

Unden, G. and Bongaerts, J. (1997) Alternative respiratory pathways if *Escherichia coli*: energetic and transcriptional regulation in response to electron acceptors. Biochim. Biophys. Acta. **1320**: 217-234

van den Berg, W.A., Stevens, A.A., Verhagen, M.F., van Dongen, W.M. and Hagen, W.R. (1994) Overproduction of the prismane protein from *Desulfovibrio desulfuricans* ATCC 27774 in *Desulfobivrio vulgaris* (Hildenborough) and EPR spectroscopy of the [6Fe-6S] cluster in different redox states. Biochim. Biophys. Acta. **1206**: 240-246

van den Berg, W.A.M., Hagen, W.R. and van Dongen, W.M.A.M. (2000) The hybrid-cluster protein ('prismane protein') from *Escherichia coli*. Characterisation of the hybrid-cluster protein, redox properties of the [2Fe-2S] and [4Fe-2S-2O] clusters and identification of an associated NADH oxidoreductase containing FAD and [2Fe-2S]. Eur. J. Biochem. **267**: 666-676

van Wonderen, J.H., Burlat, B., Richardson, D.J., Cheesman, M.R. and Butt, J.N. (2008) The nitric oxide reductase activity of cytochrome *c* nitrite reductase from *Escherichia coli*. J. Biol. Chem. **283**: 9587-9594

Varghese, S., Tang, Y. and Imlay, J.A. (2003) Contrasting sensitivities of *Escherichia coli* aconitases A and B to oxidation and iron depletion. J. Bacteriol. **185**: 221-230

Vega, J.M. and Garrett, R.H. (1975) Siroheme: a prosthetic group of the *Neurospora crassa* assimilatory nitrite reductase. J. Biol. Chem. **250**: 7980-7989

Vine, C.E. (2012) *Escherichia coli* response to nitrosative stress. PhD thesis, University of Birmingham

Vine, C.E. and Cole, J.A. (2011a) Unresolved sources, sinks, and pathways for the recovery of enteric bacteria from nitrosative stress. FEMS Microbiol. Lett. **325**: 99-107

Vine, C.E. and Cole, J.A. (2011b) Nitrosative stress in *Escherichia coli*: reduction of nitric oxide. Biochem. Soc. Trans. **39**: 213-215

Vine, C.E., Justino, M.C., Saraiva, L.M. and Cole, J.A. (2010) Detection by whole genome microarrays of a spontaneous 126-gene deletion during construction of a *ytfE* mutant: Confirmation that a *ytfE* mutation results in loss of repair of iron-sulphur centres in proteins damaged by oxidative or nitrosative stress. J. Microbiol. Meth. **81**: 77-79

Vine, C.E., Purewal, S.K. and Cole, J.A. (2011) NsrR-dependent method for detecting nitric oxide accumulation in the *Escherichia coli* cytoplasm and enzymes involved in NO production. FEMS Microbiol. Lett. **325**: 108-114

Wang, H. and Gunsalus, R.P. (2000) The *nrfA* and *nirB* nitrite reductase operons in

Escherichia coli are expressed differently in response to nitrate than to nitrite. J. Bacteriol. **182**: 5813-5822

Wang, H., Tseng, C.P. and Gunsalus, R.P. (1999) The *napF* and *narG* nitrate reductase operons in *Escherichia coli* are differentially expressed in response to submicromolar concentrations of nitrate but not nitrite. J. Bacteriol. **181**: 5303-5308

Weiss, B. (2006) Evidence for mutagenesis by nitric oxide during nitrate metabolism in *Escherichia coli*. J. Bacteriol. **188**: 829-833

Williams, C.H., Stillman, T.J., Barynin, V.V., Sedelnikova, S.E., Tang, Y., Green, J., Guest, J.R. and Artymiuk P.J. (2002) *E. coli* aconitase B structure reveals a HEAT-like domain with implications for protein-protein recognition. Nat. Struct. Biol. **9**: 447-452

Wolfe, M.T., Heo, J., Garavelli, J.S. and Ludden, P.W. (2002) Hydroxylamine reductase activity of the hybrid cluster protein from *Escherichia coli*. J. Bacteriol. **184**: 5898-5902

Yukl, E.T., Elbaz, M.A., Nakano, M.M. and Moenne-Loccoz, P. (2008) Transcription factor NsrR from *Bacillus subtilis* senses nitric oxide with a 4Fe-4S cluster. Biochemistry. **47**: 13084–13092